LID modeling and optimization at single unit and neighborhood scale

by

Yang Yu

A thesis submitted in partial fulfillment of the requirements for the degree of

Master of Science

in

Water Resources Engineering

Department of Civil and Environmental Engineering

University of Alberta

ABSTRACT

Low Impact Improvement (LID) had received great interest in the past decades to achieve sustainable urban stormwater management and improve urban ecological systems. Numerical studies were conducted in this thesis to improve the understanding of LID benefits in cold regions and explore the potentials of further improvements. This paper-based thesis mainly includes two parts: Part I "*Hydrologic and Water Quality Modeling of Bioretention Columns in Cold Regions*"; and Part II "*LID Spatial Allocation Optimization System: Integrated SWMM with PICEA-g using MATLAB as the Platform"*. Part I and II explored LID at single-unit (micro) scale and neighborhood (macro) scale, respectively.

Bioretention is widely-used in sustainable urban stormwater management. However, limited research has been conducted on its performance in cold regions, particularly for winter snowmelt, spring runoff, and large summer storm events (> 50 mm). In Part I of the thesis, HYDRUS 1D was selected and used to simulate and evaluate the hydrologic and water quality performance of four laboratory bioretention columns with different designs for cold regions. The results of the validated model reveals that the columns can remarkably reduce peak flow, ponding depth and duration for large summer storm events (even for 1:100 years). In winter snowmelt and spring runoff modeling, the saturated hydraulic conductivity (K_S) was found to be similar (approximately 0.1 cm/min) when the soil temperature was around -0.5 °C. The finer soil media would experience an increase of K_S after freeze-thaw cycles, while the opposite occurs for coarser soil media. The water quality simulation confirmed the experimental results and showed that the bioretention columns can effectively remove phosphate and ammonium, but have leaching issue for chloride and nitrate. Finally, optimization of bioretention columns was provided for summer large storm events.

Despite the growing interest in LID planning, no research, to the best of the author's knowledge, has proposed a spatial allocation optimization (SAO) system that integrates a hydrological computing engine with targeted modifications to an optimization algorithm using a programming language as the platform. In Part II of the thesis, an LID SAO system that combines SWMM and MATLAB was introduced. A preference-inspired co-evolutionary algorithm (PICEA-g) was adopted to obtain the optimal solutions for LID implementation (bioretention, rain garden, permeable pavement, and green roof) to maximize the hydrologic benefits and minimize the cost simultaneously. A typical urban residential neighborhood in western Canada was used as an example. Modifications were applied to the SAO algorithm to improve its performance, which include new methodologies for initializing candidate solutions, defining goal vector boundaries, and enhanced genetic operators. The obtained optimal solutions indicated that promising hydrologic benefits of peak flow and total inflow volume reduction, as well as peak flow delay from the catchment could be achieved with relatively low-cost LID implementations. The LID SAO system provides users with the flexibility and feasibility to apply it to a variety of drainage locations, scales, and objectives (e.g., water quality).

Finally, general conclusions were provided at the end of the thesis based on the above two (Part I and II) studies. Future research directions were also suggested.

PREFACE

The laboratory experimental data in Chapter 2 were obtained from Zhan Li and Hannah Kratky, who were MSc students supervised by Dr. Tong Yu at the University of Alberta. Their data were used for calibrating and validating the model proposed in Chapter 2.

The SWMM model in Chapter 3 was obtained from Arlette Fernandez who was a MSc. student supervised by Dr. David Zhu at the University of Alberta. The SWMM model was originally from the City of Calgary and used to simulate the proposed LID spatial allocation optimization system in Chapter 3.

All of the other parts of the thesis, including the numerical work in Chapters 2 and 3, the literature reviews in Chapters 2 and 3, the introduction in Chapter 1, and the conclusion in Chapter 4, are my own work. Partial content of Chapter 2 has been published in the following conferences:

- Yu, Y., Zhang, W., and Yu, T. (Oct, 2019). "Performance Evaluation of Bioretention Cells in Large Storm Events and Cold Climate using Numerical Modeling". Conference paper presented at *International Symposium on Sustainable Urban Drainage 2019*, Ningbo, Canada.
- Yu, Y., Zhang, W., and Yu, T. (Feb, 2020). "Modeling Rain Gardens in Cold Regions using HYDRUS 1D". Conference paper presented at *6th IAHR Europe Congress*, Warsaw, Poland.

There has been no previous publication of Chapter 3.

ACKNOWLEDGMENTS

Without the help and support of the following, I will be unable to accomplish this research. I would like to express my deepest gratitude to everyone of them.

First and foremost, I would like to express my gratitude to Dr. Wei (Victor) Liu, Dr. Tong Yu, and Dr. Evan Davies for taking the time to serve on my exam committee. I would like to express my gratitude to Dr. Wenming (William) Zhang, my supervisor, for his constant patience, guidance, support, and encouragement. I greatly appreciate your help with my academic work as well as your career planning advice.

Second, I would like to express my gratitude to Zhan Li, Hannah Kratky, and Dr. Tong Yu for sharing their valuable lab results and allowing me to do numerical simulations based on them. I really enjoy how patiently they offer extensive explanations and responses to my inquiries about their works.

I would like to express my gratitude to Arlette Fernandez for allowing me to use the SWMM model for the study area and Haibing Yan for clarifying any questions I had about it.

Finally, I would like to thank all of my friends and colleagues for making my graduate studies a wonderful experience and express my deepest appreciation to my mom and dad for their support and love.

Table of Contents

List of Tables

List of Figures

List of Algorithms

List of Appendix Context

Chapter 1 Introduction

1.1 Background

Urbanization is inevitable due to fast industrialization, commercialization, and economic and population growth worldwide (Martine and Marshall, 2007). In 2018, urban population reached 4.2 billion, i.e., approximately 55% of the global population lived in urban areas (United Nations, 2019). In Canada, about 72% of the population (27 million) lived in a census metropolitan area in 2020 and the total population is expected to reach 46.5 million by 2043 under the medium-growth scenario (Dimmell, 2021; Statistics Canada, 2021). When urbanization, impervious areas increase and result in considerable increases of peak flow and volume of urban surface runoff (Paul and Meyer, 2001). In addition to urbanization, climate change and global warming, have been increasing the frequency and severity of extreme weathers including heavy storm events, as well as the risk of urban flooding (Willems et al., 2012; Tabari, 2020). Furthermore, metropolitan areas experience urban heat island effect, which changes local weathers and increases urban flooding risks (Zhou, 2014; Kaspersen and Halsnaes, 2017; Miller and Hutchins, 2017). All of these factors have caused significant challenges for urban stormwater management system.

The conventional urban stormwater drainage system is mainly composed of underground pipes (minor system) and road surfaces (major system), which is designed to control water quantity and can be unreliable when storms exceed their design limits (Willems et al., 2012). Meanwhile, the conventional system has no control over the water quality of surface runoff, increasing the variety and quantity of contaminants and nutrients in downstream receiving water bodies such as rivers, lakes and oceans (Hatt et al., 2004; Zhou, 2014). Moreover, the grey infrastructure (underground sewers) is also costly in construction, monitoring, maintenance, rehabilitation and upgrades (Duffy

et al., 2008). These inherent drawbacks of the traditional urban stormwater drainage system, together with the challenges the traditional system has been facing, stimulated the concept of sustainable urban stormwater management.

As the key component of sustainable urban stormwater management, low impact development (LID) is a term used in North America to represent a green engineering approach that controls urban runoff at or close to the sources and uses natural-based solutions (Coffman, 2002a; HUD, 2003; Eckart et al., 2017). Typical LID-BMPs (best management practices) include bioretention, rain garden, permeable pavement, green roof, and etc. (US EPA, 2000). Review studies demonstrate the promising hydrological performance of LID-BMPs and their efficiency in pollutant removal (Dietz, 2007; Ahiablame and Engel, 2012; Eckart et al., 2017).

The benefit of LID is that it improves hydrological performance of an urban catchment by increasing the time of concentration, reducing the peak flow, and decreasing the volume of surface runoff (Hood et al., 2007; Dietz, 2007). For instance, in Guangzhou, China, a bioretention system with an area of 5% of the catchment reduced the peak flow and runoff volume by over 75% during small rainfall events (<10 mm rainfall depth) (Wang et al., 2021). Rain gardens have been shown to be quite effective at reducing rainfall runoff in residential areas, with a garden area covering 5% of the catchment reducing surface runoff from 80% to 94% (< 45 mm rainfall depth) (Tang et al., 2016). When rain depth ranges from 10 to 50 mm, a green roof system could reduce the peak flow by up to 80% (Pęczkowski et al., 2018). According to Alsubih et al. (2017)'s experiments in Edinburgh, permeable pavement could reduce total runoff volume by 40% to 92% (< 10.85 mm rainfall depth).

Meanwhile, bioretention and rain garden were reported to have the capacity of removing the loadings of TSS (total suspended solid) and heavy metals (Cu, Pb, and Zn) by over 80% (most sites > 90%), and removing total nitrogen by over 50% (Dietz, 2007; Ahiablame and Engel, 2012). Permeable pavement was reported to remove the loadings of TSS, heavy metal, and total nitrogen over 75%, 80%, and 75%, respectively (Dietz, 2007; Ahiablame and Engel, 2012). Green roof, on the other hand, demonstrated a wide range of performance in terms of nutrient and heavy metal removal, ranging from no significant retention to highly effective reduction (Ahiablame and Engel, 2012). In addition to the hydrologic and water quality benefits, LID reduces capital costs by 15 to 80% and mitigates urban heat island effect (Weitman et al., 2009; He et al., 2019). Mun-soo et al. (2021) found that LID-based pavement materials could reduce surface temperatures by 8.2 to 22.6°C when compared to dense-graded asphalt and performed significantly better at mitigating the urban heat island effect because of higher albedo, increased evaporation, and lower heat capacity.

During the last decade, LID studies have grown substantially, both in terms of experiments and numerical simulations, and in numerous areas including hydrological aspects, water quality, design optimization, and spatial allocation (Dietz, 2007; Elliott and Trowsdale, 2007; Ahiablame et al., 2012; Eckart et al., 2017; Spraakman et al., 2020). In the area of modeling single unit of LID, HYDRUS 1D, RECARGA, and GIF-MOD are considered as suitable tools for the design and optimization because of their abilities to model multiple layers of subsurface soil or porous media, surface ponding, water movement, vapor flow, root water uptake, and snow hydrology (Kaykhosravi et al., 2018). RECARGA is recommended only for estimation because of restricted options of soil types, numbers of soil layers, and boundary conditions (Kaykhosravi et al., 2018). For more accurate model calibration and flexibility in settings, GIF-MOD and HYDRUS 1D both

provide inverse modeling (auto parameter calibration) and customised soil media layers (can be > 3 layers) (Massoudieh et al., 2016; Kaykhosravi et al., 2018). Recent modeling studies established that HYDRUS 1D provides more flexibility in terms of soil structure, surface boundary conditions, underdrain options, and hydraulic flow model rather than SWMM in bioretention modeling, resulting in more accurate simulations (Liu and Fassman-Beck, 2017a, 2017b).

In the area of modeling LID spatial allocation, four modeling tools are available in the current market (HEC-HMS, MIKE Urban/MIKE+, SWMM, SWAT) that can provide stormwater management calculation and built-in LID control modules (Kaykhosravi et al., 2018). LID spatial allocation optimization (SAO) has been a huge challenge mainly due to its complex nature of the problem, which is the tradeoff between maximizing the benefits (e.g., water quantity and quality management) and minimizing the costs (Zhang et al., 2018), as well as due to the restrictions from space availability and public support. Generally, there are two types of spatial allocation optimization tools (SAOT) for LID (Zhang et al., 2018). The first one is compact optimization software (e.g., SUSTAIN) and the other one is model-algorithm integrated tools. As an example of a compact software package available on the market, SUSTAIN (the system for urban stormwater treatment and analysis integration), aggregates GIS, SWMM module, non-dominated sorting genetic algorithm (NSGA-II), Hydrological Simulation Program - FORTRAN (HSPF), and Microsoft Access database with graphical user interface (Lai et al., 2007; Shoemaker et al., 2009). The model-algorithm integrated tools are the ones that integrate a stormwater management model (e.g., SWMM) with a multi-objective evolutionary algorithm (MOEA) using a programming language as platform (e.g., MATLAB, Python) (Liu et al., 2017b; Xu et al., 2017; Zhang and Chui, 2018; Tao et al., 2019; Men et al., 2020; Dong et al., 2021). Rather than the traditional method of selecting the best scenario from some subjectively predefined scenarios of LID spatial allocation

plan, the model-algorithm integrated tools are capable of achieving near-optimal solutions (Zhang and Chui, 2018)

1.2 Knowledge gaps

In recent years, there has been significant knowledge advancement in terms of both experimental and numerical modeling and optimization of LID (Ahiablame et al., 2012; Eckart et al. 2017; Spraakman et al. 2020). Despite that, challenges and knowledge gaps still exist, which need to be studied to further understand, improve and optimize LID applications. This research focuses on the aspect of numerical modeling and optimization.

For bioretention, which is one of most commonly-used LID types and the focus of the first part of the thesis (Chapter 2), the knowledge gaps are as follows:

- There have been no studies on modeling the hydrologic performance of bioretention cells in cold climates, with consideration of preferential flow in soil media caused by freeze/thaw cycles.
- There is a paucity of literature on the modeling hydrologic performance of bioretention cells during large storm events (accumulative depth of a single event is greater than 50 mm).
- Most existing studies modeled either the hydrologic performance or the water quality improvement of bioretention cells. Limited studies integrated the modeling of both the two crucial aspects within one study mainly because of large amounts of time and effort required.

For LID spatial allocation optimization, which is the focus of the second part of the thesis (Chapter 3), the knowledge gaps are as follows:

- Relevant studies are limited, with only a small number of studies have been reported so far.

- There has been a lack of research on model-algorithm integrated tools that integrate a hydrology computing engine (e.g., SWMM, SWAT) with a classical multi-objective evolutionary algorithm (MOEA) using a programming language as platform (e.g., MATLAB, PYTHON).
- In previous studies, the original and non-modified code of MOEA (e.g., NAGA-II) was directly applied into LID spatial allocation problem, resulting in poor performance of the algorithm and lack of diversity in optimal solutions. No previous research, as far as the author know, has modified and adjusted MOEA to achieve a better performance in LID spatial allocation.

1.3 Objectives

This thesis uses numerical simulation as a tool to investigate and understand LID at different scales (single-unit scale and neighborhood scale) for urban stormwater management in cold regions such as Canada, and explore the potentials to improve the efficiency and performance of LID.

In the first part of the thesis (Chapter 2), the objectives of modeling single units of bioretention column are as follows.

- Select and use a model to examine single-unit bioretention columns of different configurations in terms of hydrologic performance for both small and large storm events. With calibration and validation of small storm events (1:2, 1:5 and 1:10 year), examine their hydrologic performance under larger storm events (1:25, 1:50 and 1:100 year).
- Simulate and examine the performance of the bioretention columns in winter snowmelt and spring runoff events, especially the effects caused by freeze/thaw cycles.
- Simulate pollutant removal of the bioretention columns, with a focus on nutrients.
- Explore potential measures to further improve the hydrologic performance of bioretention columns during large storm events in the context of climate change.

In the second part of the thesis (Chapter 3), the goals of building a new LID spatial allocation optimization (SAO) system are as follows.

- Build a new system that optimize the spatial allocation of LID implementations at neighbourhood scale, with the potentials to be adjusted depending on different project's particular situations and needs and to be further improved in the future.
- Examine the performance of the system with the new improvements of the optimization algorithm.
- Apply the new system to an urban neighborhood, and examine its performance. Select six optimal solutions for LID implementation during different storm events and evaluate their hydrologic benefits and costs under storm events of different return periods.
- Provide directions for the future improvements on the LID SAO system.

1.4 Thesis structure

This thesis is focusing on numerical modeling and optimizing of LID for cold regions. This thesis was written as paper-based, and it mainly includes two parts: Part I "Hydrologic and Water Quality Modeling of Bioretention Columns in Cold Regions" (Chapter 2 of the thesis); and Part II "LID Spatial Allocation Optimization System: Integrated SWMM with PICEA-g using MATLAB as the Platform" (Chapter 3).

Chapter 2 and 3 explores LID performances and optimizations at single-unit (micro) scale and neighborhood (macro) scale, respectively. The linkage between the two chapters is that Chapter 2 is the foundation for Chapter 3. This is because single-unit LID facilities constitute the

neighborhood LID system, and using reliable and optimized single-unit LID design, LID spatial allocation optimization can achieve further or greater hydrologic and water quality benefits. Chapter 1 above provides an overall introduction of this thesis and Chapter 4 summarizes this research work and provides suggestions on future research directions.

Chapter 2 Hydrologic and Water Quality Modeling of Bioretention Columns in Cold Regions

2.1 Introduction

Over the last few decades, increasing disturbance in land use due to urbanization has substantially changed urban hydrologic cycle and pollutant loading, causing significant impacts to aquatic environments (Rashid et al., 2018; Salerno et al., 2018; Freeman et al., 2019). Low impact development (LID) is a general term used in North America that describes a green engineering approach to achieve sustainable stormwater management in terms of both water quantity (peak and volume) and water quality (Coffman, 2002a; HUD, 2003; Eckart et al., 2017). LID facilities replace or complement the conventional storm sewer system and create a hydrologically functional landscape where runoff can be micromanaged and controlled within each LID system (Coffman, 2002b; Pour et al., 2020).

The bioretention system is one of the most recognized LID-BMPs (best management practices) for urban stormwater management (Davis et al., 2009). Bioretention captures stormwater runoff in a shallow depression treatment area, which typically consists of several layers, including ponding layer, organic or mulch layer, plants and planting soil layer, soil filtration media layer, and optional underdrain or drainage layer (US EPA, 2000; COE, 2014a; Liu et al., 2014). In recent years, bioretention has been used in more and more worldwide applications (Shrestha et al., 2018). Meanwhile, there is explosive growth in studies and research that tested bioretention's hydrologic performance and water quality treatment ability through laboratory and/or field experiments (e.g., Spraakman et al., 2020).

Bioretention has been demonstrated to significantly reduce runoff volume and peak and delay flow peak, for relatively small storm events (Davis, 2008; Hunt et al., 2008; Meng et al., 2014; Liu and Fassman-Beck, 2017a, 2017b; Shafique and Kim, 2017; Xia et al., 2018). However, limited tests and experiments have examined its hydrologic performance during large storm events, which is expected to decline when rainfall intensity increases and duration extends (Jackisch and Weiler, 2017; Sohn et al., 2019). Therefore, more efforts are required to evaluate and improve its performance for large storm events, particularly in the context of climate change that will induce more extreme rainfalls (with larger intensity and higher frequency) in the future (Sun et al., 2018; IPCC, 2021).

Bioretention has also been reported to be promising in reducing pollutants or improving water quality in recent studies (Davis, 2007; Passeport et al, 2009; Chapman and Horner, 2010; DeBusk and Wynn, 2011; Mangangka et al., 2015; Shrestha et al., 2018). Field and laboratory results illustrated that reduction rates of total suspended solids (TSS), total phosphorus (TP), total nitrogen (TN), heavy metals, and oil and grease were 54-99%, 28-85%, 32-97%, 74-99%, and greater than 90%, respectively (Hsieh and Davis, 2005a, 2005b; Davis et al., 2009). However, removal of dissolved nutrients can be highly variable, depending on the design configuration including vegetation, soil media amendments and the existence of internal water storage zone (IWS) (Hatt et al., 2009; Shrestha et al., 2018). More water quality studies are needed to examine the effectiveness of different configurations of bioretention.

In cold regions, bioretention has been insufficiently studied in terms of both hydrologic performance and pollutant removal, particularly the effects of freeze-thaw cycles (Kratky et al., 2017; Ding et al., 2019). In cold climates, soil infiltration rate is the key parameter that affects bioretention performances (Muthanna et al., 2008). When the soil temperature is below -0.5°C,

sandy loam soil becomes frozen and impermeable (Watanabe and Osada, 2017), and pore ice (frost) formed by frozen moisture blocks the soil pores and therefore reduces soil hydraulic conductivity (Flerchinger et al., 2005). Watanabe and Osada (2017) found that hydraulic conductivity of soil increased exponentially with higher unfrozen water content when the soil temperature rose from -0.5°C to -0.2°C; and it reached a constant value when the temperature was higher than -0.2°C until 0°C, which is greater than the estimated hydraulic conductivity of unfrozen soils. In the field experiments conducted by Roseen et al. (2009) in New Hampshire, US, and by Khan et al. (2012) in Calgary, Canada, bioretention maintained similar hydrologic performance during winter season when soil was partially frozen compared to that during summer season. However, some other filed studies indicated that the hydrologic performance declined with average peak flow reduction from 42% in summer to 27% in winter (partially frozen) (Muthanna et al., 2008) and approximately 80% soil infiltrability reduction after freezing (frost depth of 45 cm) (Al-Houri et al., 2009). Different factors of soil media, vegetation, snow accumulation, inflow pattern, freeze-thaw cycle frequency, preferential flow and others could contribute to the varieties of bioretention performance in cold climates, which lacks mechanism-oriented explanation (Ding et al., 2019).

Freeze-thaw cycles are frequently encountered when days are warm and nights are cold in cold regions. For example, in the City of Edmonton, Canada, the average freeze-thaw cycles are 12-18 per month in March, April, October, and November (Edmonton weather nerdery, 2019). Frequent freeze-thaw cycles can bring challenges and changes to the stability and performance of bioretention (Ding et al., 2019). For example, Wang et al. (2015) discovered that silty soil with different degrees of compactness experienced different levels of deformation and changes of strength property after repeated freeze-thaw cycles.

Another common challenge that bioretention is facing in cold regions is water quality concerns due to high concentrations of sodium chloride in runoff resulted from the use large amounts of road de-icing salts (Fay et al., 2019), which brings issues such as plant health and media clogging (Denich et al., 2013). Such inflow of high salts into bioretention during snowmelt and spring runoff events can increase effluent phosphorus concentration and consistent release of high concentrations of sodium and chloride in the spring season (Denich et al., 2013; McManus and Davis, 2020; Goor et al., 2021). One of the most significant concerns on bioretention is its long-term performance (Liu et al., 2014; Kratky et al., 2017) and it has been inadequately studied (Spraakman et al., 2020). Clogging can also be a common issue that reduces bioretention's hydraulic capacity, which had been observed with a decreasing factor of 3.6 over 72 weeks in a laboratory study conducted by Le Coustumer et al. (2012).

There are numerous models for bioretention such as MOUSE, SWMM, MUSIC, HEC-HMS, SWAT, and L-THIA-LID. These models are used typically for large-scale stormwater management and therefore more suitable for preliminary and conceptual designs of LID (Elliott and Trowsdale, 2007; Kaykhosravi et al., 2018). RECARGA, HYDRUS 1D and GIF-MOD are considered as suitable tools in Kaykhosravi et al.'s review (2018) for the design and optimization of single-unit bioretention because of their abilities to model multiple layers of subsurface soil or porous media, surface ponding, water movement, vapor flow, root water uptake, and snow hydrology. RECARGA is recommended only for estimation because of its restrictions, including pre-specified soil types, the maximum number of three soil layers, non-definable boundary conditions, and fixed underdrain location (Kaykhosravi et al., 2018). HYDRUS 1D and GIF-MOD are both capable of modeling customized soil media layers (can be > 3 layers), solute transport through soil columns, and features with inverse modeling (auto parameter calibration) for more

convenient and accurate model calibration. DRAINMOD is also used to model bioretention hydrologic performance (Brown et al., 2013; Winston et al., 2016), but its minimum temporal resolution is hours and therefore modeling a single storm event is restricted (Skaggs et al., 2012). Lisenbee et al. (2020) introduced DRAINMOD-Urban to allow high temporal resolution.

Recent modeling studies from 2011 to 2021 on bioretention columns are summarized in Table 2.1, which shows that 50% (5/10) of them used HYDRUS 1D, 20% used SWMM, 20% used DRAINMOD, and 10% used 2D variable saturated flow model. Liu and Fassman-Beck (2017a, 2017b) conducted numerical simulations using HYDRUS 1D and SWMM, and illustrated that HYDRUS 1D has better accuracy for modeling single unit of bioretention. In fact, HYDRUS 1D provides more flexibility of soil structure, surface boundary conditions, underdrain options, and different hydraulic models for flow routine rather than built-in LID module in SWMM. Meng et al. (2014) and Jiang et al. (2019) employed HYDRUS 1D to simulate the hydrologic performance of bioretention and obtained an R^2 value of over 0.70 for the outflow hydrograph. HYDRUS 1D was also used in Li et al. (2018, 2021) to simulate removal of nutrients and heavy metals in bioretention by comparing the water quality benefits with different types of soil amendments. In other publications (e.g., Brown et al., 2013; Lisenbee et al., 2020), DRAINMOD and other tools have shown their limitations in modeling single unit bioretention (e.g., limitations of time scales, boundary conditions, auto-calibration capacities, soil structure, etc.). With the overall good performance in hydrologic processes and pollutants removal, as well as its capacity to model heat transport (Xiang et al., 2012), HYDRUS 1D appears to be promising for modeling bioretention in cold regions.

Among these recent studies, no modeling studies have been reported on hydrologic performance of bioretention in cold regions when the soil temperature is near to or lower than 0 °C, nor has

there been any discussions on the existence of preferential flow due to freeze-thaw cycles. Moreover, of these studies, only Lisenbee et al. (2020) simulated rainfall events with depth larger than 50 mm using DRAINMOD-Urban, but their rainfall event lasted for days to accumulate such depth. There have been no modeling studies reported on a single large storm event within a short period (e.g., > 50 mm in a few hours) to assess the hydrologic performance of bioretention columns and to investigate the ponding situation. In addition, of these studies, only Li et al. (2018, 2021) carried out simultaneous modeling of hydrologic performance and water quality for bioretention, however, no outflow and surface ponding hydrographs were simulated.

To address the knowledge gaps mentioned above for cold region bioretention columns, this study selected HYDRUS 1D as the modeling tool to: 1) calibrate and validate the hydrologic performance during small storm events using laboratory data; 2) evaluate the hydrologic performance during large summer storm events (with rainfall depth > 50mm) and explore the design optimization of bioretention to further improve its performance; 3) reveal the hydrologic performance in cold climates including snowmelt and spring runoff events, as well as examine the influence of freeze-thaw cycles; and 4) simultaneously simulate the nutrients removal and the hydrologic performance. The findings from the simulation results will help better understand bioretention in cold regions in the context of climate change for urban flood mitigation and water quality improvement.

Table 2.1 Summary of recent numerical studies on bioretention columns

Study	Model	Modeling Layer	Rain Events/Inflows	Hydraulics Outflows	Water Quality Modeled	Ponding	Expt. for Model Calibration	Comments
This study	HYDRUS 1D	Ponding, Plant soil, Soil layer, Gravel	Design storms: 1:2, 1:5, 1:10, 1:25, 1:50, 1:100 yr Rainfall depth: 24, 35, 43, 56, 69, 84 mm Duration: 4 hrs, Chicago Also snow melt &spring runoff events CA/SA: 10	Expt.: Free drainage & IWS (Internal water storage) Model: Free drainage & IWS	NO2-N, NO3-N, NH3-N, TP, Cl	Ponding observed. Simulated results close	Lab	1. Accurate calibration & validation for summer rainfall 2. Also modeling for snowmelt & spring runoff events 3. HP1 was used for nutrient removal simulation
Li et al., 2021	HYDRUS 1D	Ponding, Plant soil, Soil layer, Gravel	Design storms: 1:2 & 1:5 yr Rainfall depth: 25 & 34 mm Duration: 120 min CA/SA: 17	Expt.: Free drainage & IWS Model: Free drainage & IWS	COD, NO3-N, NH3-N, TN, TP, Cu, Zn, Cd	None	Lab	Able to simulate pollutants removal with adding amendments
Lisenbee et al., 2020	DRAINMOD-Urban	Ponding, Soil layer, Gravel	Local storms Rainfall depth: 5 -97mm Duration: N/A CA/SA: 19.8	Expt.: IWS Model: Free drainage	None	None	Field	1. Accurate calibration and validation for single event 2. Time scale: 1 min 3. Need manual calibration
Jiang et al., 2019	HYDRUS 1D	Ponding, Plant soil, Soil layer, Gravel	Design storms: 1:2 & 1:5 yr Rainfall depth: 25 & 34 mm Duration: 120 min CA/SA: 17	Expt.: Free drainage & IWS Model: Free drainage	None	None	Field	No comprehensive calibration and validation
Li et al., 2018	HYDRUS 1D	Ponding, Plant soil, Soil layer, Gravel	Design storms: 1:2 & 1:5 yr Rainfall depth: 25 & 34 mm Duration: 120 min CA/SA: 17	Expt.: Free drainage & IWS Model: Free drainage	COD, NO3-N, NH3-N, TN, TP	None	Field	1. Conduct nutrients removal simulation 2. No comprehensive calibration & validation
Gülbaz and Kazezyilmaz-Alhan, 2017	RWB (Improved Green-Ampt method) & SWMM	Ponding, Plant soil, Soil layer, Gravel	Design storms Rainfall depth: 4,8,11,17 mm Duration: 15,20,25,30 min CA/SA: 20	Expt.: Free drainage Model: Free drainage	None	Ponding observed. Simulated results close	Field	1. RWB had better simulation results than SWMM 2. SWMM did not match peak flow 3. Both RWB and SWMM simulation did not match measured outflow after peak

Liu and Fassman-Beck, 2017a	SWMM	Ponding, Soil layer, Gravel	Design storms: 1:2 yr Rainfall depth: 13 mm Duration: 1 hr CA/SA: 43	Expt.: Free drainage & IWS Model: Free drainage	None	N/A	Lab	The simulation was not accurate
Liu and Fassman-Beck, 2017b	HYDRUS 1D	Ponding, Soil layer, Gravel	Design storms: 1:2 yr Rainfall depth: 13 mm Duration: 1 hr CA/SA: 20	Expt.: Free drainage Model: Free drainage	None	N/A	Lab	Accurate calibration & validation
Meng et al., 2014	HYDRUS 1D	Ponding, Soil layer, Gravel	Local storms & Design storms Rainfall depth: N/A Duration: N/A CA/SA: 10	Expt.: Free drainage Model: Free drainage	None	Ponding observed and simulated only for design storms Duration: 180 mins Max.: 12 cm	Field	Accurate calibration & validation
Brown et al., 2013	DRAINMOD	Ponding, Soil layer, Gravel	Local storms Rainfall depth: 2.5 ~ >38 mm Duration: N/A CA/SA: 14 & 16	Expt.: Free drainage & IWS Model: Free drainage & IWS	None	Ponding and overflow observed	Field	1. Modelled long term hydrological performance 2. Not suitable for single rainfall event due to time scale limitation
He and Davis, 2011	2D variable saturated flow model (Richards equation)	Ponding, Soil layer, surrounding gravel soil	Local storms Rainfall depth: 2.5 - >25 mm Duration: 2-24 hr CA/SA: 20	Expt.: Free drainage Model: Free drainage	None	N/A	Field	1. Discussed the influence of types of soil media & surrounding soil. 2. No validation.

2.2 Numerical Modeling for Bioretention in Cold Regions

2.2.1 Model introduction

HYDRUS 1D simulates one-dimensional movement of water, heat, and solute transport in variably-saturated porous media (Simunek et al., 2005). The governing equation is a modified form of the Richards equation with assumptions of negligible influence of air phase and thermal gradient in water flow (Simunek et al., 2005):

$$\frac{\partial \theta(h)}{\partial t} = \frac{\partial}{\partial z}\left[K(h)\left(\frac{\partial h}{\partial z} + cos\alpha\right)\right] - S \qquad (2.1)$$

where θ is the soil moisture content [L^3/ L^3], t is time [T], z is the vertical direction spatial coordinate [L], h is the water pressure head [L], and α is the angle between the vertical direction and the flow direction. K is the unsaturated hydraulic conductivity of soil media [L/T] and is a function of h and z:

$$K(h, z) = K_s(z)K_r(h, z) \qquad (2.2)$$

where K_r is the relative hydraulic conductivity [NA], and K_s is the saturated hydraulic conductivity of soil media [L/T].

2.2.1.1 Soil properties

Soil moisture content and hydraulic conductivity of unsaturated soil are highly dependent on water pressure head as shown in Eq.2.1. Van Genuchten (1980) functions were commonly used to describe unsaturated soil hydraulic properties of soil media:

$$(h) = \begin{cases} \theta_r + \dfrac{\theta_s - \theta_r}{[1 + |\alpha h|^n]^m} & h < 0 \\ \theta_s & h \geq 0 \end{cases} \tag{2.3}$$

$$K(h) = K_s S_e^l [1 - (1 - S_e^{\frac{1}{m}})^m]^2 \quad where, m = 1 - \frac{1}{n}, n > 1 \tag{2.4}$$

$$S_e = \frac{\theta - \theta_r}{\theta_s - \theta_r} \tag{2.5}$$

where θ_r and θ_s are residual and saturated water contents, respectively [L^3/ L^3], α is the inverse of the air-entry value (also called bubbling pressure) [1/L], n is a pore-size distribution index, l is a pore-connectivity parameter. θ_r, θ_s, α, n, and K_S are the five hydraulic parameters that need to be calibrated and validated.

A dual-permeability type flow is used to describe and simulate preferential flow, which involves two mobile regions of matrix and macropores (fracture) (Simunek et al., 2005). The importance of preferential flow must be recognized when the soil column is subjected to prolonged operation, particularly after freeze-thaw cycles. HYDRUS-1D implemented the approach of Gerke and van Genuchten (1993, 1996) and flow equations for the two pore regions:

$$\frac{\partial \theta_f(h_f)}{\partial t} = \frac{\partial}{\partial x}\left[K_f(h_f)\left(\frac{\partial h_f}{\partial x} + cos\alpha\right)\right] - S_f(h_f) - \frac{\Gamma_w}{w} \tag{2.6}$$

$$\frac{\partial \theta_m(h_m)}{\partial t} = \frac{\partial}{\partial x}\left[K_m(h_m)\left(\frac{\partial h_m}{\partial x} + cos\alpha\right)\right] - S_m(h_m) - \frac{\Gamma_w}{1 - w} \tag{2.7}$$

where w is the ratio of macropore (fracture) volume and total soil system, Γ_w is the transfer rate for water from one region to the other, and subscript f represents fracture region and subscript m represents matrix.

2.2.1.2 Heat transport

To model bioretention in cold climate, heat transport needs to be considered, which is expressed as a convection-dispersion equation when vapor transport is negligible:

$$\frac{\partial C_p(\theta)T}{\partial \mathrm{t}} = \frac{\partial}{\partial z}\left[\lambda(\theta)\frac{\partial T}{\partial z}\right] - C_w q\frac{\partial T}{\partial z} - C_w ST \tag{2.8}$$

where $\lambda(\theta)$ is the coefficient of apparent thermal conductivity of soil media [ML/T^{3}K], $C_p(\theta)$ is the volumetric heat capacity of the porous medium [M/LT^{2}K], and C_w is the volumetric heat capacity of the liquid phase [M/LT^{2}K]. The three terms on the right-hand side represent heat flow due to conduction, heat transported by flowing water, and energy uptake by root water uptake, respectively.

The apparent thermal conductivity $\lambda(\theta)$ can be expressed as:

$$\lambda(\theta) = \lambda_0(\theta) + \beta_t C_w|q| \tag{2.9}$$

$$\lambda_0(\theta) = b_1 + b_2 + b_3\theta^{1/2} \tag{2.10}$$

where $\lambda_0(\theta)$ is the thermal conductivity of the porous medium without flow and macrodispersivity [ML/T^{3}K], β_t is the thermal dispersity [L]. The Chung and Horton (1987) equation (Eq. 2.10) was used to describe the thermal conductivity and b_1, b_2, and b_3 are empirical parameters [ML/T^{3}K].

2.2.1.3 Solute transport

In this paper, HP1 (coupled HYDRUS 1D and PHREEQC) (Parkhurst and Appelo, 1999) was used for solute transport modeling. Chemical reactions between different pollutants used in the model can be found in PHREEQC database. PHREEQC biogeochemical code simulates chemical reactions and transport which is based on a finite equation of 1D flow path of solution transport:

$$\frac{\partial C}{\partial t} = -v\ \frac{\partial C}{\partial z} + D_L\ \frac{\partial^2 C}{\partial z^2} -\ \frac{\partial q}{\partial t} \tag{2.11}$$

where C is the solute concentration in water, t is time, v is the pore water flow velocity, D_L is the hydrodynamic dispersion coefficient, and q is the concentration in the solid phase. The three terms on the right side represent solute advection, dispersion and chemical reactions respectively.

2.2.2 Experiments for model calibration and validation

Li (2019) and Kratky (2019) at the University of Alberta, Canada, conducted laboratory experiments of four bioretention columns. The columns were typical bioretention cells, which consisted of vegetation and mulch layer at the top, topsoil with organic matters as plant soil, middle soil media layer, gravel layer, and underdrain, as shown in Figure 2.1. Outflow pipes of all the four bioretention columns were located at the bottom of the columns. Columns 1-2 used free drainage as the underdrain method all the time. Columns 3-4 had IWS (Internal water storage) zone to create an anoxic zone to promote denitrification in summer, and used free drainage (no IWS) in winter or spring. Two types of classical soil media were used in their experiments. Soil media A was a less porous soil matrix, a loam typically used in local (Edmonton, Canada) landscaping. Soil B is a more porous soil matrix which is a sandy loam.

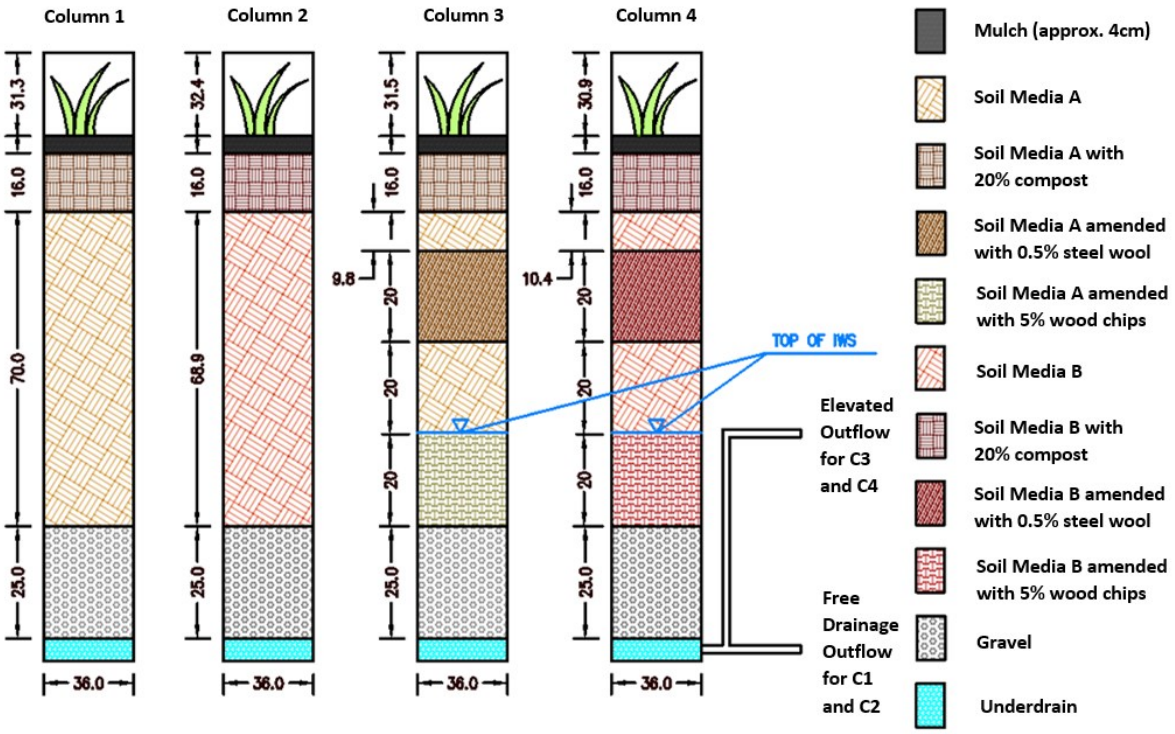

Figure 2.1 Experiment setup of bioretention columns (Li, 2019). Free drainage criteria applied for columns 1 and 2 all the time, and columns 3 and 4 during winter operations. Elevated outflow criterion with 45 cm IWS applied for column 3 and 4 during summer.

Preliminary tests (falling head tests) were first conducted in Columns 1 and 2, which was equivalent to approximately one year of precipitation in the local municipality (Edmonton, Canada). The formal experiments consisted of five stages of operation, which was equivalent to 1.6 years of typical precipitation in Edmonton: 1) Year 1 summer small storm events; 2) Year 1 winter snowmelt events; 3) Year 1 spring runoff events; 4) Year 2 summer small storm events; and 5) Year 2 summer larger storm events (Kratky, 2019). All storm events were conducted weekly to bring bioretention columns back to air dry state, and target contaminants were added (as shown in Appendix Table A2.1) into the stormwater to imitate pollutants in actual runoff. The four bioretention columns experienced a "mature" period in Year 1, which became stable in Year 2 (Li, 2019).

During the first stage (Year 1 summer), nineteen 1:2 year storm events (22.6 mm precipitation per event) were applied to the columns, followed by four snowmelt events in the second stage (Year 1 winter). Two snowmelt tests were conducted on frozen columns where the soil was fully frozen and the room temperature was -20 ℃, and two snowmelt tests were on thaw columns where the soil temperature was around -0.3 °C and the room temperature was 1 °C. After the snowmelt events, two spring runoff events in the third stage (Year 1 spring) were conducted. The first spring event was a first flush event with high concentration of salts (see Table A2.1), inflow rate of 5.8mL/min, and low volume of water (9.8 mm) in 29 hours, but the outflow hydrograph was not recorded. The second spring runoff event was a major melt of packed snow with lower concentration of salts (see Table A2.1), inflow rate of 14 mL/min, and a high volume of water (39.3mm) in 40 hours. During the fourth and fifth stages (Year 2 summer), five 1:2 year storm events were conducted, followed by one 1:5 storm event (37.3 mm precipitation) and one 1:10 year storm event (45.2 mm precipitation) (Li, 2019). In all the experiments, rainfall events were designed using the 4-hr Chicago distribution according to IDF curves in the City of Edmonton Drainage Design and Construction Standards (COE, 2014b). Detailed rainfall intensity with time for the rainfall events is provided in Appendix Table A2.2. The catchment area to surface area (CA/SA) ratio in the experiments was assumed to be 10, and the catchment area was assumed to be 100% impervious.

The experimental data of Li (2019) and Kratky (2019) were used for the HYDRUS 1D modeling in this study. Specifically, the observed outflow rate and ponding depth of all the four columns during Year 1 winter and Year 2 summer were used for model calibration and validation of hydrologic performance in this study. The inflow pollutant concentrations, leaching test results of soil media, and outflow pollutant loading of Columns 1 -2 during Year 2 summer were used for the water quality modeling in this study.

2.2.3 Model setup

2.2.3.1 Hydrologic modeling for summer storm events

One of five 1:2 year storm events tested in Year 2 was selected for model calibration on hydraulic parameters, because the hydrologic performance of the bioretention columns was more stable and mature in Year 2 (Li, 2019). A schematic diagram of calibration process using HYDRUS 1D is shown in Figure A2.1 in the Appendix. The calibrated parameters in 1:2 year storm event were then applied to 1:5 and 1:10 year storm events for model validation, assuming these parameters are transferable to larger storm events. After validations, the calibrated soil hydraulic parameters were applied for large storm events, including 1:25, 1:50, and 1:100 storm events, to test bioretention columns' hydrologic performance under extreme conditions. Note that, in this modeling study, no overflow was considered for all the four columns during large storm events to better quantify the resultant flooding (surface ponding) of the columns.

HYDRUS 1D uses a Marquardt-Levenberg type of parameter optimization algorithm for inverse estimation of soil hydraulic, heat or solute transport parameters, and a maximum of fifteen parameters can be calibrated at one time. In this study, the initial values of θ_r, θ_s, α, and n were referred to Carsel and Parrish (1988) who summarized unsaturated hydraulic parameters for different soil classifications using van Genuchten (1980) model. The initial guess of *Ks* was taken from Clapp and Hornberger (1978) whose average values of saturated conductivity were higher than Carsel and Parrish (1988)'s estimations, and the selection was based on the falling head test conducted in Li (2019) and Kratky (2019)'s experiments. Specifically, for the topsoil layer, the initial guesses of θ_r, θ_s, α, *n, and Ks* of topsoil were all larger than those for the middle soil media layer because the compost added in topsoil increases effective friction angle, saturated hydraulic

conductivity and water content (Duzgun et al., 2021). Due to the high deviation of each parameter (Carsel and Parrish, 1988) and uncertainties in the changes of soil properties caused by winter freeze-thaw cycles, this study tested a wide range of the five parameters. The initial values of soil's *Ks* and their testing ranges of topsoil and middle soil media are written as Table A2.3.

Gravel layer has very high hydraulic conductivity and sharp infiltration front, so it can turn into a dry state instantaneously making simulation unstable (Steffen, 2012). To stably simulate the gravel layer, this study adopted the method of Filipović et al. (2014), which employed hydraulic parameters of sand with higher *Ks* to replicate gravel layer behaviour in the model. In Columns 3 and 4, the gravel layer does not affect the outflow hydrograph because the entire gravel layer was submerged and saturated during a rainfall event as a result of the 45-cm anoxic zone (IWS zone) at the bottom. For Columns 3 and 4, the hydraulic conductivity of the gravel layer was set as a large value (1 cm/min) to achieve stable outflow hydrographs, because a small value would develop instability in model output (see Figure A2.2 in the Appendix).

Sensitivity analysis was conducted for the calibrated hydraulic parameters with one unit increment (depending on its highest order of decimal) and 10% increment of original value for one parameter while keeping the other four parameters unchanged. Percentage change of the peak outflow was used as the index to sort parameters' sensitivities. Using Column 1 as an example, the results indicate that *Ks* of the middle soil layer is the most sensitive parameter, followed by α and *n* of the middle layer (Table 2.2). The rest of parameters of both layers are not sensitive. The 70-cm middle soil layer's hydraulic parameters are dominant comparing to those of the 16 cm top planting soil layer for all four columns, which demonstrates the important role of the middle soil layer in bioretention.

Table 2.2 Sensitivity test of hydraulic parameters, using Column 1 as an example. The objective was to evaluate the change in peak outflow due to the change of one parameter while maintaining all other four parameters the same.

Soil	Index	Q_r	Q_s	α (1/cm)	n	K_s (cm/min)
	Increments	+0.01	+0.1	+0.01	+0.1	+0.01
Topsoil	Change in peak outflow	0.11%	-1.14%	-0.07%	-0.17%	0.16%
Middle Layer		0.03%	-0.34%	3.71%	2.34%	20.03%
	Increments	-10%	-10%	-10%	-10%	-10%
Topsoil	Change in peak outflow	-0.07%	0.59%	0.04%	0.44%	-0.46%
Middle Layer		-0.01%	0.13%	0.80%	-5.10%	-9.13%

2.2.3.2 Hydrologic modeling for winter snowmelt and spring runoff events

Soil experience compaction and expansion in cold climates, and soil hydraulic parameters would significantly change after few freeze-thaw cycles. Therefore, calibration of soil hydraulic parameters was required for snowmelt events, and then calibrated parameters were validated in spring runoff event. The soil hydraulic parameters were calibrated for cold condition using one thaw test because only this test recorded the soil temperature (-0.3°C) and room temperature (2-3°C), which are needed for the model. The parameters were validated using the second spring runoff event for the same reason. Due to the similarity between Columns 1-2 and Columns 3-4 under cold climate, only the modeling results of Columns 1-2 are presented in this study.

To examine the possibilities on the existence of preferential flow due to freeze-thaw cycles, the dual-permeability model was applied to the winter snowmelt and spring runoff events. Soil hydraulic parameters for dual-permeability model were referenced from Simunek et al. (2003) for

the fracture region (θ_{rf}= 0.0, θ_{sf}= 0.5, $\propto_f$=0.1 cm^{-1}, n_f=2.0, l=0.5, k_{sf}=1.5cm/min) and the matrix-fracture interface (β= 3, γ=0.4, a=1.0 , l=0.5, k_{as}=7x10^{-6} cm/min). w, the ratio between the volumes of the macropores or fracture domain and the total soil system, was calibrated manually for these events.

2.2.3.3 Water quality modeling

The water quality modeling focused on free drainage scenario (Columns 1-2) and nutrients (chloride, phosphate, nitrate, nitrite, and ammonium). The modeling was conducted for 1:2 year storm events in the second summer, because soil became more mature than Year 1 and hydraulic properties had been calibrated and validated. Results from the soil leaching experiment was used to describe pollutants contained inside the columns. Pollutant concentration of runoff and that contained in the bioretention column were inputs for the model (Table 2.3). The equilibrium phase of halite (NaCl) was added to the model to simulate the saturation state of chloride that existed in soil columns after winter operation with high salt concentration inflow.

Table 2.3 Pollutant concentrations in the soils (based on the leaching test) and in the rainfall/inflow (The unit is mmol/kgw, except for CEC (Cation Exchange Capacity) that uses meq/100g) (Kratky, 2019).

Pollutants	Inflow	Compost	Soil A	Soil A with 20% compost	Soil B	Soil B with 20% compost
NH_4^+	0.111	0.013	0.019	0.042	0.007	0.014
NO_3^-	0.024	0.045	0.740	3.518	0.034	0.731
NO_2^-	0.011	0.231	2.233	10.242	0.176	2.189
PO_4^-	0.021	0.001	0.070	0.348	0.001	0.070
Cl^-	0.534	0.094	0.279	1.020	0.044	0.239
K^+	0.045	0.046	0.810	3.866	0.035	0.801
Na^+	0.434	0.311	2.493	11.220	0.213	2.415
CEC	N/A	16.0	12.0	25.0	17.8	14.6

2.2.3.4 Initial and boundary conditions

In HYDRUS 1D, initial conditions can be either water content or pressure head. In our model, the initial pressure head was assigned to describe bioretention columns as air dry at the starting point. Bioretention columns were designed to be able to handle ponding at top to retain surface runoff. The upper boundary condition was set to be "atmospheric boundary condition with surface layer", which allows water to build up on the surface. Columns 1-2 have outflow pipes under the gravel layer while Columns 3-4 have elevated outflow pipes (see Figure 2.1). Because gravel has nonlinear hydraulic properties and sharp infiltration front, I assigned "free drainage" for Columns 1-2 and "seepage face h = 45 cm" for Columns 3- 4 as lower boundary conditions. "Free drainage" is a zero-gradient boundary condition that describes a freely draining soil profile, and "seepage face" indicates boundary flux that will be triggered when the pressure head reaches a given value.

2.2.3.5 Model evaluation

Two statistical measures, R-Squared for regression (R^2) and Root Mean Square Weighted Error (RMSE) were used in HYRUDS 1D to evaluate the fitness of the simulated results compared to the experimental data.

$$R^2 = \frac{\left[\sum w_i f_i y_i - \frac{\sum f_i \sum y_i}{\sum w_i}\right]^2}{\left[\sum w_i {f_i}^2 - \frac{(\sum f_i)^2}{\sum w_i}\right]\left[\sum w_i {y_i}^2 - \frac{(\sum y_i)^2}{\sum w_i}\right]} \quad (2.10)$$

$$\mathrm{RMSE} = \sqrt{\frac{\sum_{i=1}^{j} w_i (f_i - y_i)}{j}} \quad (2.11)$$

where w_i is the weight factor, f is the predicted value and y is the observed data, j is the total number of observed data. Weight factors were assumed to be 1 for all observed data.

2.3. Modeling results and discussion

2.3.1 Hydrologic model calibration and validation

Calibration results for 1:2 year storm event are shown in Figure 2.2 and Calibrated soil hydraulic parameters of four bioretention columns are provided in Table 2.4. R-squared (R^2) between the simulated outflow hydrograph and experimental data were 0.92, 0.96, 0.97, and 0.84 for Column 1, 2, 3 and 4, respectively, and RMSE were 0.06, 0.04, 0.07, and 0.13 mL/min, respectively. Meng et al. (2014) calibrated two bioretention cells' hydrologic performance using field results during natural rainfall, and R^2 were 0.76 and 0.61 for the two cells. Despite the overall good performance of the model, there were also some discrepancies. Simulated outflow hydrograph did not catch a few observed peak points for Columns 1-2. The peak outflow observed in Columns 1-2 were 94 and 210 ml/min, while the simulated peaks were 71.3 and 189.4 ml/min. The possible reason for such discrepancy is that: after one year of operation particularly the freeze-thaw cycles in winter and the use of high concentration of contaminants in spring runoff events, the soil media could have experienced the expansion, compaction, and clogging, potentially forming fractures and preferential flow paths inside the soil column. In Column 4, a sudden drop of simulated outflow occurred at around 210 min while the observed outflow showed a smooth decrease. The sudden drop of outflow occurred when the simulated ponding diminished which resulted in negative surface water pressure. The smooth decrease observed in experiments indicated that water was contained in the soil column after ponding ended. In addition to accelerating outflow, preferential

flow can also constrain outflow by retaining water in macropores and blocking flow paths in fractures (Allaire et al., 2009).

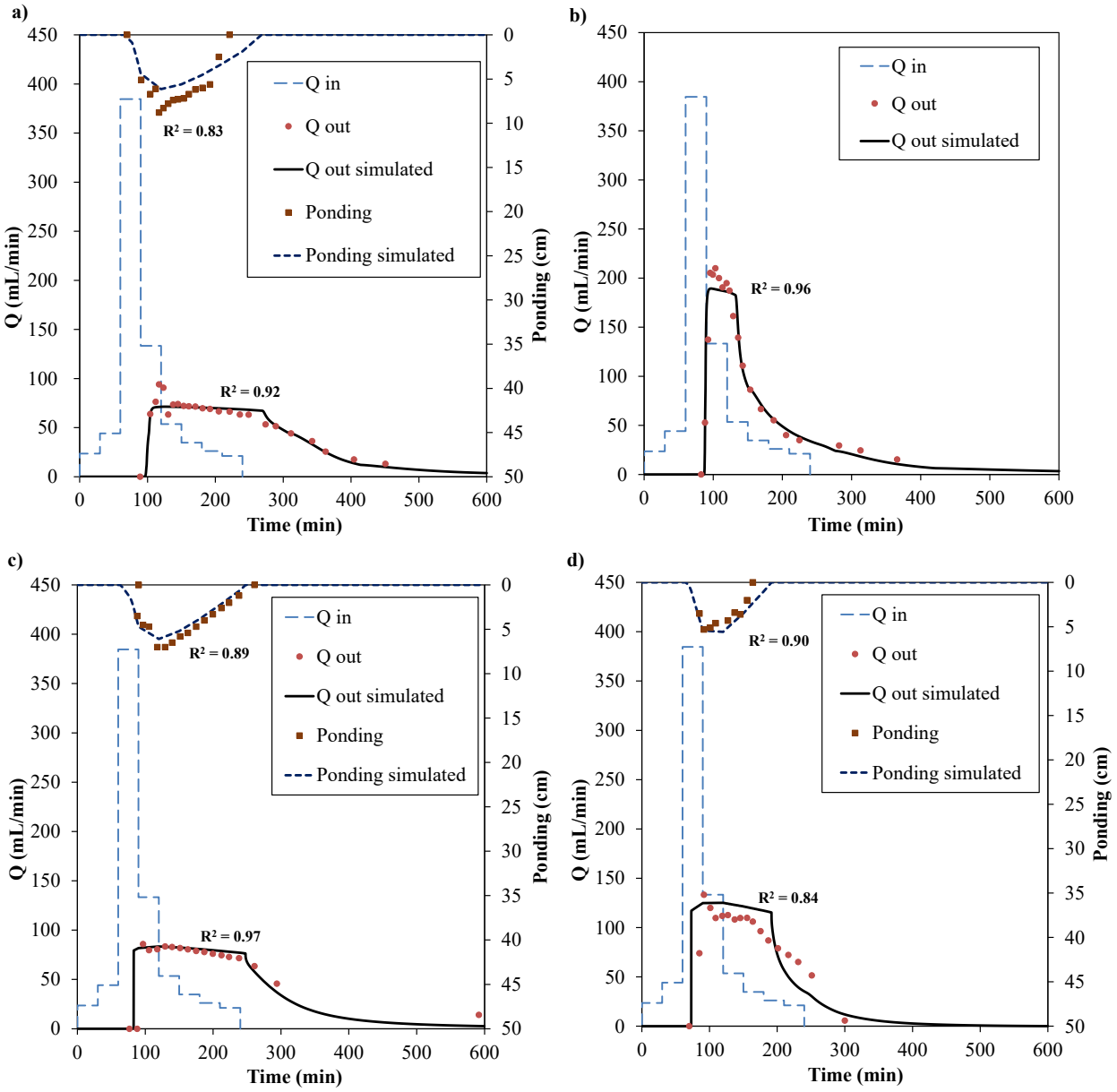

Figure 2.2 Model calibration on outflow hydrograph and ponding depth for the four bioretention columns in 1:2 year storm event in summer: a) Column 1, b) Column 2, c) Column 3, and d) Column 4. Note that no ponding was observed in both the experiment and simulation of Column 2.

Table 2.4 Calibrated hydraulic parameters of the four bioretention columns in summer

Column	Soil Layer	Q_r	Q_s	α (1/cm)	n	K_s (cm/min)
1	Top Layer	0.067	0.519	0.051	1.902	0.247
	Middle Layer	0.041	0.398	0.003	1.737	0.044
	Gravel	0.005	0.42	0.12	2.5	750
2	Top Layer	0.09	0.52	0.029	1.726	0.282
	Middle Layer	0.066	0.42	0.005	1.511	0.154
	Gravel	0.005	0.42	0.12	2.5	400
3	Top Layer	0.033	0.526	0.06	1.917	0.224
	Middle Layer	0.021	0.41	0.01	1.867	0.089
	Gravel	0.005	0.42	0.12	2.5	1
4	Top Layer	0.045	0.5	0.028	1.844	0.219
	Middle Layer	0.033	0.46	0.007	1.656	0.144
	Gravel	0.005	0.42	0.12	2.5	1

Surface ponding was observed in Columns 1, 3 and 4. R-squared (R^2) between the simulated ponding and experimental data were 0.83, 0.89, and 0.90 for these columns, respectively, and RMSE was 0.300, 0.115, and 0.180 cm. The simulated ponding depth of Columns 3 and 4 fitted well with observed values. For Column 1, the maximum simulated ponding depth was 6.1 cm, slightly lower than the maximum observed ponding of 8.4 cm; and the simulated ponding duration was approximate 3 hours, which was 30 min longer than the observed data. Overall, based on both outflow hydrograph and ponding depth, the simulated results are reliable and satisfactory.

2.3.2 Hydrologic Performance Validation

Model validation for 1:5 and 1:10 year storm events are shown in Figure 2.3 and Figure 2.4. R^2 between the observed and simulated outflows were 0.82, 0.92, 0.83, and 0.62, and RMSE were 0.11, 0.05, 0.10, and 0.17 mL/min for the four columns, respectively, during 1:5 year storm event. Similarly, R^2 between the observed and simulated outflows were 0.86, 0.80, 0.83, and 0.69, and

RMSE were 0.14, 0.09, 0.15, and 0.15 mL/min for during 1:10 year storm event. The simulated outflow hydrograph fitted well with the observed outflow in Columns 1, 2, and 3 (with $R^2 > 0.8$) during both 1:5 and 1:10 storm events, while it was satisfactory for Column 4 (with $R^2 > 0.6$). Despite the overall good performance of the model, discrepancy was also noticed. Sudden reductions were observed in the stimulated outflow for Columns 2, 3, and 4, while the experimental outflow decreased gradually. Moreover, in all the simulations, the timing of peak flow was close to observed data. The simulated peak outflows were 8.8, -0.8, 6.8, and 7.7 mL/min higher than the observed peaks for four columns during a 1:10 storm event, respectively.

In term of surface ponding, R^2 between the observed and simulated were 0.97, 0.47, 0.81, and 0.79, and RMSE were 0.04, 0.76, 0.15, and 0.15 mL/min for the four columns, respectively, during 1:5 year storm event. During 1:10 year storm event, the corresponding R^2 values were 0.82, 0.81, 0.88, and 0.86, and RMSE were 0.15, 0.14, 0.14, and 0.14 cm, respectively. The simulated ponding depth of Column 1 closely fitted with observed data from a 1:5 storm event with the same ponding duration (error < 5min). During a 1:10 storm, the simulated ponding depth was approximate 8 hours, which was 2 hours shorter than observed. The simulated peak ponding depth was 23.1 cm, which was 2.4 cm less than the observed. Column 2 had a simulated peak ponding depth of 9.9 cm, which is larger than the observed peak ponding depth of 5.4 cm, and the ponding duration is 2.5 hours (experimental ponding duration is 1.5 hours) during a 1:5 storm. Column 2's simulated ponding hydrograph fitted well with observed ponding during a 1:10 storm (the difference of duration is 14 min and that of the peak is 1.4 cm). Columns 3 and 4's simulated pond hydrograph matched well with observed data. The difference of peak ponding depth was 1.0 cm and 0.2 cm for Column 3, and 0.7 cm (did not include one "outlier peak point") and 1.1 cm for Column 4 during 1:5 and 1:10 storms, respectively. The simulated ponding durations of Colum 3 were

approximately 5.5 hours and 6.8 hours, which were about 30 min and 60 min less than the observed results, and the difference of ponding duration was 1 min and 15 min for Column 4 during 1:5 and 1:10 storms, respectively.

Even though R^2 generally decreased with the increase of rainfall intensity, the overall fitness is still promising for outflow and ponding hydrographs. The simulated peak outflow was slightly lower than the observed peak during 1:2 and 1:5 storm events, whereas it was slightly greater than the experimental data during 1:10 storm events for all four columns, which might indicate that the actual K_s of the bioretention columns declines as the intensity of storm events increases. The validation results suggest that the five hydraulic parameters including K_s do not change significantly from 1:2 to 1:10 year storm events for all four bioretention columns.

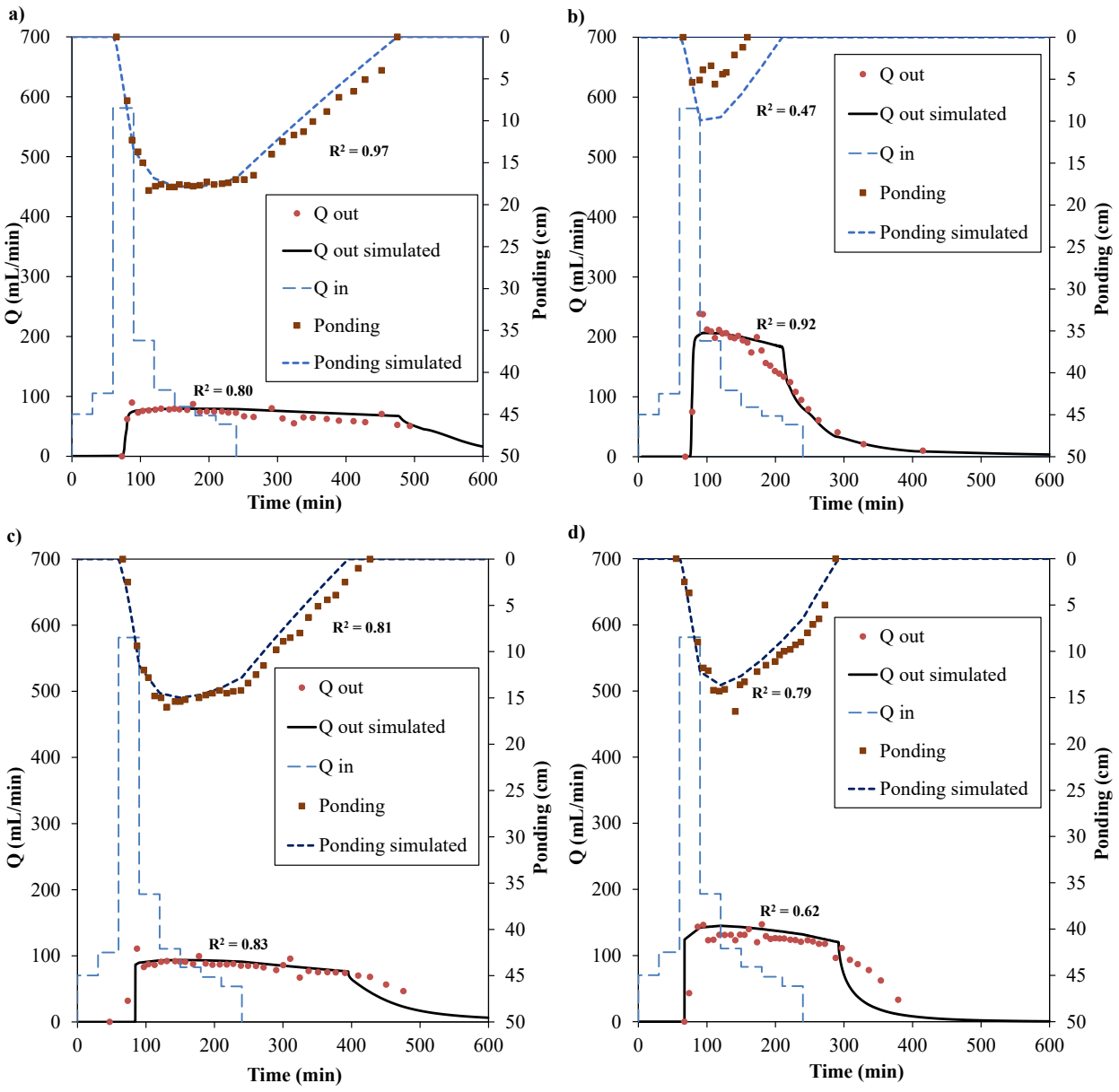

Figure 2.3 Model validation on outflow hydrograph and ponding depth for the four bioretention columns in a 1:5 year storm event in summer: a) column 1, b) column 2, c) column 3, and d) column 4.

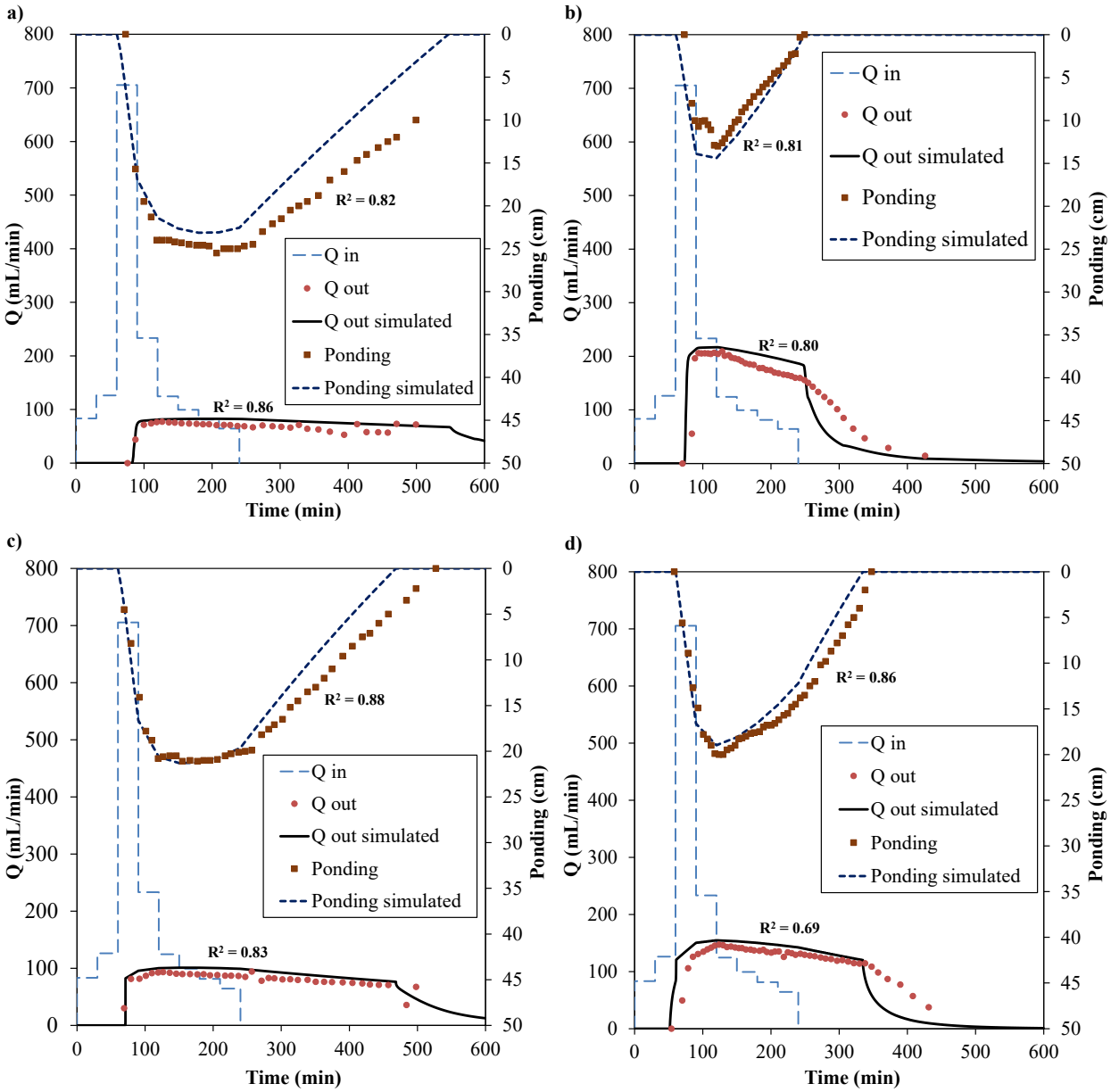

Figure 2.4 Model validation on outflow hydrograph and ponding depth for four bioretention columns in 1:10 year storm event in summer: a) column 1, b) column 2, c) column 3, and d) column 4.

2.3.3 Hydrologic performance for summer large storm events

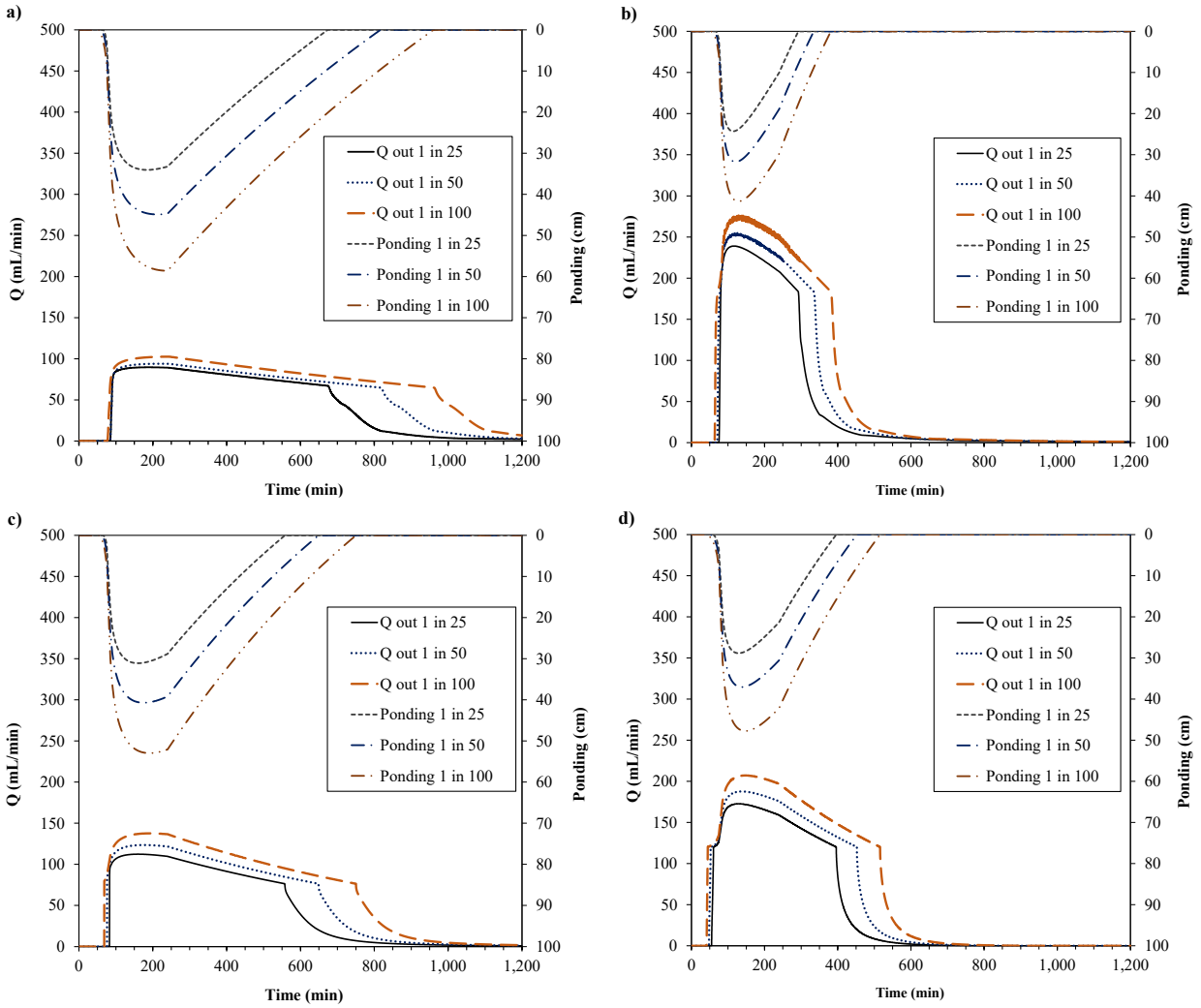

Figure 2.5 Simulated outflow hydrograph and ponding depth for four bioretention columns in large (1:25, 1:50 and 1:100) storm events in summer: a) Column 1, b) Column 2, c) Column 3, and d) Column 4.

The validated hydraulic parameters were applied in predicting bioretention performance during large storm events, including 1:25, 1:50, and 1:100 year storm events in the City of Edmonton, Canada. Detailed rainfall intensity with time for these design storms is shown in Appendix Table A2.2. The cumulative depths of 1:25, 1:50 and 1:100 year rainfall events are 56.2 mm, 68.8 mm and 83.4 mm, respectively. Simulated outflow hydrograph illustrated that four columns reduced

the peak flow by 95.7%, 88.7%, 94.3%, and 91.5% during a 1:100 storm respectively (Figure 2.5), which is promising for urban flood mitigation since LID is usually designed for small storm events, e.g., the design storm of LID is 1:5 year storm in Edmonton (COE, 2014a). The peak flow of all four columns did not increase significantly when the intensity of storm events was getting larger, because the outflow rate is mainly constrained by the saturated conductivity of the middle layer soil media of the bioretention column.

In the meantime, both ponding depth and duration significantly increased when the return period of storm events increased. Column 2 has the peak ponding depth of 24.3 cm and ponding duration of near 4 hours during a 1:25 storm, and they are 31.6 cm and near 5 hours during a 1:50 storm. The rest three columns experienced a higher peak ponding depth of around 30 cm and a longer ponding duration (approximate 10 hours, 8.3 hours, and 5.5 hours for Columns 1, 3, and 4) during 1:25 year storm. During 1:50 year storm, the maximum ponding depth of Columns 1, 3, and 4 exceeded 35 cm (approximate 44.9 cm, 40.7 cm, and 37.1 cm for Column 1, 3, and 4), which is the maximum design ponding depth as per Edmonton LID design guideline (COE, 2014a). During a 1:100 year storm, the maximum ponding depths of four columns are 58cm, 41cm, 53cmm, and 48cm respectively, and the ponding duration are approximate 15 hours, 5.5 hours, 11.5 hours, and 7.5 hours, respectively. Hydrologic performance of bioretention columns during large storm events demonstrated that coarser soil media could significantly reduce the ponding duration than finer soil media with a tradeoff of increasing peak outflow.

Sun et al. (2019) used SWMM to investigate how rainfall intensity and pattern affected bioretention hydrologic performance, and found the storms with less duration and larger intensity resulted in greater overflow and outflow and thus more severe ponding and flooding. With our test results on large storm events (rainfall depth > 50 mm in a 4-hr duration), a bioretention column

with coarser soil media and a free underdrain can effectively reduce peak flow approximately 90% while maintaining ponding depth below design standards, mitigating the pressing urban flooding issues due to extreme weathers caused by climate change.

2.3.4 Hydrologic performance for winter snowmelt and spring runoff events

Hydrologic performance of bioretention Columns 1-2 was calibrated for snowmelt events and validated for spring runoff events with the consideration of the presence of preferential flow, as shown in Figure 2.6. The calibrated soil hydraulic and thermal properties are presented in Table 2.5. For snowmelt events using the single-porosity model, R^2 of outflow for Columns 1-2 were 0.77 and 0.86, and RMSE were 0.12 and 0.09 mL/min. After using the dual-permeability model with preferential flow taken into account, R^2 of outflow increased to 0.94 and 0.96, and RMSE reduced to 0.01 and 0.005 mL/min, assuming the ratio w was 0.07 and 0.05 for Columns 1-2, respectively. The comparison between the two models indicated that preferential flow had high possibilities of existence, which created fractures and macropore flow inside soil columns and altered the flow path.

According to simulation results on spring runoff events for model validation, R^2 of outflow for Columns 1-2 were 0.72 and 0.84, and RMSE were 0.14 and 0.10 mL/min, using the single-porosity model. The R^2 values increased to 0.80 and 0.86, and RMSE reduced to 0.12 and 0.09 mL/min, using dual-permeability model with preferential flow taken into account and assuming the ratio w was 0.17 and 0.15 for Columns 1-2, respectively. Higher values of w, compared to those for the snowmelt events, suggested that more fractures could potentially occur after the first flush experiment and more severe preferential flow existed inside the soil column. The first flush event contained a high concentration of salt and high intensity of inflow, which was likely to create more

macropores inside the soil column. The observed outflow hydrograph had several fluctuations, which can potentially be caused by the instability of experimental apparatus for a long-period operation (> 60 hours).

It is interesting to notice the change of K_s from summer to winter/spring condition in both soil A and B. The K_s of Soil A in Column 1 increased from 0.044 cm/min (in summer condition when the temperature is around 21℃) to 0.10 cm/min (in winter/spring condition when the temperature is around 2-3℃ and soil temperature is around -0.5℃). However, K_s of soil B (Column 2) decreased from 0.15 cm/min in summer to 0.11 cm/min to winter/spring. The modeling results of increasing hydraulic conductivity for Soil A (loam texture) and decreasing hydraulic conductivity of Soil B (sandy loam) agreed with the laboratory experiments (Li, 2019). Weigert and Schmidt (2005) conducted lab experiments on two soil columns of sandy and loamy soil under partially frozen condition and simulated with a physical infiltration model. The calculated hydraulic conductivities of two soil types were close, indicating that hydraulic conductivities can theoretically be similar (Weigert and Schmidt, 2005). Meanwhile, due to recognized fracturing during the freezing process, the experimental hydraulic conductivity of loamy sand was underestimated by physical infiltration mode, indicating that hydraulic conductivity of soil was dominated by preferred flow when soil fractures were present (Weigert and Schmidt, 2005). Other studies have also supported that the formation of macropores in frozen soil can significantly affect the soil infiltration rate depending on the frozen water content and the formation of frost layer, both of which are, however, variable and difficult to predict (Watanabe et al., 2013; Watanabe and Kugisaki, 2017; Mohammed et al., 2018; Demand et al., 2019). The different changes of hydraulic conductivities of two types of soil were likely because finer soil media (Soil A) was expanding pore space due to freezing water

expansion and formation of macropores, while coarser soil media (Soil B) had a reduction in pore space due to compaction and pore ice blocking (Denich et al., 2013; Li, 2019).

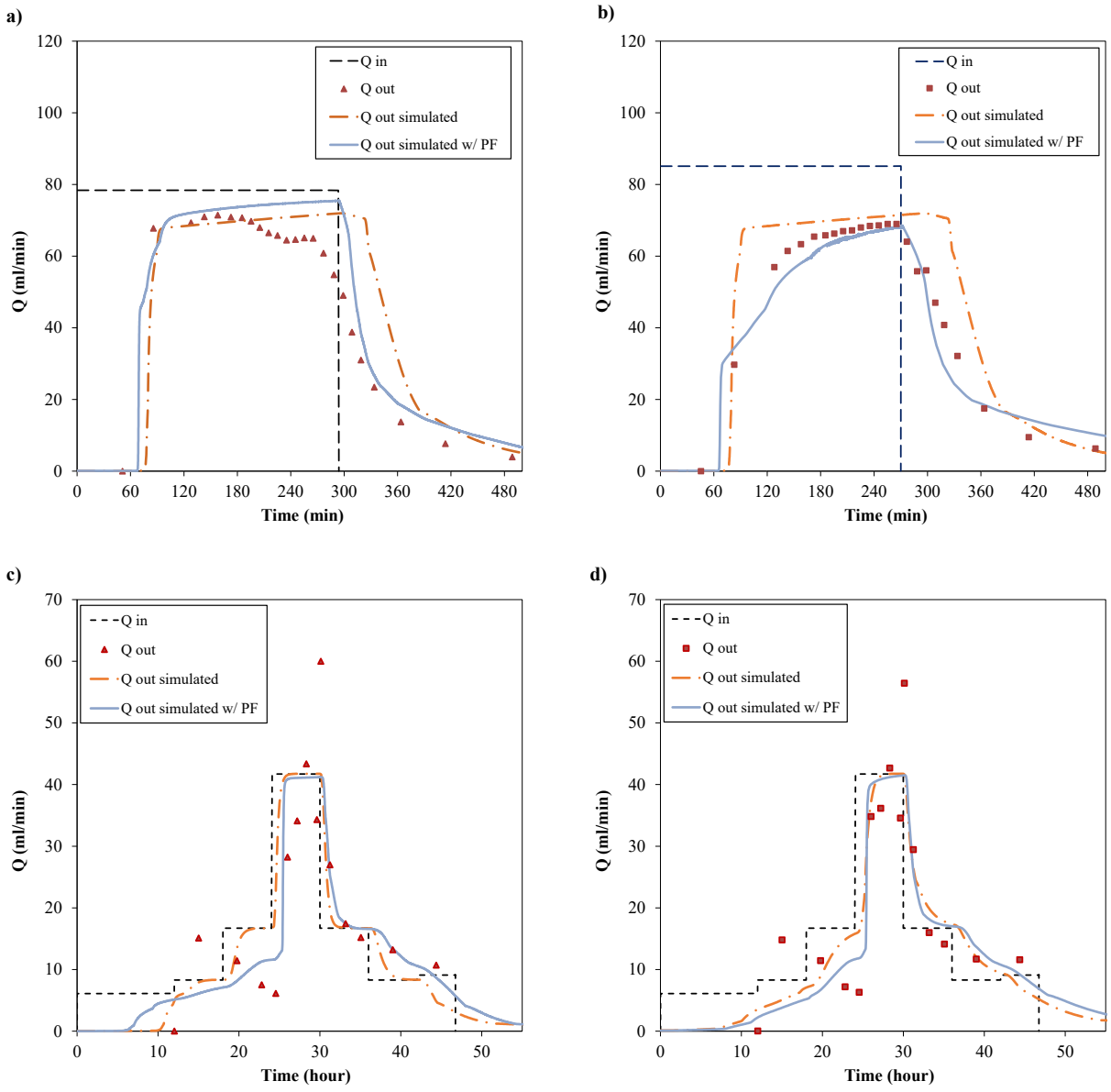

Figure 2.6 Calibrated outflow hydrograph of bioretention columns in cold region during winter snowmelt event: a) Column 1, and b) Column 2; and validated outflow hydrograph during spring runoff event: c) Column 1, and d) Column 2. PF in the figure legends stands for preferential flow.

Table 2.5 Calibrated hydraulic and heat transport parameters for bioretention Columns 1-2 in winter and spring cold climates

Column	Soil Layer	Q_r	Q_s	α (1/cm)	n	K_s (cm/min)	F	$b1$ (W/m/°C）	$b2$ (W/m/°C）	$b3$ (W/m/°C）
1	Top Layer	0.067	0.519	0.051	1.9	0.121	0.112	0.243	0.39	1.53
	Middle Layer	0.041	0.398	0.003	1.74	0.115	0.013	0.243	0.39	1.53
	Gravel	0.005	0.42	0.120	2.5	500	0.005	0.228	-2.40	4.92
2	Top Layer	0.09	0.55	0.029	1.73	0.120	0.216	0.228	-2.40	4.92
	Middle Layer	0.066	0.42	0.005	1.51	0.114	0.003	0.228	-2.40	4.92
	Gravel	0.005	0.42	0.113	2.5	500	0.005	0.228	-2.40	4.92

2.3.5 Water quality modeling

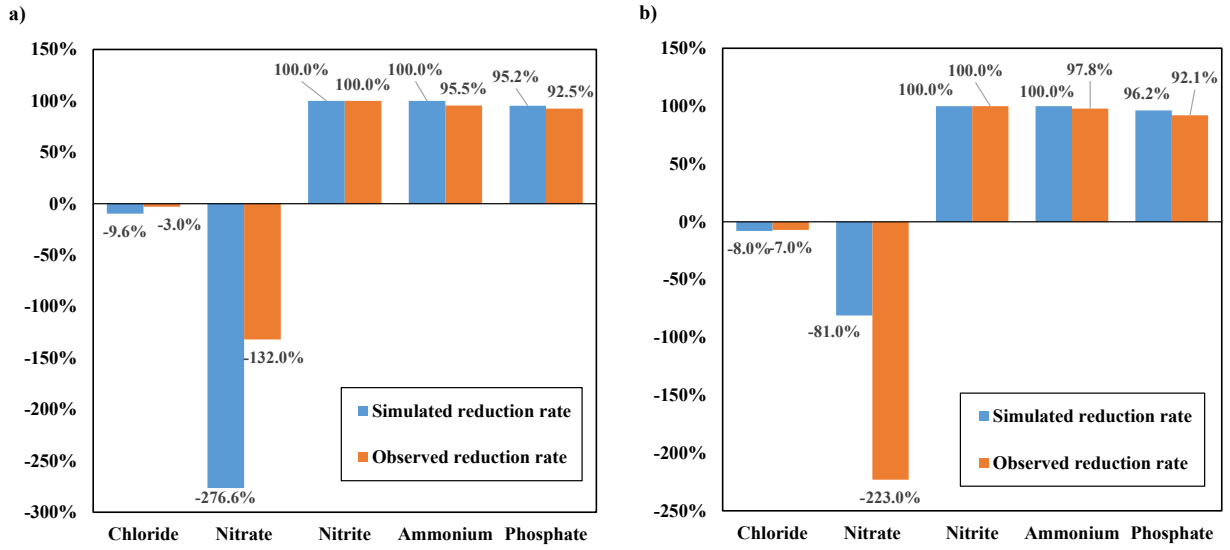

Figure 2.7 Comparison of the simulated pollutant loading reduction rates (%) with the measurements for bioretention Columns 1-2 during a 1:2 year storm event: a) Column 1; and b) Column 2. The initial pollutant concentrations are listed in Table A2.1.

In comparison with the observed results, the simulation results on water quality performance of bioretention during a 1:2 year storm event were generally reasonable, as shown in Figure 2.7. Both bioretention columns demonstrated a high loading reduction capability in phosphate, nitrite, and ammonium, but chloride and nitrate loading increased after the bioretention due to leaching effect. During the winter experiments, influent with a high concentration of sodium chloride flowed into the soil columns (Li, 2019), which made soil reach the saturation state of solute NaCl and salt precipitated. Chloride concentration was significantly larger in the outflow with 142% and 22% increase than that of inflow in the first summer week in Year 2 right after the winter season. After the first week of summer, chloride concentration reduction of both columns was around 0% with an error of approximately 7% during the next four weeks. The simulated reduction of chloride was -9.6% and -8.0% for Columns 1 and 2, which are very close to observed chloride concentration

reduction following summer weeks. Mile High Flood District, Colorado (2020) summarized that bioretention and other types of LID were ineffective at treating road salts in several studies, suggesting that bioretention temporarily stored the salts and chloride leaching occurred during the first flush in spring, and that bioretention was not effective in chloride removal (MHFD, 2020).

The increase of nitrate in the outflow was because of nitrogen rich soil used in the columns and nitrification process that converted ammonium to nitrite and further to nitrate (US EPA, 2002). Organic nitrogen and ammonia nitrogen can be effectively contained by the medium of bioretention systems and transformed into nitrate (Wan et al., 2017). The simulated nitrate reduction of -276% and -81% for Columns 1-2 was different from the observed results of -132% and -223% that were the average value for five 1:2 year storm events in the summer of Year 2. In the experiments, nitrate reduction for both columns differed significantly

in the second summer from weeks to weeks (Kratky, 2019). In the first week, the reductions of Columns 1-2 were -200% and -515%, but it decreased to -10% and -94% in the fifth week. Nitrite is unstable in solution, which is why it is barely seen in the outflow of bioretention columns (Moeller, 2012). Meanwhile, no evident nitrite inhibition was observed in experiments, and therefore no nitrite accumulation occurred. Li et al. (2018) tested three bioretention columns through lab experiments and numerical simulations using HYDRUS 1D, and demonstrated that average reduction rates of nitrate, ammonium, and total phosphate were approximately 65%, 75% and 80%, respectively, in all design scenarios of different fillers. Because IWS was used in their bioretention, they were able to achieve positive nitrate removal, which is in opposite to our findings. IWS creates an anoxic zone that stimulates the denitrification process and has been demonstrated with successive nitrogen removal in a few studies (Palmer et al., 2013; Li et al., 2014; Qiu et al., 2019). Mulch or wood chips can also be considered as one possible denitrification measure since

they convert to a carbon source for denitrifying bacteria (Liu et al., 2021) and promote anaerobic condition at top layer (Wan et al., 2017). Mulch was used in Li (2019) and Kratky (2019)'s experiments, however owing to its thin thickness of 4 cm, the denitrification benefits of mulch were deemed insignificant. The simulated results and observed results illustrated significant removal capacity of bioretention columns for ammonium and phosphate in the outflow, but negative removal for nitrate and chloride without appropriate denitrification measures.

In the present model, one error source is that the initial concentration of pollutants in the soils was assumed to be the same as the leaching test results, which could be different from actual conditions. To achieve more convincing modeling results, it is recommended that the initial concentrations of different contaminants inside the soil column be tested at different positions.

2.3.6 Optimization of bioretention columns

Three measures can be used to improve the design of bioretention columns. The first measure is to replace soil media B in the bioretention column with a coarser soil media. In bioretention's practice, the fundamental design component is its soil media, and many studies and design guidelines have suggested coarse soil media as engineering soil media because of its higher permeability (Hunt and Lord, 2006; Davis et al., 2009; Dhalla and Zimmer, 2010; Liu et al., 2014; Dell and Brim, 2017). The second measure is to increase the soil layer depth inside the bioretention column because a larger layer thickness of soil indicates additional storage space for stormwater. Decreasing the CA/SA is the last measure. Using coarser soil media for surrounding soil was one measure reported by He and Davis (2011) because higher hydraulic conductivity of surrounding soil reduces outflow. HYDRUS 1D neglects side wall effects in simulation, so this measure is not considered in this paper.

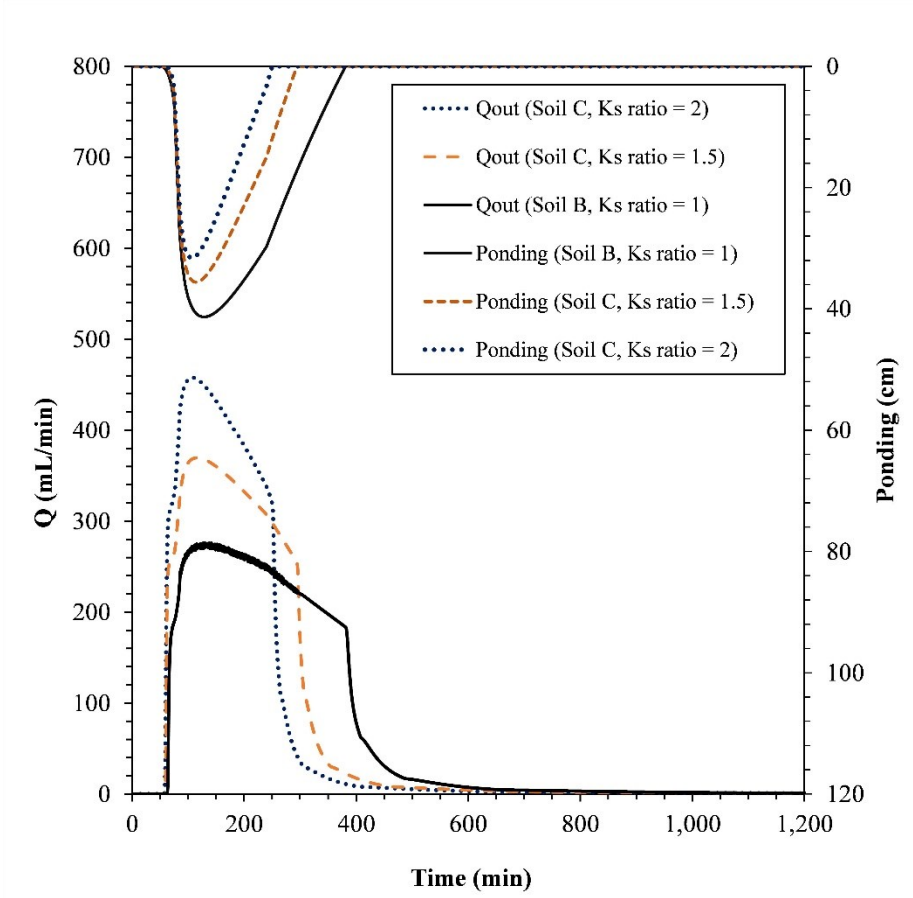

Figure 2.8 Hydrologic performance of bioretention Column 2 modified by replacing Soil B with Soil C for 1:100 year storm event. Two different values of *Ks* of Soil C were tested.

Loamy sand is considered a replacement of sandy loam (soil B) to avoid overflow (flooding) caused by exceeding maximum ponding depth during large storm events. Sandy soil has higher permeability and lower water content, which reduce clogging potential (Tirpak et al., 2021), has better performance in cold weather and increases permeability following the thawing process (Moghadas et al., 2016). Coarser media with larger pores is helpful to prevent concrete frost (one type of frost in soil) and form granular or porous frost instead in cold conditions (Kratky et al., 2017). Soil media has a premature period and hydraulic parameters of soil change significantly during that period and after freeze-thaw cycles in winter. Accurate determination of hydraulic parameters of a new soil media at a mature state requires experiments, testing, and model

calibration. A soil C classified as the loamy sand texture is proposed by increasing sand percentage in soil B. The ratio of *Ks* between loamy sand and sandy loam is approximate 3 to 5 according to Clapp and Hornberger (1978) and Carsel and Parrish (1988). To simulate the hydrologic performance of bioretention column replaced with soil C, saturated hydraulic conductivity of soil C is assumed to be 0.23 and 0.31 cm/min (*Ks* ratio = 1.5 and 2).

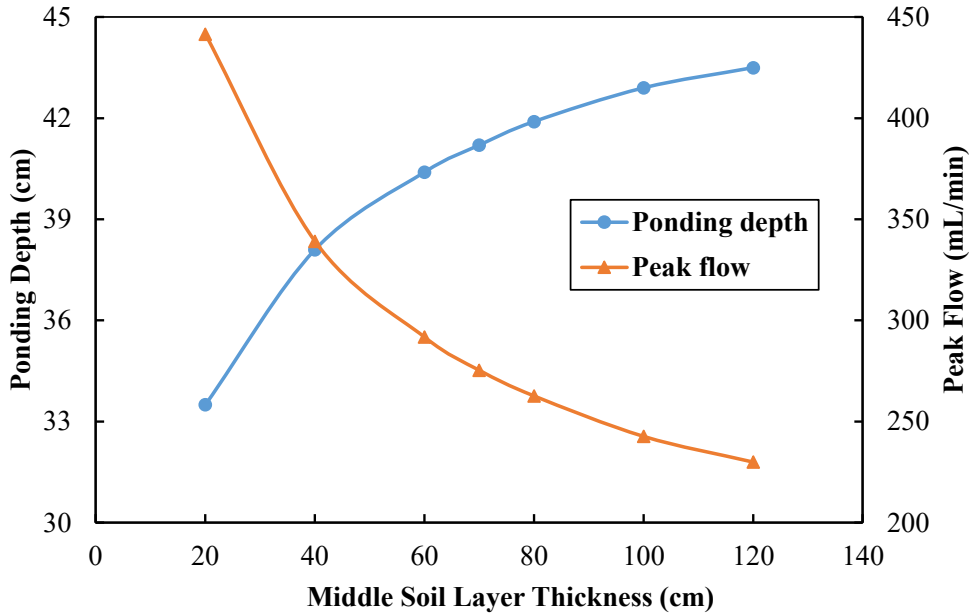

Figure 2.9 Hydrologic performance of bioretention Column 2 modified by changing the thickness of middle soil layer. Storm event modeled: 1:100 year.

The hydrologic performance of replacing Soil B in the middle layer of Column 2 with Soil C (loamy sand texture) during 1:100 year storm is illustrated in Figure 2.8. The ponding depth reduced from 41.5 cm to 35.6 cm and 31.6 cm when the saturated hydraulic conductivities of two types of Soil C were 0.23 and 0.31 cm/min, respectively, but the peak outflow increased from 276 mL/min to 370 and 458 mL/min. The peak inflow of 1:100 year storm was 2436 mL/min, and therefore the bioretention columns replaced by two types of Soil C could still reduce the peak flow by 85% and 81%. To achieve more accurate hydraulic performance, experiments are necessary to

test the values of all the five hydraulic parameters of the loamy sand. Loamy sand with a higher ratio of sand is likely to manage a local 1:100 storm event without flooding.

With ±10 cm, ±30 cm, and ±50 cm increments added to the original 70 cm middle layer of Soil B in Column 2, the hydrologic performance (peak flow and pond depth) during 1:100 year storm event is shown in Figure 2.9. As the thickness of the middle soil layer decreased, ponding depth became smaller and peak outflow increased due to the shorter duration of water flow through this layer. Increasing the thickness resulted in opposite outcome. An exponential trend was shown in the correlation between ponding depth and soil thickness, as well as between peak outflow and soil thickness. When the soil thickness increased from 20 cm to 40 cm, 4.6 cm increase in peak ponding depth and 102.3 mL/min decline in peak outflow were observed. When the soil thickness was in the higher range and increased from 100 cm to 120 cm, there was only 0.6 cm increase in ponding depth and 12.7 mL/min decline in peak flow.

For bioretention column filled with sandy loam such as Column 2, the middle soil layer thickness is recommended to be smaller to reduce ponding depth. Meanwhile, higher soil layer thickness provided extra pollutant reduction capacity (Li et al., 2020). Therefore, 60-80 cm of middle layer thickness is suggested to achieve promising peak flow reduction, contaminants removal with minor overflow.

The third option of modifications was decreasing the catchment area to surface area (CA/SA) ratio. Figure A2.3 illustrated that ponding depth, ponding duration and outflow decreased when the ratio became larger. The ponding depth decreased from 41.5 to 14.8 cm, and the peak outflow decreased from 276 to 218 mL/min when CA/SA ratio reduced from 10 to 5. Ponding depth was approximately 30 cm when the CA/SA was 8, which meets the requirements of COE design

guidelines, in which the maximum permitted ponding depth is 35 cm. The maximum outflow was 252 mL/min, which means 90% reduction of peak flow with CA/SA = 8.

2.4 Conclusions and future research directions

Bioretention is one of the most cost-effective LID facilities that has been widely studied and practiced. However, limited studies have been conducted on its hydrologic performance during large storm events (rainfall depth > 50 mm) and in cold climates, and on simultaneous modeling of hydrologic processes and water quality improvement. In this paper, HYDRUS 1D was selected and proved to be an appropriate software to model four single unit bioretention columns (with CA/SA = 10) to explore these knowledge gaps.

The model was calibrated and validated for 1:2, 1:5, 1:10 year storm events, with rainfall depth of 22.6, 37.3 and 45.2 mm, respectively. The R^2 of simulated outflow and ponding hydrographs were typically greater than 0.8. The soil hydraulic parameters appeared to not change significantly from a 1:2 to a 1:10 storm event. The four bioretention columns reduced the peak flow by 95.7%, 88.7%, 94.3%, and 91.5% respectively during 1:100 storm, although the maximum ponding depth of all exceeded the design limits of 35 cm for approximately 6.8, 1.8, 4.8, and 2.2 hours, respectively.

To address the ponding depth issue, (1) loamy sand can be used as a replacement soil media, e.g., it decreases the ponding depth of Column 2 to 31.6 cm with 81% peak flow reduction during 1:100 storm. (2) The soil thickness of 60-80 cm is recommended to achieve the tradeoff balance of ponding depth, peak flow reduction, and contaminants removal. (3) Smaller CA/SA ratio can be also used, e.g., the CA/SA = 8 decreases the ponding depth of Column 2 to 30 cm with 90% peak flow reduction during 1:100 storm.

Due to the limited data from the experiments as a result of complexity of experiments under cold conditions, only one winter snowmelt event and one spring runoff event were calibrated and validated using both single-porosity and dual-permeability models. Therefore, the findings below are still preliminary. Higher fitness of dual-permeability model indicated a high potential of preferential flow in bioretention in cold climates, which was likely caused by freeze-thaw cycles and high concentrations of contaminants in the inflow. The simulation results also demonstrated that the finer texture soil experienced increasing hydraulic conductivity in cold climates, while it was opposite for the coarser soil texture.

Based on limited experimental data and this modeling work, bioretention columns had high contaminant removal rates for phosphate, nitrite, and ammonium. At the meantime, leaching of chloride and nitrate occurred. High concentration of chloride in outflow was caused by a large amount of de-icing salts in winter flowed into bioretention columns which saturated NaCl in soil and precipitated salts. The nitrification process causes an increasing concentration of nitrate observed in outflow while the total nitrogen reduction rate was positive. Overall, bioretention demonstrated a promising capability for nutrients removal in this study.

To improve efficiency and reliability of bioretention modeling, it is recommended to measure (1) the hydraulic and heat transport parameters of each soil media so that initial condition can be accurately set; (2) water content at different heights of bioretention to provide boundary condition and alternative validation for models; and (3) the change of hydraulic properties of soil with time and temperature to better simulate bioretention with time and climates. Future research directions are suggested on (1) more research of bioretention in cold climates including field monitoring, lab experiments and numerical simulation; (2) long-term performance of bioretention; and (3)

clogging of bioretention due to sediments in stormwater. Detailed suggestions for future research directions are provided in Chapter 4.

Chapter 3 A New LID Spatial Allocation Optimization System: Integrated SWMM with PICEA-g using MATLAB as the Platform

3.1 Introduction

Conventional urban stormwater drainage systems, composed of underground pipes (grey infrastructure) and road surfaces, have the sole purpose of conveying the water quantity, and may be unreliable in rainfall extremes that exceed the design standards (Willems et al., 2012). In recent decades, low impact development (LID), also known as green infrastructure, has been widely and extensively studied and practiced worldwide as a new approach to achieve sustainable stormwater management in terms of both water quantity (peak and volume reductions) and water quality (US EPA, 2000; Coffman, 2002b; HUD, 2003). Typical LID-BMPs (best management practices) include bioretention, grass swale, green roof, and permeable pavement (US EPA, 2000). Numerous studies summarized the promising hydrological performance of LID-BMPs and their efficiency in pollutant loading removal (US EPA, 2000; Dietz, 2007; Ahiablame and Engel, 2012; Eckart et al., 2017).

As LID research grows, more municipalities adopt and apply LID-BMPs in their neighborhoods (Weitman et al., 2009; Chang et al., 2018). One of the most critical challenges of implementing LID is spatial allocation. Optimization of LID spatial allocation is complex due to different restrictions, including space availability, public support, and trade-offs among maximizing different benefits of LID such as flood mitigation, water quality improvement, other environmental effects and ecological influence (Zhang and Chui, 2018). Installation location, quantity, and type of LID generate infinite combinations of spatial allocation, making finding optimal solutions practically challenging.

A considerable number of studies have made great efforts to optimize LID spatial allocation using numerical models (Zhang and Chui, 2018; Huang et al., 2018; Men et al., 2020). There are several modeling tools in the market (e.g., MIKE Urban/MIKE+, SWMM), which provide both the capabilities of stormwater management designs and built-in LID control modules (Kaykhosravi et al., 2018). A straightforward methodology is to establish some representative scenarios based on geographical, landscape, and other existing information about the project area and designers' judgment, which reduces computation complexity to an acceptable level (Zhang and Chui, 2018). Cano and Barkdoll (2017) designed their LID allocation scenarios with the assumption that only one LID-BMP type would be implemented in one sub-catchment. They used SWMM to compute all the scenarios, acquired cost-benefit-ratio and maintenance probability factor, and finally applied an entitled multi-objective algorithm called MOSEBEND to choose the best solutions. One disadvantage of this methodology is that only a small number of scenarios are selected based on designers' subjective judgment (while the quantity of scenarios is infinite), which means a strong possibility of missing the optimal scenarios.

Zhang and Chui (2018) proposed a term called "spatial allocation optimization tool (SAOT)" in their review paper, and introduced two types of SAOT structures. The first one is single compact (commercially available) software packages on the market (e.g., SUSTAIN, GreenPlan-IT, InfoSWMM, etc.). For example, SUSTAIN (the system for urban stormwater treatment and analysis integration), aggregates GIS, the SWMM module, a non-dominated sorting genetic algorithm (NSGA-II), Hydrological Simulation Program - FORTRAN (HSPF), and Microsoft Access database (Lai et al., 2007; Shoemaker et al., 2009). Mao et al. (2017) used SUSTAIN to optimize the cost and benefits of LID-BMPs at a regional scale. The second SAOT structure in Zhang and Chui (2018) is a new methodology that interacts with a stormwater management model

(e.g., HEC-HMS, MIKE Urban/MIKE+, SWMM, SWAT) and a programming language (e.g., MATLAB, Python). Using multi-objective evolutionary algorithms (MOEA), a numeric computing environment provides a route to evolve selected scenarios, provides feedback to the stormwater management model, and forms a loop to achieve near-optimal solutions instead of selecting the best scenarios from pre-defined scenarios (Liu et al., 2016; Xu et al., 2017; Tao et al., 2019; Men et al., 2020; Dong et al., 2021).

Table 3.1 summarizes the recent studies on LID SAO from 2016 to 2021 that used a programming language as a platform to link an optimization algorithm with a stormwater computing engine. For example, Xu et al. (2017) coupled NSGA-II with SWMM using platform Python in a LID-BMPs optimization case study in Tianjin, China, which considered runoff quantity, water quality, and cost. Men et al. (2020) combined PICEA-g with SWMM through MATLAB to find optimal LID layout solutions with objectives of minimizing cost, total runoff, peak flow at outfall, and TSS pollutants loading. The strength of interacting with a programming language is to provide: 1) the flexibility to use different optimization algorithms and stormwater management modules based on project characteristics; 2) the flexibility to set up objective functions and decision variables; and 3) the potential to further improve optimization algorithms.

As shown in Table 3.1, despite the recent progress, no research, to the author's best knowledge, has modified a multi-objective evolutionary algorithm (MOEA) and applied it to the LID spatial allocation problem. Applying original and non-modified code of classical MOEA (e.g., NAGA-II, PICEA-g) directly into LID spatial allocation problem can result in unsatisfying performance of algorithm and lack of diversity in optimal solutions. In Men et al. (2020), the LID cost ranged from 5 million to 27 million CNY (Currency CNY:CAD was about 5.1:1.0 in 2021) for a 2-year storm event and it didn't cover the entire cost range of LID (from zero to maximum cost of full installation

(maximum constraints of decision variables)). Meanwhile, the Pareto front of optimal solutions didn't form a smooth curve, indicating that there is potential for improving the diversity of optimal solutions and algorithm effectiveness (Men et al., 2020).

This study introduced a new LID SAO system that used MATLAB as a platform to integrate SWMM with a modified PICEA-g algorithm, with upgraded functions for candidate solution initialization, goal vector boundary definition, and genetic operators. These upgraded functions increase the diversity of solutions, enhance solution evolution, and improve the performance and effectiveness of PICEA-g in the LID SAO problem.

Table 3.1 Summary of SAO models for LID that used a programming language to combine optimization algorithm and a stormwater engine

Study	Stormwater model	Programming language	Optimization Algorithm	Objectives	Decision Variables	LID Facility	Algorithm Modifications	Limitations
This Study	SWMM	MATLAB	PICEA-g	Peak inflow of retention pond; Total inflow volume of retention pond; Cost	Area of each LID type installed in each subcatchment	Bioretention; Rain Garden; Green Roof; Permeable Pavement	Initializing candidate solutions; defining goal vector boundaries; Enhanced genetic operators	No prescreening methodology
Dong et al. (2021)	SWMM	Python	NSGA-II	Non-point source pollution; Cost	Area of each LID type installed in each subcatchment and area of storage tanks	Green Roof; Permeable Pavement; Vegetative Swale; Storage Tank (non-LID)	None	No algorithm modifications; Small area (number of decision variable is small)
Men et al. (2020)	SWMM	MATLAB	PICEA-g	Surface runoff; Outfall peak flow; SS pollutant; Cost	Implementation area ratio of each LID type installed each subcatchment	Vegetative Swale; Green Roof; Permeable Pavement	None	No algorithm modifications; Small area (number of decision variable is small)
Xu et al. (2017)	SWMM	Python	NASA-II	Target control rate of total runoff volume; Water quality score; Cost	Area ratio of each LID type in block scale	Raised Flower Bed; Vegetative Swale; Permeable Pavement; Rain Garden	None	No algorithm modifications; Optimization in block scale
Liu et al. (2016)	L-THIA-LID 2.1	MMLSOPT	AMALGAM	cumulative runoff/pollutant fraction value; Cost	Area ratio of chosen LID and BMPs in suitable locations	Retention Pond; Detention Basin; Wetland Basin; Grassed Swale; Grass Strip; Wetland Channel; Bioretention; Permeable Pavement	None	No algorithm modifications; Optimization in block scale

3.2 Optimization System Algorithms

3.2.1 Study area and SWMM model

The study area is a residential neighborhood located in the northwest of the City of Calgary, Alberta, Canada (Figure 3.1). The total area of the catchment is 15.2 hectares, with 51% imperviousness and an average surface slope of 1%. The study area is mainly composed of single-family and multi-family dwelling units without any commercial or industrial buildings. Surface runoff from the catchment is directed into a downstream retention pond, which has two inlets and one outlet. The pond has a surface area of 5,500 m^2, a normal depth of 0.8 meters, and the side slope is 2:1 (H:V). It is designed to retain 9,570 m^3 of water during a 1:100 year storm event.

An existing SWMM model of the study area catchment was calibrated and validated based on a 2-year field monitoring program as described in Fernandez et al. (2019). In this study, LID units were added to the existing model to test the new LID SAO system. The existing SWMM model contained a dual drainage system (road surfaces as major system and underground storm sewers as minor system) with 240 subcatchments (based on topography and distribution of manholes), 126 junctions, and 119 conduits. The infiltration method used in this model was the Modified Green-Ampt model, and its parameters and other hydraulic parameters of the model can be found in Table A3.1. The “Dynamic Wave” option was chosen as the routing method for the SWMM model with a minimum variable time step of 0.5 sec, and the detailed parameters are shown in Table A3.2. Three types of land use were assigned to each subcatchment: greenspace, concrete (comprising the roadways, sidewalks, and driveways), and roof (see Table A3.3 for examples). Land use information was used in this study to determine the area limitation of LID units in each subcatchment.

Figure 3.1 Aerial photo and location of the study area (MapTrove, 2021; Google Map, 2021)

Instead of using natural rainfall data, single design storm events were used in this study to better evaluate LID performance. According to the Stormwater Management and Design Manual of the City of Calgary (2011), a single event analysis with a storm duration of 1 hour is suitable for a small drainage area as in our case, because overflow and flooding issues tend to occur preferentially with LID implementations when the enduring storm events have shorter duration

and higher intensity (Sun et al., 2014). The 1 hour, Chicago rainfall distribution of 1:2, 1:5, 1:10, 1:25, 1:50, and 1:100 year design storm events (rainfall depth are 13.7, 19.4, 23.1, 28.0, 31.6, and 35.1 mm respectively) were applied in this study, and detailed storm information is provided in Table A**3.**4.

3.2.2 Process structure of the LID SAO system

3.2.2.1 Overview of PICEA-g algorithm

PICEA-g is a multi-objective evolutionary algorithm (MOEA) that was first introduced by Wang (2013) as a more effective algorithm for the multi-objective problem (MOP). By proposing a family of goals (goal vectors) in PICEA-g, candidate solutions gain a new fitness assignment and are guided to move towards the Pareto optimal front (Pareto front is a set of optimal solutions, which leaves no space for improvements in multi-objective optimization problem) in two ways: 1) move closer to the Pareto optimal front (convergence); and 2) spread out towards the regions with fewer solutions (diversity). PICEA-g overcomes the challenges of poor performance when the objective number is large, which many state-of-the-art MOEAs (e.g., NSGA-II, MOGA (multi-objective genetic algorithm)) face (Wang, 2013).

An elitist framework of PICEA-g is shown in Figure A3.1 to represent how candidate solutions and goal vectors are co-evolved. *S* (fixed size of *N*) represents solutions, and *G* (fixed size of *Ng*) represents goal vectors. They will co-evolve for a preset number of generations. In each generation, parent solutions *S* goes through genetic variation operators (crossover and mutation) and generate offspring solutions *Sc* (fixed size of *N*). Meanwhile, new goal vectors *Gc* (fixed size of *Ng*) are generated randomly in a defined space. Fitness is then calculated for each population of *S*, *Sc*, *G,* and *Gc*. After sorting the fitness of individuals in the combined population of *(S + Sc)* and *(G +*

Gc), the best *N* solutions and *Ng* goal vectors will become the new population of *S* and *G* in the next generation (this selection process is called truncation selection). The pseudo code of PICEA-g is in the Appendix Algorithm A3.1.

3.2.2.2 Decision variables

The decision variables in this optimization system were the installed area of each type of LID facility in each subcatchment. Four types of LID were used in this study, which are the widely-used bio-retention cell (BR), rain garden (RG), green roof (GR), and permeable pavement (PP). For simplicity, the detailed design parameters of these four types were adopted from the City of Edmonton LID Design Guidelines (COE, 2014a) (Table 3.2). Other LID practices and parameters could have been adopted, however, it is beyond the current scope of work . The approach of placing LID within a subcatchment in this study was to replace the pervious and impervious area with a mix of LID practices (based on land use type) (Figure 3.2), and each LID unit catches runoff generated from a portion of the impervious area (Rossman, 2015). Bioretention, rain garden, and permeable pavement were set to treat runoff from a portion of the impervious area and send it to the outlet of the current subcatchment, while the green roof was set to only treat rainfall directly on the roof and send outflow to the pervious area of the current subcatchment. Seven scenarios regarding how much impervious areas (in percentage) were treated by BR, RG, and PP, respectively, are listed in Table 3.3. For example, in Scenario 1, BR, RG, and PP are implemented in one subcatchment and treat 30%, 30%, and 30% of the impervious area (totally 90% of the impervious area) of the subcatchment, respectively.

With 240 subcatchments in the SWMM model and 4 types of LID selected (i.e., 4 decision variables in each subcatchment), there were a total of 960 decision variables in this study. A single decision variable *D* can be expressed as

$$D = Area(\#S, T) \tag{3.1}$$

where #*S* is the subcatchment number, and *T* is the type of LID facility (BR, RG, GR, PP).

The only geographic information available on the study area was the area percentage of green space, concrete, and roof in each subcatchment. Due to the limited geographic information, assumptions of spatial availability were made to determine the range of each decision variable. A maximum 20% of green space area was assumed to be available for bioretention and rain garden installations, separately. A maximum 20% of concrete and roof area was assumed to be available for permeable pavement and green roof installation, respectively. These assumptions can be easily changed based on the actual conditions and have no effects on the SAO system. For a project with sufficient geographic information, detailed spatial availabilities for different types of LID facilities can be specified or determined, for example, using SUSTAIN that has a LID siting tool to find suitable locations for different types of LID facilities based on suitability criteria and GIS data sets (Tetra Tech, 2013). With this information, the optimal solutions will have more practicability for LID implementation.

Table 3.2 LID control settings in this study (COE, 2014a)

LID control	Layer	Layer Parameters	Value
Bioretention	surface	Berm height (mm)	150
	soil	Thickness (mm)	500
		Porosity (Volume fraction)	0.44
		Field Capacity (volume fraction)	0.11
		Wilting Point (volume fraction)	0.05
		Conductivity (mm/hr)	30
		Conductivity Slope	10
		Suction Head (mm)	61
	storage	Thickness (mm)	300
		Void Ratio (voids/solids)	0.66
		Seepage Rate (mm/hr)	1
	Drain	Flow Coefficient	0.36
		Flow Exponent	0.5
		Offset (mm)	100
Rain Garden	surface	Berm height (mm)	150
	soil	Thickness (mm)	500
		Porosity (volume fraction)	0.44
		Field Capacity (volume fraction)	0.11
		Wilting Point (volume fraction)	0.05
		Conductivity (mm/hr)	30
		Conductivity Slope	10
		Suction Head (mm)	61
	storage	Thickness (mm)	10
		Void Ratio (voids/Solids)	0.66
		Seepage Rate (mm/hr)	1

Permeable Pavement	surface	Berm Height (mm)	150
		Surface Roughness (Manning's n)	0.03
		Surface Slope (%)	1
	Pavement	Thickness (mm)	150
		Void Ratio (voids/Solids)	0.15
		Permeability (mm/hr)	500
	storage	Thickness (mm)	10
		Void Ratio (voids/Solids)	0.66
		Seepage Rate (mm/hr)	1
	Drain	Flow Coefficient	0.34
		Flow Exponent	0.5
		Offset (mm)	100
Green roof	Surface	Berm height (mm)	25
	Soil	Thickness (mm)	150
		Porosity (volume fraction)	0.58
		Field Capacity (volume fraction)	0.34
		Wilting Point (volume fraction)	0.04
		Conductivity (mm/hr)	64
		Conductivity Slope	5
		Suction Head (mm)	75
	Drain Mat	Thickness (mm)	150
		Void Fraction	0.66

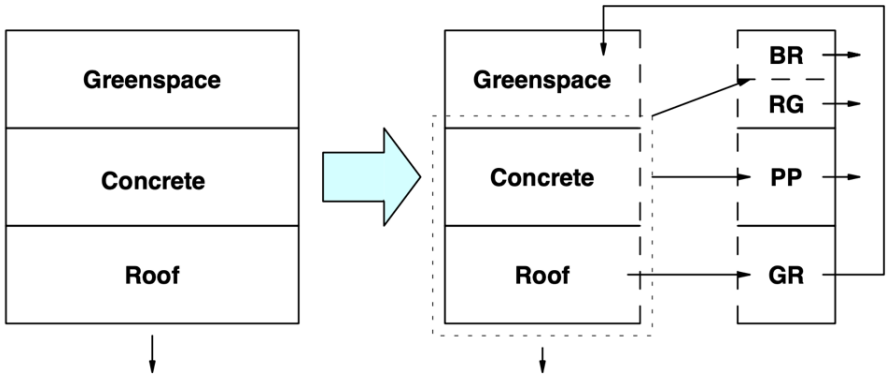

Figure 3.2 Schematic diagram of LID practice placement approach (example of one subcatchment)

Table 3.3 Modeling scenarios on the percentage of impervious area treated by bioretention (BR), rain garden (RG) and permeable pavement (PP)

	Percentage (%) of Impervious Area Treated by		
Scenario	**BR**	**RG**	**PP**
#1	30	30	30
#2	60	0	30
#3	0	60	30
#4	60	30	0
#5	90	0	0
#6	0	90	0
#7	0	0	60

3.2.2.3 Objective functions

The objective functions were the hydrologic performance of LID and cost in this study. Typically, the intent of a LID spatial optimization is to achieve the best hydrologic and/or water quality benefits of LID implementation with a fixed cost, or to achieve the minimum cost with required hydrologic and/or water quality benefits. SWMM currently only simulates pollutant removal of

LID practices resulting from the reduction in runoff flow volume, which would underestimate the water quality improvements (Rossman, 2015). Therefore, water quality benefits were not considered in this study, but can be added easily into the current LID SAO system.

In this study, all the surface runoff from the study area was directed into a downstream retention pond (Fig. 1). Therefore, the three objective functions of this study selected to assess the LID were: 1) peak inflow into the retention pond, 2) total inflow volume to the retention pond, and 3) total cost of LID implementations. The PICEA-g algorithm can optimize three or more goals (Wang, 2013). However, the performance of any MOEA deteriorates considerably as the number of objectives grows (particularly when it exceeds three), because the difficulty of generating optimal solutions in multi-objective problem (MOP) grows exponentially (Ishibuchi et al., 2008; Wang, 2013). In this study, only two objective functions, the peak inflow to the retention pond and the total cost of LID, were optimized (minimized) to have a better performance of the MOD-PICEA algorithm. The total inflow volume was achieved based on the optimal solutions from the peak inflow and cost optimization, and was automatically optimized with cost, as discussed later in results.

The total cost (*TC*) of LID considered was as a life cycle (*LC*) accumulated cost, which includes capital cost (construction and material cost, *CMC*), annual operation and maintenance cost (*OMC*), and periodic maintenance cost (*PMC*). The detailed costs of each type of LID facility (BR, RG, GR, PP) are listed in Table 3.4 (COE, 2014a). The life cycle of all LID facilities in this study was assumed to be 25 years. The calculation formula of the total cost of LID implementation is:

$$TC = \sum_{i=1}^{S=240} \sum_{j=1}^{T=4} (D_{i,j} \times CMC_j + D_{i,j} \times OMC_j \times LC + D_{i,j} \times PMC_j) \quad (3.2)$$

Table 3.4 LID costs used in this study (COE, 2014a)

LID control	Material and Construction Cost ($/m^2)	Operations and Maintenance Cost ($/m^2/year)	Periodic Maintenance Cost ($/m^2)
Bioretention	140	21.5	87
Rain Garden	190	21.5	12.5
Permeable Pavement	390	0.23	430
Green Roof	420	23.5	16

3.2.2.4 Overview of the SAO process structure

The three fundamental elements of this optimization system were: 1) hydrologic process computation module - SWMM, 2) optimization algorithm - PICEA-g, and 3) a platform and framework manager that interacts and integrates all the components of the system - MATLAB. As shown in Figure 3.3, the system started with setting up the objective functions (cost, peak inflow to the pond, total inflow volume to the pond) and decision variables (installation areas of LID units). User-determined amount of candidate solutions (one solution is one possible configuration of LID implementation in the study area, i.e., one possible combination of 960 decision variables) were then created based on the determined range of each decision variable. With the generated candidate solutions, the total cost of LID facilities was calculated with Eq. 3.2. The next step was to modify the SWMM input file according to the decision variables in each candidate solutions and run SWMM simulation by calling the dynamic link library files of SWMM (run one SWMM

simulation for one candidate solution). Running the SWMM engine function was adapted from MATSWMM, an open-source package developed by Riaño-Briceño et al. (2016).

The objective function value (peak inflow) was extracted from the SWMM report file once the simulation was completed. Each candidate solution corresponded to one SWMM simulation and one set of objective function values (cost and peak inflow). The optimization algorithm, PICEA-g, would next generate a new solution matrix based on objective function values, which were closer to the Pareto optimal solutions than the first candidate solutions. The follow-up steps were the same as the previous steps, and formed a loop of modifying SWMM inputs, running SWMM simulation, obtaining objective function values, and generating new solutions. The loop would stop when the generation of solutions met the maximum iteration number specified in the user's set up (i.e., in this study, the maximum number of iterations was set to 20).

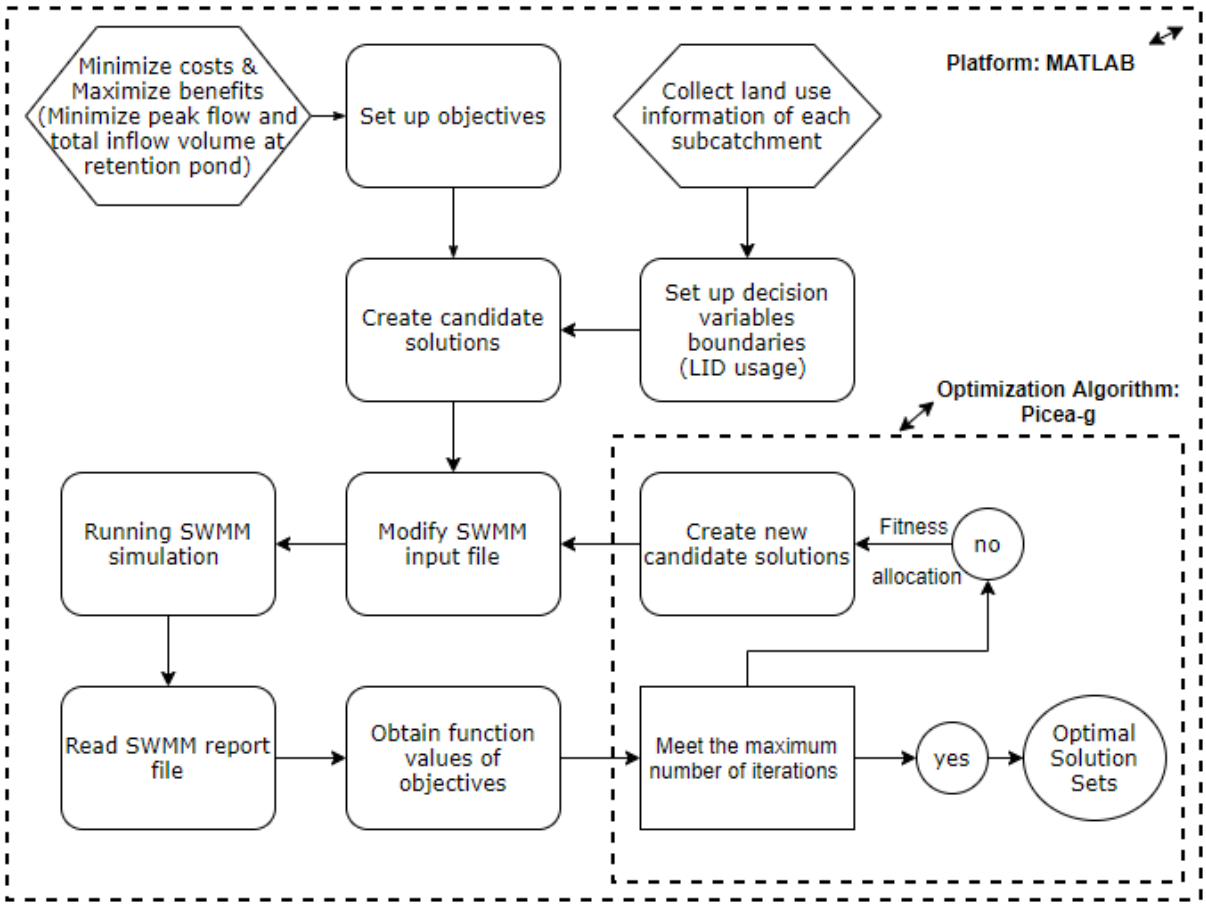

Figure 3.3 Overall process structure of LID layout optimization methodology

3.2.3 Modification on PICEA-g

3.2.3.1 Initialize candidate solutions

In the original PICEA-g algorithm, the value of each decision variable from the first candidate solutions is randomly generated inside the range of decision variable bounds. When the number of decision variables is small, diversity and randomness of candidate solutions can be acquired; however, when the number is large, the sum of decision variables gets close to the mean of the sum of decision variables' bounds (e.g., if there are 500 decision variables and each decision variable has a random value between 0 and 5, then the sum of these 500 decision variables would be close to $500 \times 5/2 = 1250$) and the diversity of candidate solutions diminishes. In this study,

there were 960 decision variables. With the original randomly-generated values of decision variables, the total area (sum of decision variables) and total cost (sum of objective functions) of LID implemented in the study area were mostly within ±5% range for the first candidate solution. This resulted in scenarios of low or high percentage of LID implementation not being considered. Therefore, the following modifications were made in initializing the first candidate solutions: (1) values of candidate solutions were linear uniformly distributed within constraints throughout the sets (reflecting diversity), and (2) the value was set to zero (i.e., no LID implementation) for randomly selected individual decision variables in half of the sets of candidate solutions (reflecting randomness). An example of 4 decision variables and 4 sets of solutions is represented in Figure A3.2 to better explain the modifications on initializing candidate solutions.

3.2.3.2 Enhanced goal vectors generation methodology – *cutting plane*

Because PICEA-g's performance is affected by goal vectors, especially the bounded space of goal vectors, Wang (2013) proposed an enhanced strategy called *cutting plane* to help in the generation of goal vectors that are more effective in guiding candidate solutions towards the Pareto optimal front. The *cutting plane* is used in this study to redefine the bound space of goal vectors, guaranteeing that no single goal vector dominates or is dominated by all candidate solutions. As shown in Figure A3.3, an example of an optimization problem of minimizing two objectives is used to explain the strategy of *cutting plane*.

3.2.3.3 Enhanced Fitness calculation

The fitness value is a mark of how individual of candidate solution population performs in reaching the Pareto optimal front (Wang, 2013). In the PICEA-g algorithm, the fitness value (*Fit*) of candidate solutions (*cs*) and goal vectors (*gv*) are calculated as Eqs. 3.3-3.5 (Wang, 2013):

$$Fit_{cs} = \sum_{g \in G \uplus G_C | s \preccurlyeq g} \frac{1}{n_{gv}} \tag{3.3}$$

$$Fit_{gv} = \frac{1}{1+\gamma} \tag{3.4}$$

$$\gamma = \begin{cases} 1 & n_{gv} = 0 \\ \dfrac{n_{gv}-1}{2N-1} & otherwise \end{cases} \tag{3.5}$$

where g and G represents goal vectors; G_C is the offspring goal vectors; s represents solutions; n_{gv} is the number of solutions that dominate the goal vector gv; and N is the population size of candidate solutions. One point dominates another point means the value of one point's position in all dimensions are smaller than those of another point when all objectives are minimized.

As shown in Appendix Context A3.2, two candidate solutions could have the same fitness value while one of them dominates the other. Therefore, the current fitness calculation method cannot sort candidate solutions adequately without considering the domination relationships among the candidate solutions themselves. Paknejad et al. (2021) proposed a new method to improve fitness value calculation as shown in Eqs. 3.6 – 3.7.

$$Fit_{cs} = \sum_{g \in G \uplus G_C | s \preccurlyeq g} \frac{1}{n_{gv}} \times Fit_{gv} + \frac{1}{rank_{cs}} \tag{3.6}$$

$$Rank_{cs} = 1 + P \tag{3.7}$$

where P is how many individuals dominate CS_i at the current population. Then, the new fitness values can sort the domination relationships between the candidate solutions. An example calculation is shown in Appendix Context A3.3.

3.2.3.4 Enhanced genetic operator – crossover and mutation

PICEA-g uses three types of crossover (i.e., single-point crossover, uniform crossover, and simulated binary crossover (Deb and Agrawal, 1994), and polynomial mutation (Deb et al., 2002) as genetic operators. The genetic operators are essential for the production of offspring solutions and the evolution of solutions. Adjustments or the acquisition of various genetic operators are required for different problems and scenarios in order to improve the algorithm performance (Srinivas and Patnaik, 1994). Paknejad et al. (2021) proposed a strategy for applying a *logistic map* and a *roulette wheel* in crossover and mutation operators, which was used and adjusted in this study to improve the LID spatial allocation solutions.

Logistic map

The *logistic map* was introduced by May (1976) to produce chaotic sequences, and its mathematical equation is written as:

$$X_{n+1} = rX_n(1 - X_n) \tag{3.8}$$

where X_n is a number bounded on [0, 1], and r is a parameter in the range of [0, 4]. The r value changes the behavior of the logistic sequence, e.g., when $3.57 < r \leq 4$, the logistic sequence develops chaotic behavior. The *logistic map* was applied in crossover and a mutation operator to increase the variation among the individual population and solution sets (Paknejad et al., 2021).

Roulette Wheel

The *roulette wheel* was applied in crossover operator for selecting one solution set from the entire solution population. The probability of selecting one CS_i is:

$$P(CS_i) = Fit_{CS_i} / \sum_{j=1}^{N} Fit_{CS_j} \quad (3.9)$$

Higher fitness value of one solution set means higher chance of being selected.

Crossover

The pseudo code of the crossover operator for this study is in Appendix Algorithm A3.2. The crossover operator extracts one individual solution from one of the two selected sets (one pair) of parent solutions at each index and combines them into one set of offspring solutions. For each set of parent solutions, its paired set of parent solutions were selected using *roulette wheel*. When a random number was less than a pre-set crossover probability, the crossover would operate on this pair of parent solutions. For each individual index of the new offspring solution, if the generated chaotic sequence by the *logistic map* was ≤ 0.5, this individual offspring solution was extracted from the first parent solution at the same index. Otherwise, it was extracted from the second parent solution.

Mutation

Detailed calculations are illustrated in the pseudo code of the enhanced mutation operator in Appendix Algorithm A3.3. With the enhanced mutation operator, solutions were guided to implement more cost-effective types of LID facilities in this study. The mutation operator increased the area of one type of LID facility (randomly selected from the four types) while decreasing the area of another type of LID facility (randomly selected from the rest three types). The adding and reducing areas of LID facilities were randomly chosen based on the *logistic map*.

3.2.4 Numerical experiments for evaluating algorithm modifications

Numerical experiments were conducted to evaluate the improvements of the LID SAO system after the modifications to the algorithm. Five scenarios were compared to demonstrate the improvements: 1) O-PICEA (the original PICEA-g algorithm without any modifications), 2) CS-PICEA (the PICEA-g algorithm with modification of initializing *CS*), 3) GV-PICEA (the PICEA-g algorithm with modification of new goal vectors methodology – *cutting plane*), 4) GV-CS-PICEA (the PICEA-g algorithm with modification of initializing *CS* and *cutting plane*), and 5) MOD-PICEA (the PICEA-g algorithm with modification of initializing *CS*, *cutting plane*, genetic operator including fitness, crossover, and mutation).

All the five scenarios were run with the identical parameters for the comparison: two objective functions (cost and peak inflow), 100 *CS* and *GV* population sizes, 20 maximum generations, and 1:2 year design storm events. MOD-PICEA was used to examine the hydrologic performance of LID implementation for all storm events (1:2, 1:5, 1:10, 1:25, 1:50, and 1:100) in the end. There are two types of optimal solutions: solutions with the highest fitness value; and non-dominated solutions. In this study, the quality of solution sets in any given generation was fully represented by solutions with the highest fitness value (fixed population), which were utilized to analyze the comparison and improvements across different scenarios. Non-dominated solutions (unfixed population) are the "absolute" optimal solutions in any given generation, and they were utilized to illustrate the optimized performance of LID in the final step.

3.3 Results and discussion

3.3.1 Improvement of optimization with the new *CS* initializing method

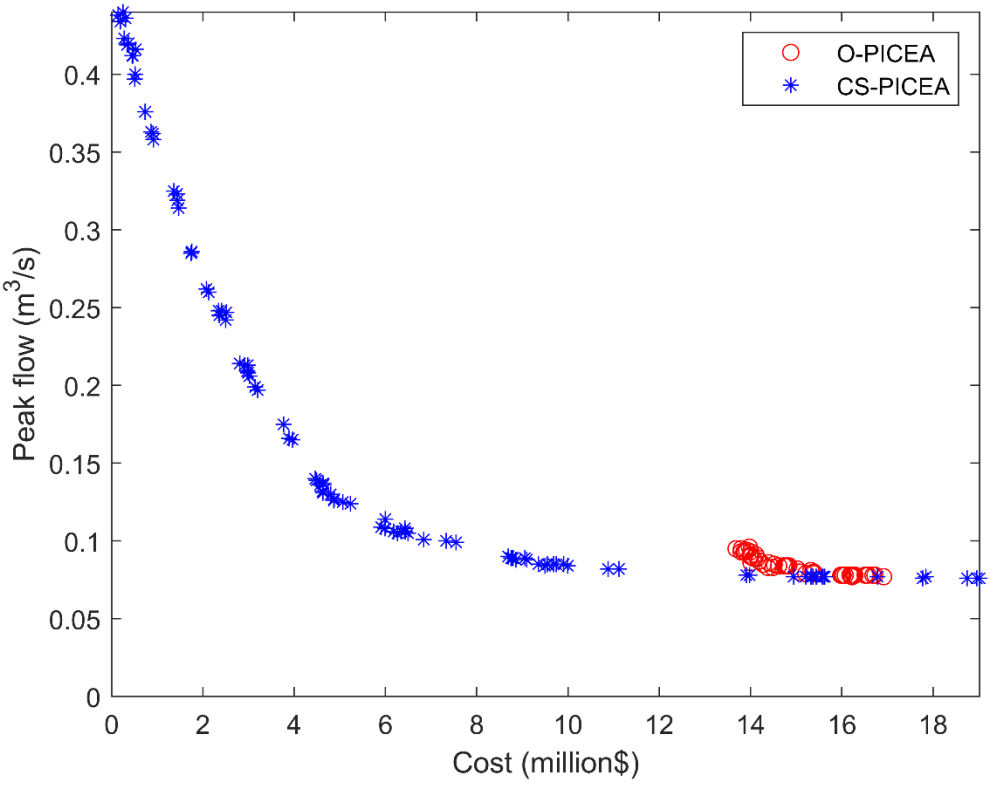

Figure 3.4 Comparison of 100 solutions with highest fitness values between O-PICEA and CS-PICEA

The optimal solutions (with highest fitness values) of O-PICEA and CS-PICEA were compared in Figure 3.4 to examine how initializing candidate solutions (*CS*) affects the algorithm's performance. In the figure, each dot represents one optimal solution, which is the combination of optimal values of 960 decision variables (installation areas of the 4 types of LID facilities in 240 subcatchment). The total cost of LID implementations from O-PICEA is between 13 million and 17 million dollars after candidate solutions evolves for 20 generations; while, from CS-PICEA, the total cost can be as low as 0 dollars (no LID implemented) and as high as approximately 19

million dollars. A wider price range gives the LID implementation more flexibility to meet the needs of project owner and designers. If the project budget is less than $10 million, for example, answers could be identified from CS-PICEA rather than O-PICEA. Furthermore, within the cost range of O-PICEA, CS-PICEA solutions dominated O-PICEA solutions, as shown by the fact that CS-PICEA solutions have a smaller peak flow than O-PICEA solutions with the same cost in the figure. This demonstrates that the diversity of candidate solutions (reflected in the variation of objective function values of candidate solutions) not only assists the algorithm in obtaining a complete perspective of optimal solutions, but also improves genetic operator performance.

When the quantity of decision variables is large (>100) in a MOP, it is essential to generate first candidate solutions diversely to cover all the possible extent of objective functions and avoid the precision of produced optimal solutions. Generating first candidate solutions by random values individually centralizes objective function values of solutions. Hence, initializing candidate solutions is critical to the algorithm's performance, and it is necessary for a range of issues with a large number of decision variables, depending on the MOP circumstance.

3.3.2 Improvement of optimization with cutting plane for *GV*

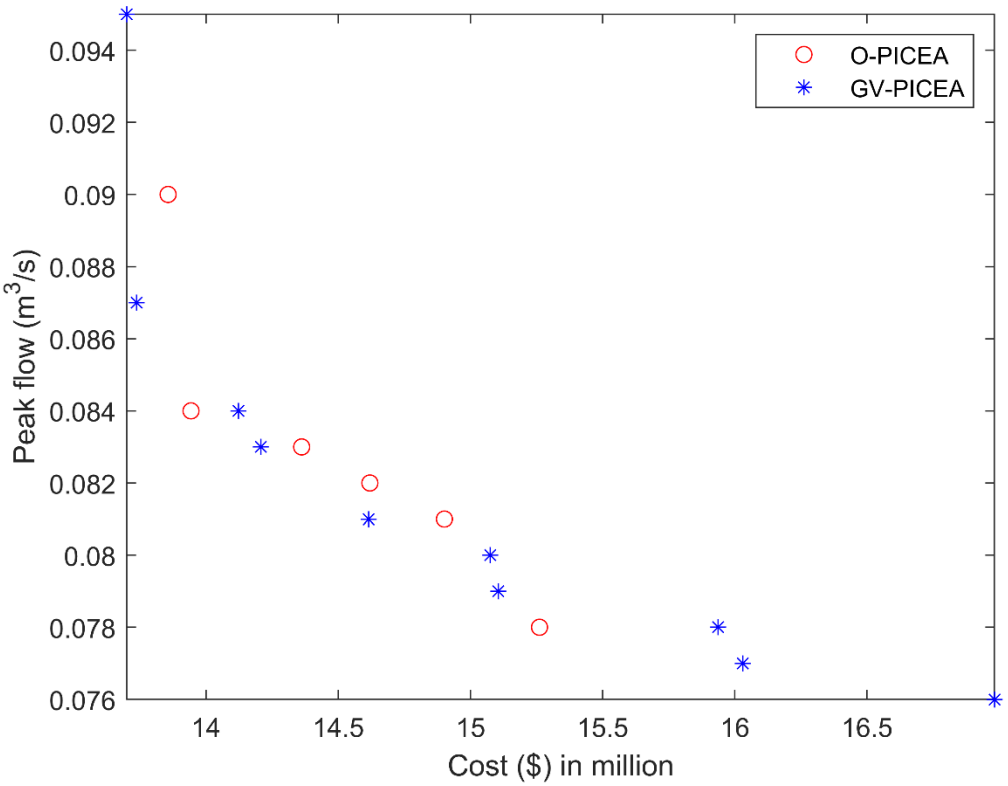

Figure 3.5 Comparison of the nondominated solutions between O-PICEA and GV-PICEA

The difference between the nondominated solutions of O-PICEA and GV-PICEA represents how efficient the *cutting plane* guides candidate solutions toward Pareto optimal front (Figure 3.5). The *cutting plane* increases the number of nondominated solutions from 6 (O-PICEA) to 10 (GV-PICEA). The total cost of the optimal solutions from O-PICEA is between 13.9 million and 15.2 million dollars. The *cutting plane* extends the cost range to be 13.8 – 17.0 million dollars. Meanwhile, within the cost range of 14.0 – 15.0 million dollars, the GV-PICEA optimal solutions dominate O-PICEA optimal solutions. From the comparison between the nondominated solutions of O-PICEA and GV-PICEA, it reveals that the *cutting plane* can more effectively direct candidate

solutions towards the Pareto optimal front while simultaneously increasing the diversity of candidate solutions.

3.3.3 Improvement of optimization with new genetic operators

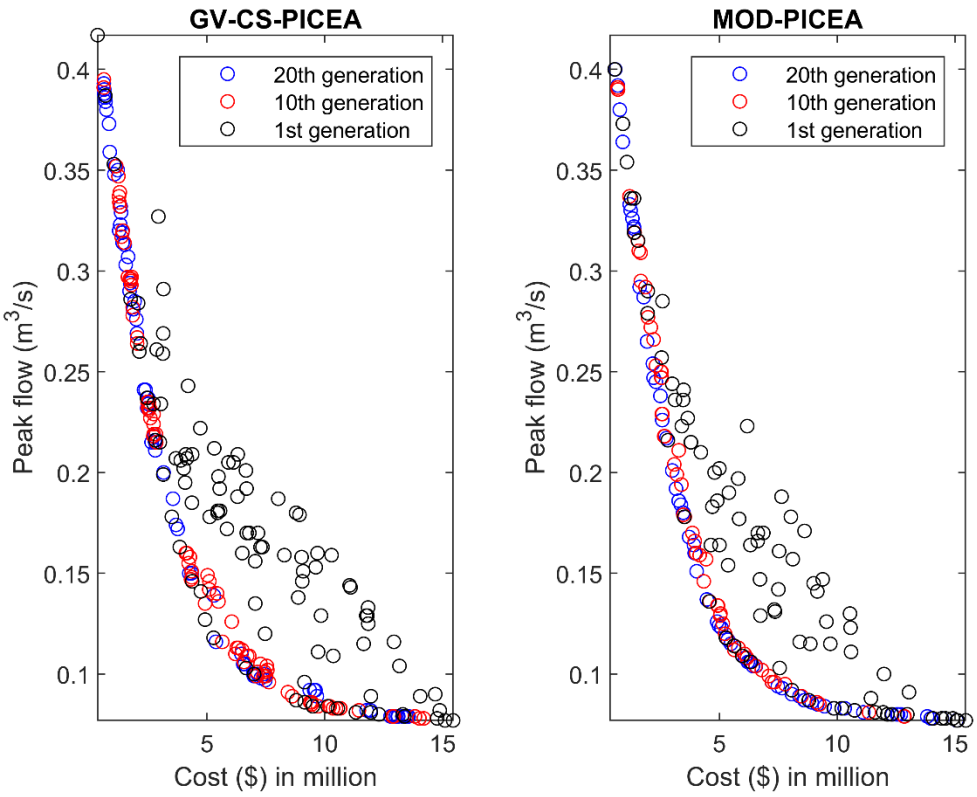

Figure 3.6 Evolving process of candidate solutions in GV-CS-PICEA and MOD-CS-PICEA

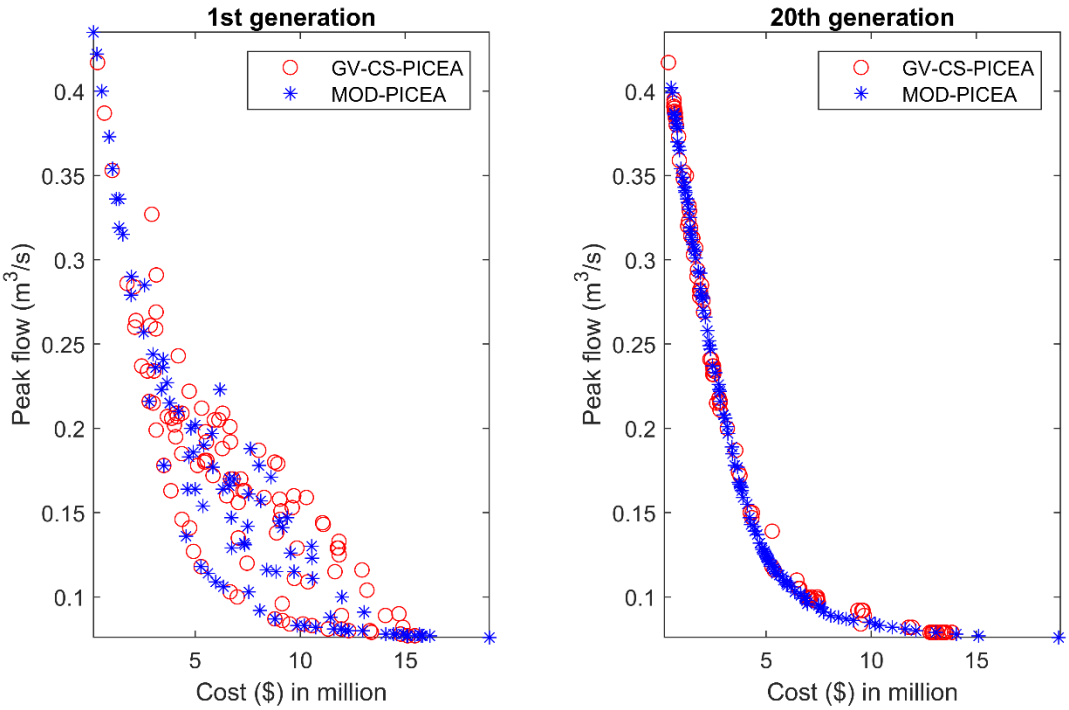

Figure 3.7 Comparison of optimal solutions between GV-CS-PICEA and MOD-CS-PICEA

The evolving processes of GV-CS-PICEA and MOD-PICEA are shown in Figure 3.6 by plotting solutions after evolving for 1, 10 and 20 generations. In both GV-CS-PICEA and MOD-PICEA, candidate solutions improve significantly from the 1st to the 10th generation, and are close to the Pareto optimum front, with a slight improvement from the 10th to the 20th generation in both cases. Comparison of optimal solutions (with highest fitness value) between GV-CS-PICEA and MOD-PICEA at the 1st generation and the 20th generation is illustrated in Figure 3.7. In the 1st generation, more candidate solutions from GV-CS-PICEA are dominated by the candidate solutions from MOD-PICEA rather than the opposite way. Optimal solutions form a smooth curve at the 20th generation from both GV-CS-PICEA and MOD-PICEA, although a few optimal solutions from GV-CS-PICEA lay outside the curve in the cost range of 5 – 15 million dollars. In brief,

modifications of initializing candidate solutions, the *cutting plane*, and the new approach of genetic operators, i.e., MOD-PICEA, improve the PICEA-g's performance on LID spatial allocation.

3.3.4 Performance of MOD-PICEA for the design storms

Nondominated solutions of the LID SAO system under 1:2, 1:5, 1:10, 1:25, 1:50, and 1:100 year design storm events are displayed as peak inflow to the pond versus cost in Figure 3.8. The total inflow volume corresponding to the optimal solutions is presented in Figure 3.9. The solution points of peak inflow and total inflow volume have a similar trend due to the close correlation between them for the same catchment. As the intensity of design storms increases from 1:2 to 1:100 year event, the trend of solution points transforms from a convex curve towards a straight line.

The peak inflows into the retention pond are 0.47, 0.71, 0.86, 1.08, 1.26, and 1.44 m^3/s with zero cost of LID (i.e., no LID implementation) during 1:2, 1:5, 1:10, 1:25, 1:50, and 1:100 year design storm events, respectively. The peak inflows reduce to 0.07, 0.14, 0.24, 0.41, 0.54, 0.67 m^3/s, respectively, when LID is fully installed at available space with a capital cost of around 10 million and a total cost of 34 million dollars for 25 years. The reduction rates in peak inflow are 85%, 80%, 73%, 62%, 57%, and 54% for 1:2, 1:5, 1:10, 1:25, 1:50, and 1:100 year storm events, respectively. Without any LID implementation, the total inflow volumes are 0.86, 1.35, 1.74, 2.35, 2.83, and 3.31 thousands m^3 for these storm events. With the maximum LID implementation at a cost of approximately \$34 million, the total inflow volumes are 0.18, 0.32, 0.50, 0.82, 1.07, and 1.33 thousands m^3, respectively, which correspond to 79%, 76%, 71%, 65%, 62%, and 60% reductions, respectively.

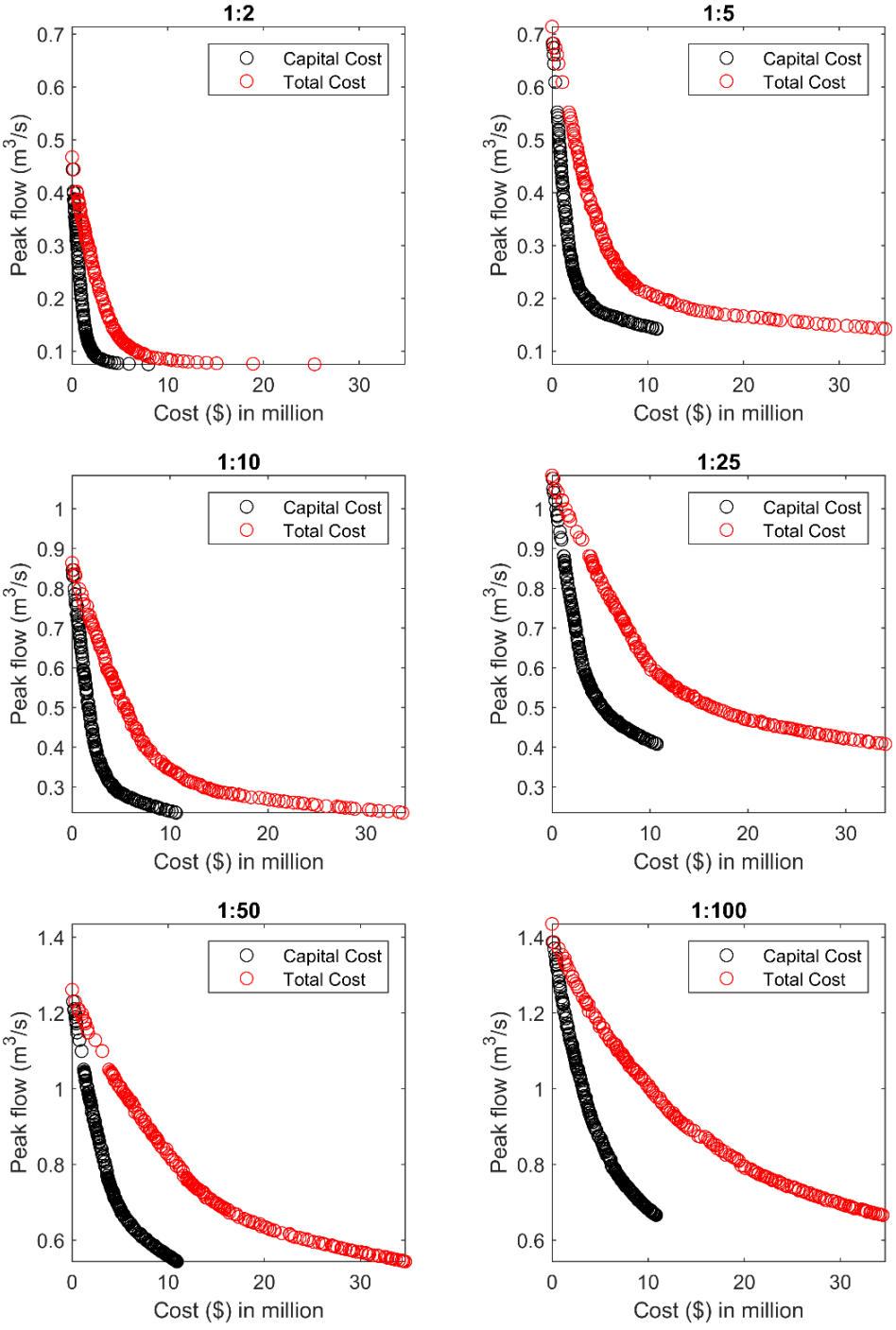

Figure 3.8 Nondominated solutions of peak inflow to the retention pond versus cost during 1:2, 1:5, 1:10, 1:25, 1:50, and 1:100 year design storm events.

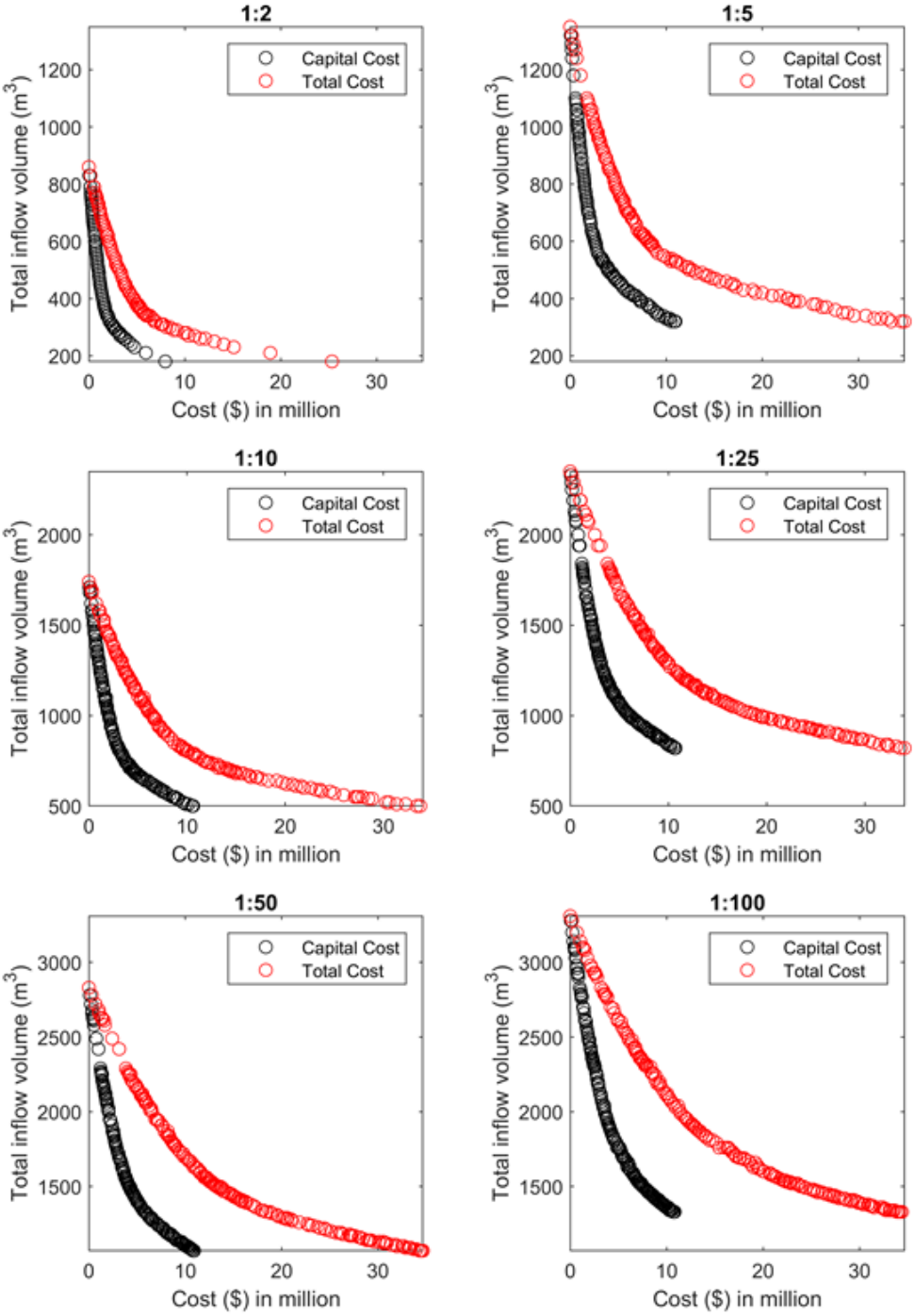

Figure 3.9 Nondominated solutions of total inflow volume to the retention pond versus cost during 1:2, 1:5, 1:10, 1:25, 1:50, and 1:100 design storm events.

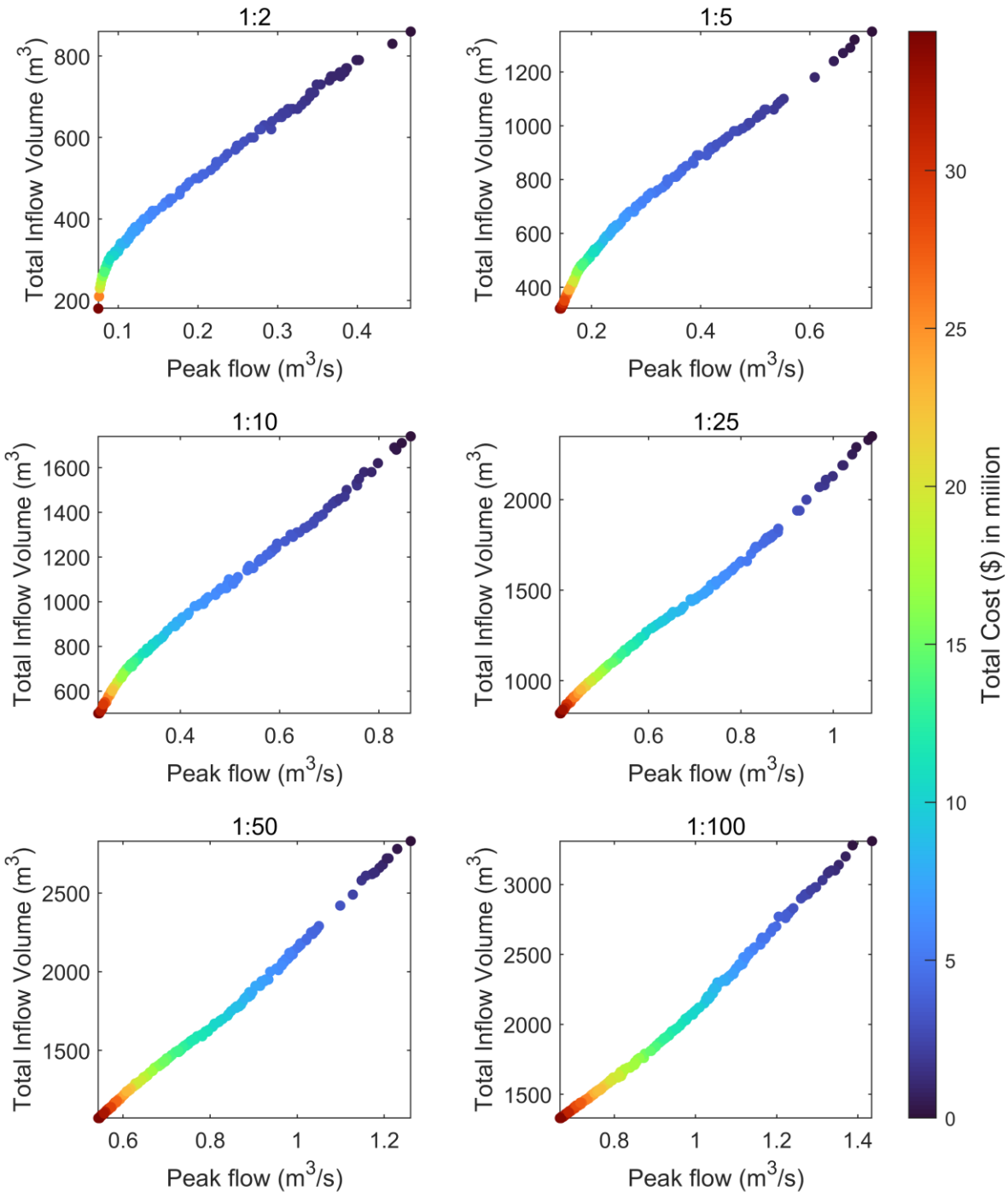

Figure 3.10 Scatter plot of solutions with total inflow volume and peak inflow to the retention pond, as well as cost for 1:2, 1:5, 1:10, 1:25, 1:50 and 1:100 year design storms.

A 3D scatter plot with a color bar of the three variables (total inflow volume, peak inflow, and total cost) is shown in Figure 3.10 to further understand the correlation between the total inflow volume and the optimized peak inflow. In the case of a fixed total cost, the solution points of the total inflow volume versus peak inflow display approximately linear trends for all design storms, indicating that total inflow volume was auto-optimized simultaneously with the optimization of peak inflow and cost. The total inflow volume is the sum of the area under the inflow hydrograph, and the high relevance between the two hydrologic parameters could be the explanation for this approximately linear correlation.

Table 3.5 Solutions A, B, C, D, E, and F as examples of optimal solutions during 1:2, 1:5, 1:10, 1:25, 1:50, and 1:100 year design storm events

Design Storm	Capital Cost ($ million)	Total Cost ($ million)	Peak flow (m^3/s)	Peak flow reduction (%)	Total Inflow Volume (m^3)	Total Inflow Volume Reduction (%)	Total LID implementation area (m^2)
1:2	1.83	5.83	0.11	75.8%	350	59.3%	7257
1:5	2.85	9.73	0.22	68.8%	550	58.5%	11322
1:10	3.76	12.03	0.31	62.3%	740	57.5%	15015
1:25	5.19	16.51	0.50	52.5%	1050	55.3%	20574
1:50	6.64	21.10	0.62	49.8%	1270	55.1%	26288
1:100	7.51	26.10	0.75	47.5%	1460	54.7%	29758

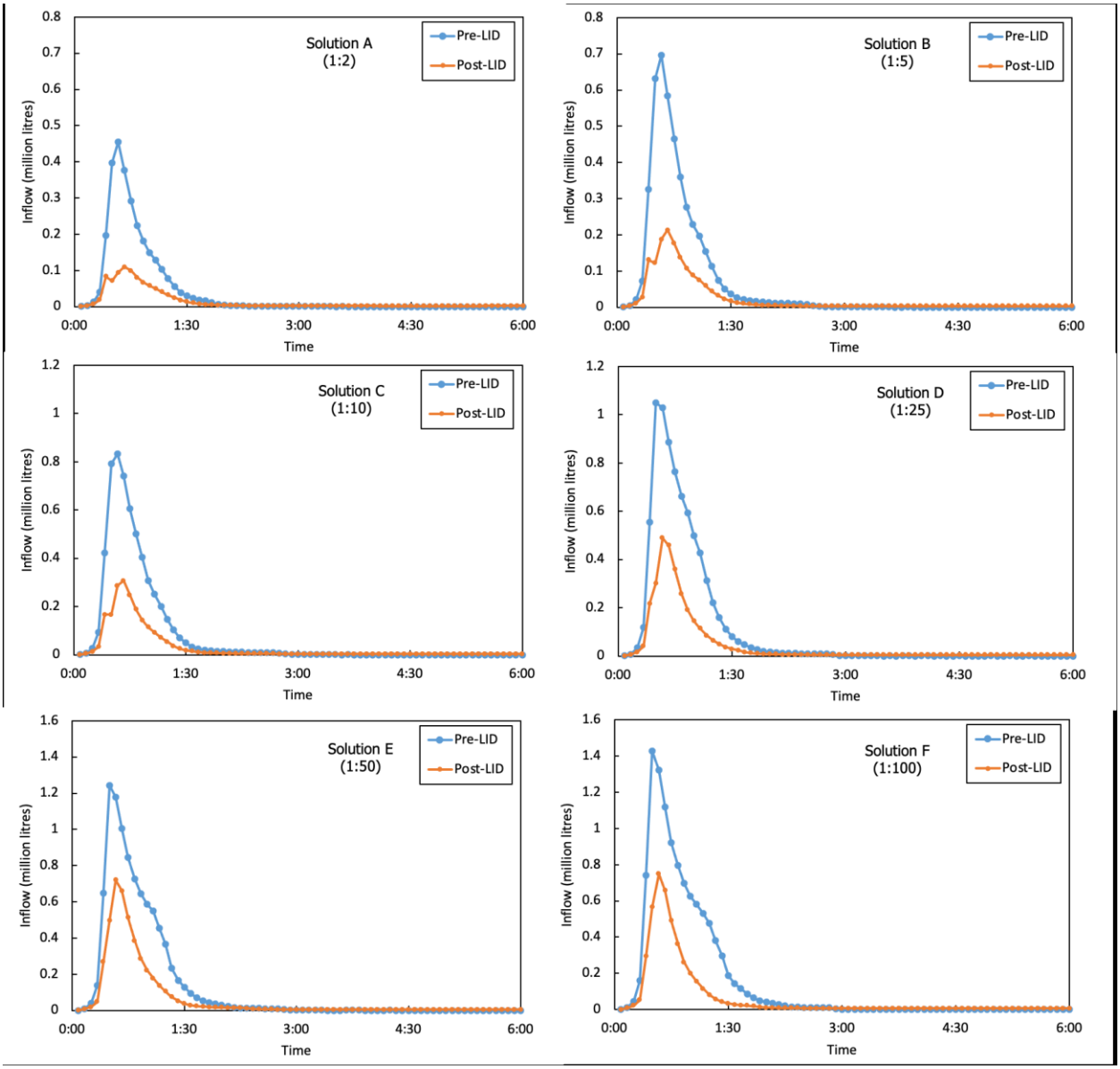

Figure 3.11 Time series of inflow rate to the retention pond during 1:2, 1:5, 1:10, 1:25, 1:50, and 1:100 year storm events. The two lines in each sub-figure represent those before and after LID installations (for Solutions A, B, C, D, E, and F).

Using the 1:2 year storm event as an example, the optimal solutions can be divided into three parts: an upper part (with total cost of 0- 5 million), a middle part (with total cost of 5-10 million), and a lower part (with total cost of 10 – 30 million), as shown in Figure 3.8. In the upper and lower parts, the solution points follow a linear trend, while they follow a convex curve in the middle part. The

density of the solution points is higher in the middle part than in the upper and lower parts, because the number of combinations of decision variables is much larger in the middle range. There is little opportunity to improve the LID spatial allocation when there is nearly little to no LID implementation in the study area (i.e., with close to zero cost) or when LID is implemented with coverage that is close to the maximum area constraints (i.e., the decision variables of one solution at each index are close to the upper bounds). Therefore, the candidate solutions in the upper and lower parts are closer to the Pareto optimal front, while the solutions in the middle part have more potential to evolve in the early generations. A small increase in the total cost of LID could yield a relatively significant peak inflow reduction in the upper part where the benefit-cost ratio (i.e., the slope of the solution points) is high, while the peak inflow would hardly decrease incrementally by adding a large cost of LID in the lower part where the benefit-cost ratio is low.

A turning point occurs where the slope of solution points ($\Delta y/\Delta x$) starts to decrease, i.e., the endpoint of the upper part. This point is interpreted as the optimal solution that maximizes the benefit-cost ratio among all the solutions. Based on the trend of solution points, three points, A, B, C, D, E, and F were chosen from the 1:2, 1:5, 1:10, 1:25, 1:50 and 1:100 year storms events, respectively, as examples. These six solutions are listed in Table 3.5. The total LID implementation area of solutions A, B, C, D, E, and F is 7257, 11322, 15015, 20574, 26288, and 29758 m^2, respectively. The capital costs are 1.83, 2.85, 3.76, 5.19, 6.64, and 7.51 million dollars, respectively, and their total costs for 25 years are 5.83, 9.73, 12.03, 16.51, 21.10, and 26.10 million dollars, respectively. The peak inflow reductions of solutions A, B, C, D, E, and F are 75.8%, 68.8%, 62.3%, 52.5%, 49.8%, and 47.5%, respectively, and their total inflow volume reductions are 59.3%, 58.5%, 57.5%, 55.3%, 55.1%, and 54.7%. The results demonstrate that LID has promising benefits of peak inflow reduction (over 60% of peak inflow reduction) with relatively

low cost (under 5 million dollars of capital cost) for small storm events (1:2, 1:5, and 1:10 year). Figure 3.11 shows the time series of the inflow rate for solutions A, B, C, D, E, and F. After LID implementation, a dual peak of the inflow can be detected for solutions A, B, and C. This observation reflecting the 5 minute delay in the flow arriving from the area where the LID is implemented relative to the area surrounding the detention pond which drains more quickly in the retention pond and creates the first peak.

Men et al. (2020) studied LID spatial allocation optimization and three optimal solutions were also selected for 1:2, 1:10, and 1:50 year storm events (rainfall intensity information is not available in Men et al. (2020)'s paper; total runoff depth was 28.2, 47.9, and 69.2 mm, respectively) under peak flow-cost optimization scheme. With total construction cost of 9.8, 10.4, and 7.6 million CNY (The construction cost of permeable pavement, green roof, vegetable swale, and rain barrel is 193 CNY/m^2, 500 CNY/m^2, 220 CNY/m^2, and 350 CNY/each; Currency CNY:CAD = 5.1:1.0), LID implementation reduced runoff by 21.8, 17.3, and 17.0%, and reduced peak flow by 15.6%, 11.8%, and 8.0%, respectively. The total area of Men et al. (2020)'s study area was 94 hectares, which is approximately 6.2 times the total area of this paper's study area. Because of the difference at construction cost and the lack of detail LID implementation area for each selected optimal solution in Men et al. (2020)'s study, a rough estimate of LID implementation area is calculated as 39,000, 42,000, and 30,000 m^2 for 1:2, 1:10, and 1:50 year storm events. For 1:2 and 1:10 storm events, the LID implementation area in Men et al. (2020)'s study is approximately 6 and 3 times the LID implementation area in our study. The optimal solutions with BR, RG, PP, and GR installation in this study appear to have better hydrologic performance with similar area ratios of LID implementation. The hydrologic performance of LID implementation, on the other hand, is affected by the type of LID facility, drainage region topography, and rainfall pattern.

3.3.5 Application of the LID SAO system in other neighborhoods and its limitations

The LID SAO system introduced in this study provides the flexibility and feasibility for users to adapt it to other objectives or different drainage areas, with minor code adjustments. Optimization of LID implementation to achieve water quality benefits can be easily added into the SAO system by incorporating one or more additional objective functions reflecting water quality, setting up the water quality parameters in the SWMM model, and processing the relevant results from the output file, similarly as how the hydrologic objective functions were implemented in this study. Users can incorporate different water quality objectives or other objectives as project requirements into the SAO system by using the corresponding equations for computing the objectives, as demonstrated by Liu et al. (2016), Xu et al. (2017), Men et al. (2020), and Dong et al. (2021). Other objectives, such as maximum hydrologic benefits/cost ratio or maximum water quality benefits/cost ratio, can also be accomplished by changing objective functions of the SAO system.

The SAO system can be applied at a variety of study scales. Users can identify lumped areas as subcatchments within a much larger study area, such as a city, as done by Liu et al. (2016) and Xu et al. (2017), distinguish land use information (e.g., with the help of GIS information) to find suitable locations for different LID facilities, and change decision variable bounds accordingly. For a large drainage area, an area ratio rather than a particular LID footprint can be considered for the decision variables. Different LID practices or LID design parameters can be changed to suit different design preferences and standards in different cities or countries by simply changing/adding LID controls to the SWMM model or changing the LID control parameters in the SWMM input file with a simple adjustment on the input file modification function. The SAO system provides users a conceptual appreciation of the approximated area sizes

and types of LID throughout the study area, yielding maximum hydrologic benefits and/or water quality benefits at minimized cost (Pareto front of optimized solutions).

This SAO system also provides the flexibility to use any open source stormwater management software by calling the dynamic link library (DLL) file in the loop of MOEA. Instead of using SWMM as a hydrologic process computation engine, any other stormwater management software (e.g., MIKE) can also take the place of SWMM for different projects if the access of external use is acquired. Other optimization algorithms (e.g. NSGA-II) can replace PICEA-g in this system, and modifications can be made.

When implementing an LID SAO system, a few ground rules apply. First, SWMM model itself should have been calibrated. Secondly, users should use representative LID control parameters in the SWMM model to ensure that they properly represent the hydrologic or water quality benefits of actual LID installations. Last, the representation of the configuration of the LID implementation and flow routine in SWMM model should be adjusted to reflect the intended configuration (e.g., when a LID facility is installed along the roadside and collects all runoff from the road, the LID facility's treatment area must be configured to be equivalent to the road area).

The application of the LID SAO system as presented in this study has a few limitations. First, no pre-screening was implemented to determine potentially suitable locations for each LID practice. Maximum allowable usage for each type of LID facility in each subcatchment was evaluated in this study as a constraint purely based on the area of different land use. SUSTAIN and similar software packages could have an adequate LID spatial availability analysis to set up more practical constraints for the system, reduce unnecessary decision variables, and improve the performance of the optimization algorithm with more detailed geographical information (comprehensive GIS data).

Second, the current LID SAO system may not be able to achieve good optimal solutions for a single subcatchment because the optimization is based on the entire sets of solutions (one set of solutions considers the entire drainage area). When the number of generations and the size of the solution population increase, the computing time will become a concern. After the 20^{th} generation, the incremental improvements in the overall solutions have become minimal, as seen in Figure 3.10. This problem can be solved using the divide and conquer technique and this method has been used to solve complicated multi-objective optimization problems in several studies that are not for LID (Cooper et al., 2014; Lü et al., 2016; Friese, 2016; Qian, 2019). Instead of optimizing the spatial allocation of LID practices for the entire drainage area, SAO system can be decomposed to optimize LID installation for each individual subcatchment, and then combine those optimal solutions into new sets of optimal solutions for the entire drainage area as a possible option to improve the SAO system.

3.4 Conclusions and future research

LID has been attracting more and more attention for sustainable urban stormwater management, and various LID spatial allocation optimization tools have been developed to seek cost-effective implementation plans. This study proposes an efficient optimization system that integrated SWMM and PICEA-g using MATLAB as a platform, which was then applied to optimize LID implementations in a neighborhood area located in Calgary, Canada. Through numerical experiments, modifications such as enhanced functions of initializing candidate solutions, cutting plane, and genetic operators adopting the *logistic map* and *roulette wheel* have been shown to increase the algorithm performance. The selected optimal solutions in this study area showed that LID implementation provides hydrologic benefits of reducing peak inflow, lowering total runoff volume, and delaying peak inflow with relatively low capital cost (compared to the capital cost of

maximum allowable LID implementations). Due to the high correlation between the objective functions of peak inflow and total inflow volume to the downstream retention pond, optimal solutions by optimizing peak inflow and cost automatically optimize the total inflow volume.

Comparison of different stages of modifications to the optimization system demonstrated that it is essential to generate first candidate solutions diversely to cover all the possible extent of the objective function values, and avoid the precision of produced optimal solutions, to obtain the diversity and improve the convergence (closer to the Pareto optimal front) of non-dominated solutions. The cutting plane helps to sort candidate solutions and increase the diversity of candidate solutions by making every goal vectors useful. However, application of only the cutting plane approach does not improve the algorithm performance noticeably if genetic operators are not modified. The *logistic map* produces a chaotic sequence which improves the diversity and randomness of offspring solutions. The Roulette wheel gives the parent solution with a higher fitness value a higher chance to be selected, which accelerates the convergence of the offspring solutions. Applying the *logistic map* and roulette wheel with advanced fitness calculation proposed by Pajnejad (2021) demonstrated a significant improvement in the algorithm performance.

The LID SAO system proposed in this paper gives users a lot of flexibility, allowing them to use it in different study areas in different scales, different objectives (water quality), and different optimization algorithms with customized modifications, as well as replace SWMM with other stormwater computing engines. The LID SAO system can be further improved in the future. A pre-screening that preliminarily screens suitable places for LID implementations can improve the performance of the optimization algorithm and provide a more practicable plan. In order to determine the spatial availability of LID, it is necessary to collect appropriate geographic information about the study area. In addition, using MOEA with divide and conquer (decompose

decision variables) techniques and parallel computing to improve optimization system performance can be a viable alternative.

Chapter 4 General conclusions and future research directions

Numerical simulation is a powerful, cost-effective tool for LID design and implementation to achieve sustainable urban stormwater management. Lab and field experiments provide benchmark data for numerical simulation, while numerical simulation can further improve the understanding on LID performances and mechanisms under different conditions (e.g., cold climates) and at different scales (e.g., single-unit and neighborhood scale), based on which LID design, planning, operation and maintenance can be improved and optimized. Moreover, numerical simulation can provide insights on future experiments.

Detailed conclusions on single-unit LID (bioretention) modeling and neighborhood scale modeling have been provided in Chapters 2 and 3 of the thesis, respectively. General conclusions from these two studies are summarized below.

- Based on calibrated and validated soil hydraulic parameters using experimental data, bioretention shows the great potential to handle or mitigate large storm events (> 50 mm in cumulative depth) in terms of peak inflow, volume and ponding depth.
- According to calibration and validation with limited experimental data in winter condition, bioretention has high potential of preferential flow in cold climates due to freeze/thaw cycles. The hydraulic conductivity is still high when the soil is partially frozen. The finer soil media experiences an increase of K_S after freeze-thaw cycles, while the opposite for coarser soil media, based on the limited data so far.
- Bioretention has high contaminant removal rates for phosphate and ammonium, but low removal rate for nitrate due to the soil itself (nitrogen rich) and denitrification based on the current data from the experiments.

- A new LID spatial allocation optimization (SAO) system was developed by integrating SWMM and PICEA-g and using MATLAB as the platform to optimize LID implementation at neighborhood scale.
- By applying the new LID SAO system in Calgary, Canada, LID implementation at neighbourhood scale has significant hydrologic benefits in reducing peak inflow (> 60%), lowering total runoff volume (> 55%), and delaying peak inflow with relatively low capital cost (< 5 million dollars) for small storm events (< 25 mm rainfall depth).

Future research directions on bioretention modeling are suggested below:

- To improve the model calibration of bioretention, it is suggested to a) measure hydraulic properties of each soil layer, b) conduct simple storm event experiments for each soil layer (one soil column contains only one type of soil layer) to calibrate initial soil hydraulic parameters, c) record soil water content throughout the columns in the experiments, and d) record soil temperature throughout the columns in cold condition.
- More numerical studies and laboratory and field experiments on LID (including bioretention) are needed to understand their performances of both hydrologic and water quality aspects in cold climates (for cold regions or winter seasons of warm regions). Specifically, it is important to examine the changes in soil parameters caused by soil freezing, the presence of preferential flow, and the impact of freeze/thaw cycles. Current relevant studies are rather scarce.
- More work is needed on 2-D or 3-D modeling of LID (including bioretention) to examine the spatial variability of LID performance. This need is particularly true in practical LID application, in which the inflow to LID is typically from one side and therefore spatial

variability of LID performance (both hydrologic and water quality aspects) is expected. Current software packages on the market are not able to conduct such simulations.

- More modeling studies (and experiments) are needed on the temporal variability of LID (including bioretention), particularly examining the long-term operation on LID performance (both hydrologic and water quality aspects). For instance, the impact of compaction, weather impact, and pollutants (e.g., TSS) to soil media. Currently, long-term modeling and monitoring on LID are limited.
- More studies are needed for modeling more parameters of water quality such as TSS. It is important to understand the LID's ability to remove pollutants from all perspectives in order to evaluate its water quality performance comprehensively. Currently, limited studies have modelled various pollutants removal parameters simultaneously, and TSS removal is particularly challenging due to the complexity of the physical process of flow through soil pores.
- More modeling (and experimental) studies are needed to examine the impact of extreme weather (e.g., droughts and severe storms) in the context of climate change to LID performance (both hydrologic and water quality aspects).

Future research directions on LID spatial allocation optimization (SAO) system are suggested below:

- More studies are needed to modify and enhance the optimization algorithm to improve its performance in LID spatial allocation problem. Current optimization algorithms are typically tested only on mathematical multi-objective optimization problems (e.g., functions that contain variables of x, y, z) and do not take into account practical problems with complicated objectives

and constraints on decision variables (e.g., LID spatial allocation problem with objectives related to hydrologic performance and water quality and a large amount of decision variables with different bound range for each decision variable). No previous studies have modified the optimization algorithm for the purpose of LID spatial allocation.

- More work is needed to evaluate the performance of the optimization algorithm with more than two objectives. When considering both hydrology and water quality with cost, achieving optimal solutions with a good balance of all objectives are challenging. Meanwhile, the difficulty of modifying the algorithm increases as the number of solution dimension increases. To the best of the author's knowledge, there are no studies that compare three-objective optimization to two-objective optimization. Optimization solutions form a plane in three-objective optimization instead of a line in two-objective optimization and picking one adequate optimal solution from a plane is complicated. To solve this problem, adding weights to different objective functions can be a feasible way.
- More studies are needed for decomposing the optimization process from total drainage area into some defined subarea (e.g., the total drainage area can be divided into headwater zone, middle zone, and outlet zone) or the individual subcatchments. This can be used to screen out potentially unsuitable locations where LID implementation has a negligible effect on overall hydrologic and water quality performance. This concept has been overlooked in previous studies. Applying MOEA with a divide and conquer strategy using parallel computing is a possible alternative for improving the performance of the optimization system.
- More efforts are needed to develop a graphical user interface for the system to make it more user-friendly for the public.

- It is suggested to collect sufficient geographic information about the study area to help determine the spatial availability for LID implantation before conducting the spatial allocation optimization.

References

Ahiablame, L. M., Engel, B. A., & Chaubey, I. (2012). Effectiveness of low impact development practices: literature review and suggestions for future research. *Water, Air, & Soil Pollution*, *223*(7), 4253-4273.

Al-Houri, Z. M., Barber, M. E., Yonge, D. R., Ullman, J. L., & Beutel, M. W. (2009). Impacts of frozen soils on the performance of infiltration treatment facilities. *Cold Regions Science and Technology*, *59*(1), 51-57.

Allaire, S. E., Roulier, S., & Cessna, A. J. (2009). Quantifying preferential flow in soils: A review of different techniques. *Journal of Hydrology*, *378*(1-2), 179-204.

Alsubih, M., Arthur, S., Wright, G., & Allen, D. (2017). Experimental study on the hydrological performance of a permeable pavement. *Urban Water Journal*, *14*(4), 427-434.

Brown, R. A., Skaggs, R. W., & Hunt Iii, W. F. (2013). Calibration and validation of DRAINMOD to model bioretention hydrology. *Journal of hydrology*, *486*, 430-442.

Cano, O. M., & Barkdoll, B. D. (2017). Multiobjective, socioeconomic, boundary-emanating, nearest distance algorithm for stormwater low-impact BMP selection and placement. *Journal of Water Resources Planning and Management*, *143*(1), 05016013.

Carsel, R. F., & Parrish, R. S. (1988). Developing joint probability distributions of soil water retention characteristics. *Water resources research*, *24*(5), 755-769.

Chang, N. B., Lu, J. W., Chui, T. F. M., & Hartshorn, N. (2018). Global policy analysis of low impact development for stormwater management in urban regions. *Land Use Policy*, *70*, 368-383.

Chapman, C., & Horner, R. R. (2010). Performance assessment of a street-drainage bioretention system. *Water Environment Research*, *82*(2), 109-119.

Chung, S. O., & Horton, R. (1987). Soil heat and water flow with a partial surface mulch. *Water Resources Research*, *23*(12), 2175-2186.

Clapp, R. B., & Hornberger, G. M. (1978). Empirical equations for some soil hydraulic properties. *Water resources research*, *14*(4), 601-604.

COE (City of Edmonton). 2014a. Low Impact Development Best Management Practices Design Guide. City of Edmonton, Edmonton, Alberta. Edition 1.1: 1-269.

COE (City of Edmonton). 2014b. Drainage Design and Construction Standards. City of Edmonton, Edmonton, Alberta. Volume 3: 1-129.

Coffman, L. S. (2002a). Low Impact Development: Smart technology for clean water-Definitions, issues, roadblocks, and next steps. In *Global Solutions for Urban Drainage* (pp. 1-11).

Coffman, L. S. (2002b). Low-impact development: an alternative stormwater management technology. In R. L. France (Ed.), Handbook of water sensitive planning and design (pp. 97–124). Washington, D.C.: Lewis.

Cooper, I. M., John, M. P., Lewis, R., Mumford, C. L., & Olden, A. (2014, July). Optimising large scale public transport network design problems using mixed-mode parallel multi-objective evolutionary algorithms. In *2014 IEEE Congress on Evolutionary Computation (CEC)* (pp. 2841-2848). IEEE.

Da-Bang, J. I. A. N. G., & Na, W. A. N. G. (2021). Water cycle changes: interpretation of IPCC Sixth Assessment Report. Advances in Climate Change Research, 0.

Davis, A. P. (2007). Field performance of bioretention: Water quality. *Environmental Engineering Science*, *24*(8), 1048-1064.

Davis, A. P. (2008). Field performance of bioretention: Hydrology impacts. *Journal of Hydrologic Engineering*, *13*(2), 90-95.

Davis, A. P., Hunt, W. F., Traver, R. G., & Clar, M. (2009). Bioretention technology: Overview of current practice and future needs. *Journal of environmental engineering*, *135*(3), 109-117.

Deb, K., & Agrawal, R. B. (1994). Simulated binary crossover for continuous search space (Technical Report No. IITK/ME/SMD-94027). *Indian Institute of Technology, Kanpur*.

Deb, K., Thiele, L., Laumanns, M., & Zitzler, E. (2002, May). Scalable multi-objective optimization test problems. In *Proceedings of the 2002 Congress on Evolutionary Computation. CEC'02 (Cat. No. 02TH8600)* (Vol. 1, pp. 825-830). IEEE.

DeBusk, K. M., & Wynn, T. M. (2011). Storm-water bioretention for runoff quality and quantity mitigation. *Journal of Environmental Engineering*, *137*(9), 800-808.

Dell, T., & Brim, J. (2017). Bioretention Media Mixtures–A Literature Review. *City of Fort Collins*.

Demand, D., Selker, J. S., & Weiler, M. (2019). Influences of macropores on infiltration into seasonally frozen soil. *Vadose Zone Journal*, *18*(1), 1-14.

Denich, C., Bradford, A., & Drake, J. (2013). Bioretention: assessing effects of winter salt and aggregate application on plant health, media clogging and effluent quality. *Water Quality Research Journal of Canada*, *48*(4), 387-399.

Dhalla, S., & Zimmer, C. (2010). Low Impact Development Stormwater Management Planning and Design Guide. *Toronto and Toronto and Region Conservation Authority: Toronto, ON, Canada*, *300*.

Dietz, M. E. (2007). Low impact development practices: A review of current research and recommendations for future directions. *Water, air, and soil pollution*, *186*(1), 351-363.

Dimmell, M. (2021). Our Weight in Canada: Western Canadian population growth tips the scales. *Canada West Foundation.* https://cwf.ca/research/publications/our-weight-in-canada-western-canadian-population-growth-tips-the-scales/

Ding, B., Rezanezhad, F., Gharedaghloo, B., Van Cappellen, P., & Passeport, E. (2019). Bioretention cells under cold climate conditions: Effects of freezing and thawing on water infiltration, soil structure, and nutrient removal. *Science of the Total Environment*, *649*, 749-759.

District, M. H. F. (2020). Engineered Bioretention Media Literature Review.

Dong, X., Yuan, P., Song, Y., & Yi, W. (2021). Optimizing Green-Gray Infrastructure for Non-Point Source Pollution Control under Future Uncertainties. *International Journal of Environmental Research and Public Health*, *18*(14), 7586.

Duffy, S., Shackelton, L. A., & Holmes, E. C. (2008). Rates of evolutionary change in viruses: patterns and determinants. *Nature Reviews Genetics*, *9*(4), 267-276.

Duzgun, A. O., Hatipoglu, M., & Aydilek, A. H. (2021). Shear and Hydraulic Properties of Compost-Amended Topsoils for Use on Highway Slopes. *Journal of Materials in Civil Engineering*, *33*(8), 04021192.

Eckart, K., McPhee, Z., & Bolisetti, T. (2017). Performance and implementation of low impact development–A review. *Science of the Total Environment*, *607*, 413-432.

Edmonton weather nerdery. (2019). *Freeze/Thaw Cycles: Part 1.* http://edmontonweathernerdery.blogspot.com/2019/03/freezethaw-cycles-part-1.html.

Elliott, A. H., & Trowsdale, S. A. (2007). A review of models for low impact urban stormwater drainage. *Environmental modelling & software*, *22*(3), 394-405.

EPA, U. (2000). Low Impact Development (LID), A Literature Review. *Washington, DC, US Environmental Protection Agency, Office of Water and Low Impact Development Center*.

EPCOR. (2018). *2018 EPCOR IDF CURVES.* https://www.epcor.com/products-services/drainage/service-for-new-developments/Documents/2018-EPCOR-IDF-Curves.pdf.

Fay, L., Ament, R., Hartshorn, T., & Powell, S. (2019). *Evaluating the Potential Effects of Deicing Salts on Roadside Carbon Sequestration*.

Fernandez, A., Ghobrial, T. R., Zhang, W., Zhu, D. Z., Loewen, M. R., van Duin, B., ... & Chen, L. (2019). PCSWMM modeling of storm runoff and sediment and nutrients loading to stormwater wetlands in Calgary Alberta. *CSCE Annual Conference, Laval, QC*.

Filipović, V., Mallmann, F. J. K., Coquet, Y., & Šimůnek, J. (2014). Numerical simulation of water flow in tile and mole drainage systems. *Agricultural Water Management*, *146*, 105-114.

Flerchinger, G. N., Lehrsch, G. A., & McCool, D. K. (2005). Freezing and thawing processes.

Freeman, L. A., Corbett, D. R., Fitzgerald, A. M., Lemley, D. A., Quigg, A., & Steppe, C. N. (2019). Impacts of urbanization and development on estuarine ecosystems and water quality. *Estuaries and Coasts*, *42*(7), 1821-1838.

Friese, R. D. (2016, May). Efficient genetic algorithm encoding for large-scale multi-objective resource allocation. In *2016 IEEE International Parallel and Distributed Processing Symposium Workshops (IPDPSW)* (pp. 1360-1369). IEEE.

Gerke, H. H., & Van Genuchten, M. T. (1993). A dual-porosity model for simulating the preferential movement of water and solutes in structured porous media. *Water resources research*, *29*(2), 305-319.

Gerke, H. H., & van Genuchten, M. T. (1996). Macroscopic representation of structural geometry for simulating water and solute movement in dual-porosity media. *Advances in Water Resources*, *19*(6), 343-357.

Goor, J., Cantelon, J., Smart, C. C., & Robinson, C. E. (2021). Seasonal performance of field bioretention systems in retaining phosphorus in a cold climate: Influence of prolonged road salt application. *Science of The Total Environment*, *778*, 146069.

Gülbaz, S., & Kazezyılmaz-Alhan, C. M. (2017). An evaluation of hydrologic modeling performance of EPA SWMM for bioretention. *Water Science and Technology*, *76*(11), 3035-3043.

Hatt, B. E., Fletcher, T. D., & Deletic, A. (2009). Hydrologic and pollutant removal performance of stormwater biofiltration systems at the field scale. *Journal of Hydrology*, *365*(3-4), 310-321.

Hatt, B. E., Fletcher, T. D., Walsh, C. J., & Taylor, S. L. (2004). The influence of urban density and drainage infrastructure on the concentrations and loads of pollutants in small streams. *Environmental management*, *34*(1), 112-124.

He, B. J., Zhu, J., Zhao, D. X., Gou, Z. H., Qi, J. D., & Wang, J. (2019). Co-benefits approach: Opportunities for implementing sponge city and urban heat island mitigation. *Land use policy*, *86*, 147-157.

He, Z., & Davis, A. P. (2011). Process modeling of storm-water flow in a bioretention cell. *Journal of Irrigation and Drainage Engineering*, *137*(3), 121-131.

Hood, M. J., Clausen, J. C., & Warner, G. S. (2007). Comparison of Stormwater lag times for low impact and traditional residential development 1. *JAWRA Journal of the American Water Resources Association*, *43*(4), 1036-1046.

Hsieh, C. H., & Davis, A. P. (2005a). Evaluation and optimization of bioretention media for treatment of urban storm water runoff. *Journal of Environmental Engineering*, *131*(11), 1521-1531.

Hsieh, C. H., & Davis, A. P. (2005b). Multiple-event study of bioretention for treatment of urban storm water runoff. *Water Science and Technology*, *51*(3-4), 177-181.

Huang, C. L., Hsu, N. S., Liu, H. J., & Huang, Y. H. (2018). Optimization of low impact development layout designs for megacity flood mitigation. *Journal of hydrology*, *564*, 542-558.

Hunt, W. F., & Lord, W. G. (2006). *Bioretention performance, design, construction, and maintenance*. NC Cooperative Extension Service.

Hunt, W. F., Smith, J. T., Jadlocki, S. J., Hathaway, J. M., & Eubanks, P. R. (2008). Pollutant removal and peak flow mitigation by a bioretention cell in urban Charlotte, NC. *Journal of Environmental Engineering*, *134*(5), 403-408.

Ishibuchi, H., Tsukamoto, N., & Nojima, Y. (2008, June). Evolutionary many-objective optimization: A short review. In *2008 IEEE congress on evolutionary computation (IEEE world congress on computational intelligence)* (pp. 2419-2426). IEEE.

Jackisch, N., & Weiler, M. (2017). The hydrologic outcome of a Low Impact Development (LID) site including superposition with streamflow peaks. *Urban Water Journal*, *14*(2), 143-159.

Jiang, C., Li, J., Li, H., & Li, Y. (2019). Experiment and simulation of layered bioretention system for hydrological performance. *Journal of Water Reuse and Desalination*, *9*(3), 319-329.

Kaspersen, P. S., & Halsnæs, K. (2017). Integrated climate change risk assessment: A practical application for urban flooding during extreme precipitation. *Climate services*, 6, 55-64.

Kaykhosravi, S., Khan, U. T., & Jadidi, A. (2018). A comprehensive review of low impact development models for research, conceptual, preliminary and detailed design applications. *Water*, *10*(11), 1541.

Khan, U. T., Valeo, C., Chu, A. V., & Van Duin, B. (2012). Bioretention cell efficacy in cold climates: Part 1—hydrologic performance. *Canadian Journal of Civil Engineering*, *39*(11), 1210-1221.

Kratky, H. (2019). Stormwater Quality Improvement through Bioretention in a Continental, Cold Climate. A thesis submitted to the University of Alberta.

Kratky, H., Li, Z., Chen, Y., Wang, C., Li, X., & Yu, T. (2017). A critical literature review of bioretention research for stormwater management in cold climate and future research recommendations. *Frontiers of Environmental Science & Engineering*, *11*(4), 1-15.

Lai, F. H., Dai, T., Zhen, J., Riverson, J., Alvi, K., & Shoemaker, L. (2007). SUSTAIN-AN EPA BMP process and placement tool for urban watersheds. *Proceedings of the water environment federation*, *2007*(5), 946-968.

Le Coustumer, S., Fletcher, T. D., Deletic, A., Barraud, S., & Poelsma, P. (2012). The influence of design parameters on clogging of stormwater biofilters: A large-scale column study. *Water research*, *46*(20), 6743-6752.

Li, J., Liu, Z., Jiang, C., Li, Y., Li, H., & Xia, J. (2021). Optimization design of key parameters for bioretention cells with mixed filter media via HYDRUS-1D model and regression analysis. *Ecological Engineering*, *164*, 106206.

Li, J., Zhao, R., Li, Y., & Chen, L. (2018). Modeling the effects of parameter optimization on three bioretention tanks using the HYDRUS-1D model. *Journal of environmental management*, *217*, 38-46.

Li, J., Zhao, R., Li, Y., & Li, H. (2020). Simulation and optimization of layered bioretention facilities by HYDRUS-1D model and response surface methodology. *Journal of Hydrology*, *586*, 124813.

Li, M. H., Swapp, M., Kim, M. H., Chu, K. H., & Sung, C. Y. (2014). Comparing bioretention designs with and without an internal water storage layer for treating highway runoff. *Water Environment Research*, *86*(5), 387-397.

Li, Z. (2019). Laboratory Study on the Hydraulic Performance of Bioretention for Stormwater Management in Cold Climates. A thesis submitted to the University of Alberta.

Lisenbee, W., Hathaway, J., Negm, L., Youssef, M., & Winston, R. (2020). Enhanced bioretention cell modeling with DRAINMOD-Urban: Moving from water balances to hydrograph production. *Journal of Hydrology*, *582*, 124491.

Liu, J., Sample, D. J., Bell, C., & Guan, Y. (2014). Review and research needs of bioretention used for the treatment of urban stormwater. *Water*, *6*(4), 1069-1099.

Liu, L., Wang, F., Xu, S., Sun, W., Wang, Y., & Ji, M. (2021). Woodchips bioretention column for stormwater treatment: Nitrogen removal performance, carbon source and microbial community analysis. *Chemosphere*, *285*, 131519.

Liu, R., & Fassman-Beck, E. (2017a). Hydrologic experiments and modeling of two laboratory bioretention systems under different boundary conditions. *Frontiers of Environmental Science & Engineering*, *11*(4), 10.

Liu, R., & Fassman-Beck, E. (2017b). Hydrologic response of engineered media in living roofs and bioretention to large rainfalls: experiments and modeling. *Hydrological Processes*, *31*(3), 556-572.

Liu, Y., Cibin, R., Bralts, V. F., Chaubey, I., Bowling, L. C., & Engel, B. A. (2016). Optimal selection and placement of BMPs and LID practices with a rainfall-runoff model. *Environmental Modelling & Software*, *80*, 281-296.

Lü, R., Guan, X., Li, X., & Hwang, I. (2016). A large-scale flight multi-objective assignment approach based on multi-island parallel evolution algorithm with cooperative coevolutionary. *Science China Information Sciences*, *59*(7), 1-17.

Mangangka, I. R., Liu, A., Egodawatta, P., & Goonetilleke, A. (2015). Performance characterisation of a stormwater treatment bioretention basin. *Journal of environmental management*, *150*, 173-178.

Mao, X., Jia, H., & Shaw, L. Y. (2017). Assessing the ecological benefits of aggregate LID-BMPs through modelling. *Ecological Modelling*, *353*, 139-149.

MapTrove. (2020). Where is Calgary Alberta? [online image]. https://www.maptrove.ca/info/where/canada/calgary

Martine, G., & Marshall, A. (2007). State of world population 2007: unleashing the potential of urban growth. *State of world population*.

Massoudieh, A., Aflaki, S., & Panguluri, S. (2016). User's manual for green infrastructure flexible model (GIFMod). *GIFMod: Washington, DC, USA*.

May, R. M. (2004). Simple mathematical models with very complicated dynamics. *The Theory of Chaotic Attractors*, 85-93.

McManus, M., & Davis, A. P. (2020). Impact of periodic high concentrations of salt on bioretention water quality performance. *Journal of Sustainable Water in the Built Environment*, *6*(4), 04020014.

Men, H., Lu, H., Jiang, W., & Xu, D. (2020). Mathematical Optimization Method of Low-Impact Development Layout in the Sponge City. *Mathematical Problems in Engineering*, *2020*.

Meng, Y., Wang, H., Chen, J., & Zhang, S. (2014). Modelling hydrology of a single bioretention system with HYDRUS-1D. *The Scientific World Journal*, *2014*.

Miller, J. D., & Hutchins, M. (2017). The impacts of urbanisation and climate change on urban flooding and urban water quality: A review of the evidence concerning the United Kingdom. *Journal of Hydrology: Regional Studies*, *12*, 345-362.

Moeller, T. (2012). *Chemistry: with inorganic qualitative analysis*. Elsevier.

Moghadas, S., Gustafsson, A. M., Viklander, P., Marsalek, J., & Viklander, M. (2016). Laboratory study of infiltration into two frozen engineered (sandy) soils recommended for bioretention. *Hydrological Processes*, *30*(8), 1251-1264.

Mohammed, A. A., Kurylyk, B. L., Cey, E. E., & Hayashi, M. (2018). Snowmelt infiltration and macropore flow in frozen soils: Overview, knowledge gaps, and a conceptual framework. *Vadose Zone Journal*.

Mun-Soo, N., Woo-Bin, B., Hee-Man, K., Yong-Gil, K., & Sang-Rae, K. (2021). Quantitative evaluation of the mitigation effect of low-impact development pavement materials on urban heat island and tropical night phenomena. *Water Science and Technology*, *83*(10), 2452-2462.

Muthanna, T. M., Viklander, M., & Thorolfsson, S. T. (2008). Seasonal climatic effects on the hydrology of a rain garden. *Hydrological Processes: An International Journal*, *22*(11), 1640-1649.

Paknejad, P., Khorsand, R., & Ramezanpour, M. (2021). Chaotic improved PICEA-g-based multi-objective optimization for workflow scheduling in cloud environment. *Future Generation Computer Systems*, *117*, 12-28.

Palmer, E. T., Poor, C. J., Hinman, C., & Stark, J. D. (2013). Nitrate and phosphate removal through enhanced bioretention media: mesocosm study. *Water Environment Research*, *85*(9), 823-832.

Parkhurst, D. L., & Appelo, C. A. J. (1999). User's guide to PHREEQC (Version 2): A computer program for speciation, batch-reaction, one-dimensional transport, and inverse geochemical calculations. *Water-resources investigations report*, *99*(4259), 312.

Passeport, E., Hunt, W. F., Line, D. E., Smith, R. A., & Brown, R. A. (2009). Field study of the ability of two grassed bioretention cells to reduce storm-water runoff pollution. *Journal of Irrigation and Drainage Engineering*, *135*(4), 505-510.

Paul, M. J., & Meyer, J. L. (2001). Streams in the urban landscape. *Annual review of Ecology and Systematics*, *32*(1), 333-365.

Pęczkowski, G., Kowalczyk, T., Szawernoga, K., Orzepowski, W., Żmuda, R., & Pokładek, R. (2018). Hydrological performance and runoff water quality of experimental green roofs. *Water*, *10*(9), 1185.

Pierce, J. (2011). Logistic Bifurcation map High Resolution [online image]. https://commons.wikimedia.org/wiki/File:Logistic_Bifurcation_map_High_Resolution.png

Pour, S. H., Abd Wahab, A. K., Shahid, S., Asaduzzaman, M., & Dewan, A. (2020). Low impact development techniques to mitigate the impacts of climate-change-induced urban floods: Current trends, issues and challenges. *Sustainable Cities and Society*, *62*, 102373.

Qian, C. (2019). Distributed Pareto optimization for large-scale noisy subset selection. *IEEE Transactions on Evolutionary Computation*, *24*(4), 694-707.

Qiu, F., Zhao, S., Zhao, D., Wang, J., & Fu, K. (2019). Enhanced nutrient removal in bioretention systems modified with water treatment residuals and internal water storage zone. *Environmental Science: Water Research & Technology*, *5*(5), 993-1003.

Rashid, H., Manzoor, M. M., & Mukhtar, S. (2018). Urbanization and its effects on water resources: An exploratory analysis. *Asian Journal of Water, Environment and Pollution*, *15*(1), 67-74.

Riaño-Briceño, G., Barreiro-Gomez, J., Ramirez-Jaime, A., Quijano, N., & Ocampo-Martinez, C. (2016). MatSWMM–an open-source toolbox for designing real-time control of urban drainage systems. *Environmental modelling & software*, *83*, 143-154.

Roseen, R. M., Ballestero, T. P., Houle, J. J., Avellaneda, P., Briggs, J., Fowler, G., & Wildey, R. (2009). Seasonal performance variations for storm-water management systems in cold climate conditions. *Journal of Environmental Engineering*, *135*(3), 128-137.

Rossman, L. A. (2015). *Storm water management model user's manual, version 5.1* (p. 276). Cincinnati: National Risk Management Research Laboratory, Office of Research and Development, US Environmental Protection Agency.

Rui (2021). PICEAg MATLAB.zip (https://www.mathworks.com/matlabcentral/fileexchange/47620-piceag-matlab-zip), MATLAB Central File Exchange. Retrieved June 19, 2021.

Salerno, F., Gaetano, V., & Gianni, T. (2018). Urbanization and climate change impacts on surface water quality: Enhancing the resilience by reducing impervious surfaces. *Water research*, *144*, 491-502.

Shafique, M., & Kim, R. (2017). Green stormwater infrastructure with low impact development concept: a review of current research. *Desalination and Water Treatment*, *83*(7), 16-29.

Shoemaker, L., Riverson, J., Alvi, K., Zhen, J. X., Paul, S., & Rafi, T. (2009). *SUSTAIN: a framework for placement of best management practices in urban watersheds to protect water quality*. Washington, DC: National Risk Management Research Laboratory, Office of Research and Development, US Environmental Protection Agency.

Shrestha, P., Hurley, S. E., & Wemple, B. C. (2018). Effects of different soil media, vegetation, and hydrologic treatments on nutrient and sediment removal in roadside bioretention systems. *Ecological Engineering*, *112*, 116-131.

Šimůnek, J., Jarvis, N. J., Van Genuchten, M. T., & Gärdenäs, A. (2003). Review and comparison of models for describing non-equilibrium and preferential flow and transport in the vadose zone. *Journal of hydrology*, *272*(1-4), 14-35.

Simunek, J., Van Genuchten, M. T., & Sejna, M. (2005). The HYDRUS-1D software package for simulating the one-dimensional movement of water, heat, and multiple solutes in variably-saturated media. *University of California-Riverside Research Reports*, *3*, 1-240.

Skaggs, R. W., Youssef, M. A., & Chescheir, G. M. (2012). DRAINMOD: Model use, calibration, and validation. *Transactions of the ASABE*, *55*(4), 1509-1522.

Sohn, W., Kim, J. H., Li, M. H., & Brown, R. (2019). The influence of climate on the effectiveness of low impact development: A systematic review. *Journal of environmental management*, *236*, 365-379.

Spraakman, S., Rodgers, T. F., Monri-Fung, H., Nowicki, A., Diamond, M. L., Passeport, E., & Drake, J. (2020). A Need for Standardized Reporting: A Scoping Review of Bioretention Research 2000–2019. Water, 12(11), 3122.

Srinivas, M., & Patnaik, L. M. (1994). Adaptive probabilities of crossover and mutation in genetic algorithms. *IEEE Transactions on Systems, Man, and Cybernetics*, *24*(4), 656-667.

Statistics Canada. (2021). Canada's population estimates: Sub provincial areas, July 1, 2020. *The Daily*. https://www150.statcan.gc.ca/n1/daily-quotidien/210114/dq210114a-eng.htm.

Steffen, J. R. (2012). *Bioretention hydrologic performance in a semiarid climate*. A thesis submitted to the University of Utah.

Sun, F., Roderick, M. L., & Farquhar, G. D. (2018). Rainfall statistics, stationarity, and climate change. *Proceedings of the National Academy of Sciences*, *115*(10), 2305-2310.

Sun, Y. W., Li, Q. Y., Liu, L., Xu, C. D., & Liu, Z. P. (2014). Hydrological simulation approaches for BMPs and LID practices in highly urbanized area and development of hydrological performance indicator system. *Water Science and Engineering*, *7*(2), 143-154.

Sun, Y. W., Pomeroy, C., Li, Q. Y., & Xu, C. D. (2019). Impacts of rainfall and catchment characteristics on bioretention cell performance. *Water Science and Engineering*, *12*(2), 98-107.

Tabari, H. (2020). Climate change impact on flood and extreme precipitation increases with water availability. *Scientific reports*, *10*(1), 1-10.

Tang, S., Luo, W., Jia, Z., Liu, W., Li, S., & Wu, Y. (2016). Evaluating retention capacity of infiltration rain gardens and their potential effect on urban stormwater management in the sub-humid loess region of China. *Water resources management*, *30*(3), 983-1000.

Tao, T., Xiao, T., Wang, L., & Yan, H. (2019). Multi-objective optimization design of low-impact development plan in sponge city construction. *Journal of Tongji University (Natural Science)*, *47*(01), 92-96.

Tetra Tech, Inc. (2013). *BMP Siting Tool Step-by-step Guide.* ArcGIS 10.1 Service Pack 1 (Build 3143).

The City of Calgary Water Resources. (2011). *Stormwater Management & Design Manual*.

The City of Edmonton, (2014). Low Impact Development Best Management Practices Design Guide. *Edition 1.1*.

Tirpak, R. A., Afrooz, A. N., Winston, R. J., Valenca, R., Schiff, K., & Mohanty, S. K. (2021). Conventional and amended bioretention soil media for targeted pollutant treatment: A critical review to guide the state of the practice. *Water Research*, 116648.

U.S. Department of Housing and Urban Development. (2003). The Practice of Low Impact Development. *Office of Policy Development and Research, Washington, D.C.*

U.S.EPA. (2000). Low impact development (LID): A literature review. *Washington, DC, US Environmental Protection Agency, Office of Water and Low Impact Development Center*.

U.S.EPA. (2002). Nitrification. *Washington, DC, US Environmental Protection Agency, Office of Ground Water and Drinking Water*.

United Nations, Department of Economic and Social Affairs, Population Division (2019). World Urbanization Prospects: The 2018 Revision (ST/ESA/SER.A/420). *New York: United Nations*.

Van Genuchten, M. T. (1980). A closed-form equation for predicting the hydraulic conductivity of unsaturated soils. *Soil science society of America journal*, *44*(5), 892-898.

Wan, Z., Li, T., & Shi, Z. (2017). A layered bioretention system for inhibiting nitrate and organic matters leaching. *Ecological Engineering*, *107*, 233-238.

Wang, M., Zhang, D., Wang, Z., Zhou, S., & Soon, K. (2021). Long-term performance of bioretention systems in storm runoff management under climate change and life-cycle condition. *Sustainable Cities and Society*, 102598.

Wang, R. (2013). *Preference-inspired co-evolutionary algorithms* (Doctoral dissertation, University of Sheffield).

Wang, T. L., Liu, Y. J., Yan, H., & Xu, L. (2015). An experimental study on the mechanical properties of silty soils under repeated freeze–thaw cycles. *Cold Regions Science and Technology*, *112*, 51-65.

Watanabe, K., & Kugisaki, Y. (2017). Effect of macropores on soil freezing and thawing with infiltration. *Hydrological Processes*, *31*(2), 270-278.

Watanabe, K., & Osada, Y. (2017). Simultaneous measurement of unfrozen water content and hydraulic conductivity of partially frozen soil near 0 C. *Cold Regions Science and Technology*, *142*, 79-84.

Watanabe, K., Kito, T., Dun, S., Wu, J. Q., Greer, R. C., & Flury, M. (2013). Water infiltration into a frozen soil with simultaneous melting of the frozen layer. *Vadose Zone Journal*, *12*(1), vzj2011-0188.

Weigert, A., & Schmidt, J. (2005). Water transport under winter conditions. *Catena*, *64*(2-3), 193-208.

Weitman, D., Weinberg, A., & Goo, R. (2009). Reducing stormwater costs through LID strategies and practices. In *Low Impact Development for Urban Ecosystem and Habitat Protection* (pp. 1-10).

Willems, P., Arnbjerg-Nielsen, K., Olsson, J., & Nguyen, V. T. V. (2012). Climate change impact assessment on urban rainfall extremes and urban drainage: Methods and shortcomings. *Atmospheric research*, *103*, 106-118.

Willems, P., Arnbjerg-Nielsen, K., Olsson, J., & Nguyen, V. T. V. (2012). Climate change impact assessment on urban rainfall extremes and urban drainage: Methods and shortcomings. *Atmospheric research*, *103*, 106-118.

Winston, R., Smolek, A., Dorsey, J., & Hunt, W. (2016). Modeling Bioretention Hydrologic Performance using DRAINMOD under Current and Future Climate Scenarios. *Modélisation/Models*.

Xia, J., Wang, H., Stanford, R. L., Pan, G., & Yu, S. L. (2018). Hydrologic and water quality performance of a laboratory scale bioretention unit. *Frontiers of environmental science & engineering*, *12*(1), 14.

Xiang, L., Yu, Z., Chen, L., Mon, J., & Lü, H. (2012). Evaluating coupled water, vapor, and heat flows and their influence on moisture dynamics in arid regions. *Journal of Hydrologic Engineering*, *17*(4), 565-577.

Xu, T., Jia, H., Wang, Z., Mao, X., & Xu, C. (2017). SWMM-based methodology for block-scale LID-BMPs planning based on site-scale multi-objective optimization: a case study in Tianjin. *Frontiers of Environmental Science & Engineering*, *11*(4), 1-12.

Zhang, K., & Chui, T. F. M. (2018). A comprehensive review of spatial allocation of LID-BMP-GI practices: Strategies and optimization tools. *Science of the total environment*, *621*, 915-929.

Zhou, Q. (2014). A review of sustainable urban drainage systems considering the climate change and urbanization impacts. *Water*, *6*(4), 976-992.

Appendix

Chapter 2

Tables:

Table A2.1 The stormwater pollutant concentrations to the bioretention columns for the experiments of Li (2018) and Kratky (2019)

Parameter	Source	Concentration (mg/L)
Ammonium (NH_4^+ - N)	NH_4Cl	2
Nitrate (NO_3^--N)	KNO_3	1.5
Nitrite (NO_2^--N)	$NaNO_2$	0.5
Phosphate ($PO4_3^-$-P)	KH_2PO_4	2
Chloride (Cl^-)	NaCl	15[a]
		320[b]
		1280[c]

Note: [a] During summer operation including the 1:5 and 1:10 year storm events;

[b] During Year 1 winter operation and the second spring runoff event (major snow melt);

[c] During Year 1 the first spring runoff event (first flush).

Table A2.2 The 4-hr design storm intensity in Chicago Distribution. The 1:2, 1:5, and 1:10 year storms were from COE (2014), and 1:25, 1:50, and 1:100 year storms were from EPCOR (2018).

Time (min)	Return Frequency (mm/hr)					
	2-yr	5-yr	10-yr	25-yr	50-yr	100-yr
0	0.00	0.00	0.00	0	0	0
5	1.39	4.15	4.91	3.82	4.92	6.25
10	1.39	4.15	4.91	4.04	5.19	6.58
15	1.39	4.15	4.91	4.28	5.49	6.97
20	1.39	4.15	4.91	4.56	5.84	7.41
25	1.39	4.15	4.91	4.89	6.25	7.92
30	1.39	4.15	4.91	5.27	6.73	8.52
35	1.39	4.15	4.91	5.74	7.31	9.24
40	2.60	6.20	7.44	6.31	8.01	10.12
45	2.60	6.20	7.44	7.02	8.89	11.22
50	2.60	6.20	7.44	7.95	10.03	12.63
55	2.60	6.20	7.44	9.2	11.57	14.54
60	2.60	6.20	7.44	11	13.76	17.26
65	2.60	6.20	7.44	13.82	17.18	21.48
70	2.60	6.20	7.44	18.89	23.26	28.94
75	22.67	34.27	41.58	30.69	37.26	45.9
80	22.67	34.27	41.58	103.56	122.26	143.62
85	22.67	34.27	41.58	103.56	122.26	143.62
90	22.67	34.27	41.58	55.17	66.01	80
95	22.67	34.27	41.58	35.36	42.79	52.54
100	22.67	34.27	41.58	26.01	31.74	39.26
105	22.67	34.27	41.58	20.63	25.34	31.48
110	22.67	11.39	13.75	17.15	21.18	26.4
115	7.86	11.39	13.75	14.72	18.26	22.81
120	7.86	11.39	13.75	12.93	16.1	20.14
125	7.86	11.39	13.75	11.55	14.43	18.08
130	7.86	11.39	13.75	10.46	13.1	16.44
135	7.86	6.52	7.34	9.57	12.02	15.1
140	7.86	6.52	7.34	8.83	11.12	13.98
145	3.16	6.52	7.34	8.21	10.36	13.04
150	3.16	6.52	7.34	7.68	9.71	12.23
155	3.16	6.52	7.34	7.22	9.14	11.52
160	3.16	6.52	5.86	6.82	8.65	10.91
165	3.16	4.88	5.86	6.46	8.21	10.36
170	3.16	4.88	5.86	6.15	7.82	9.87
175	2.05	4.88	5.86	5.87	7.47	9.44
180	2.05	4.88	5.86	5.61	7.15	9.04

185	2.05	4.88	4.80	5.38	6.86	8.68
190	2.05	4.00	4.80	5.17	6.6	8.36
195	2.05	4.00	4.80	4.98	6.36	8.06
200	1.54	4.00	4.80	4.8	6.14	7.78
205	1.54	4.00	4.80	4.64	5.94	7.53
210	1.54	4.00	4.80	4.49	5.75	7.29
215	1.24	3.17	3.80	4.35	5.57	7.07
220	1.24	3.17	3.80	4.21	5.41	6.86
225	1.24	3.17	3.80	4.09	5.26	6.67
230	1.24	3.17	3.80	3.98	5.12	6.49
235	1.24	3.17	3.80	3.87	4.98	6.33
240	1.24	3.17	3.80	3.77	4.86	6.17

Table A2.3 The initial values and testing ranges of hydraulic parameters for model calibration

Soil	Setting	Q_r	Q_s	α (1/cm)	n	K_s (cm/min)
Soil Media A and Compost	Initial value	0.08	0.5	0.05	2	0.25
	Range	0 ~ 0.1	0.1 ~ 0.6	0 ~ 0.01	1 ~ 2	0 ~ 1
Soil Media A (Loam)	Initial value	0.078	0.43	0.036	1.56	0.0417
	Range	0 ~ 0.1	0.1 ~ 0.6	0 ~ 0.01	1 ~ 2	0 ~ 1
Soil Media B and Compost	Initial value	0.08	0.5	0.08	2	0.25
	Range	0 ~ 0.1	0.1 ~ 0.6	0 ~ 0.01	1 ~ 2	0 ~ 1
Soil Media B (Sandy Loam)	Initial value	0.065	0.41	0.075	1.89	0.208
	Range	0 ~ 0.1	0.1 ~ 0.6	0 ~ 0.01	1 ~ 2	0 ~ 1

Figures:

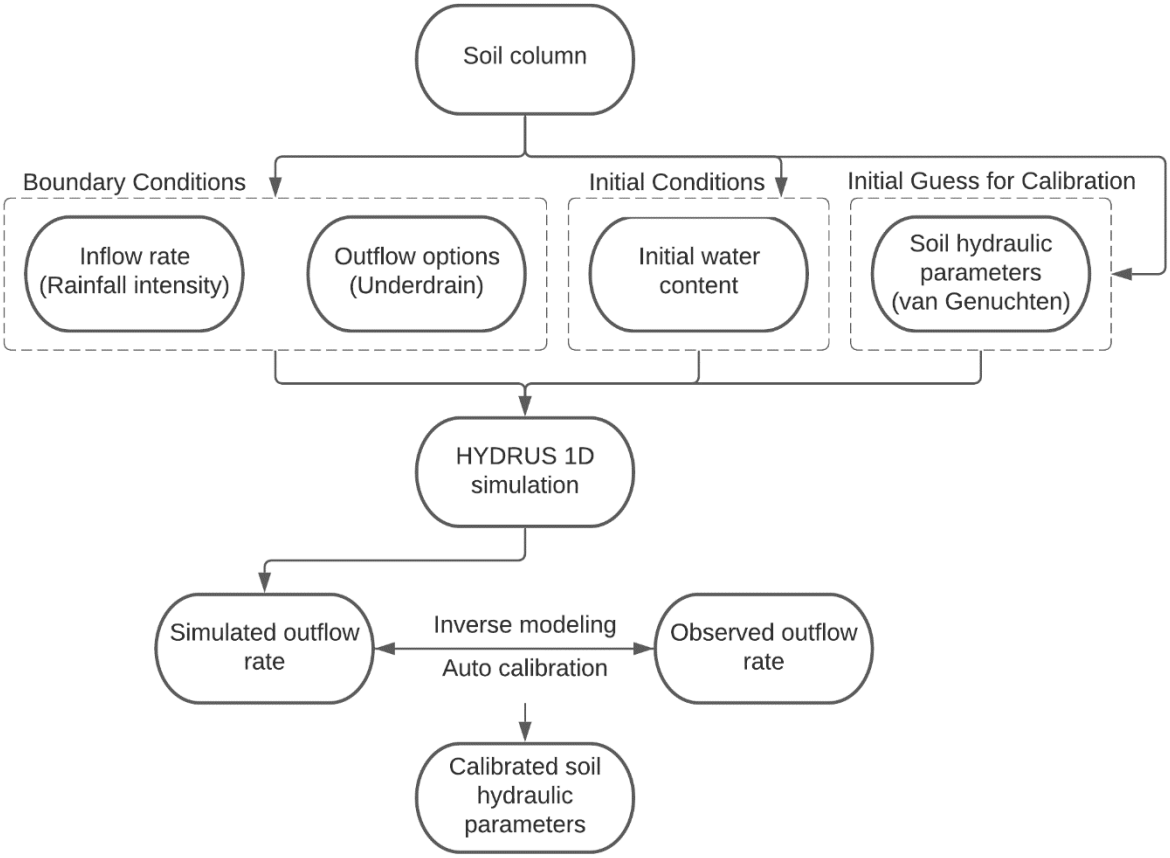

Figure A2.1 Schematic diagram of soil hydraulic parameters calibration process using HYDRUS 1D

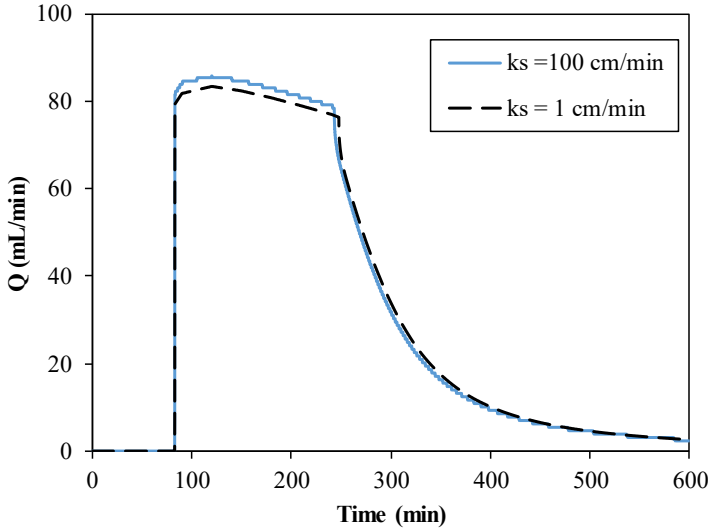

Figure A2.2 Sensitivity of the outflow hydrograph with different *Ks* values of gravel layer for bioretention Column 3 with anoxic zone. Storm event modeled: 1:2 year.

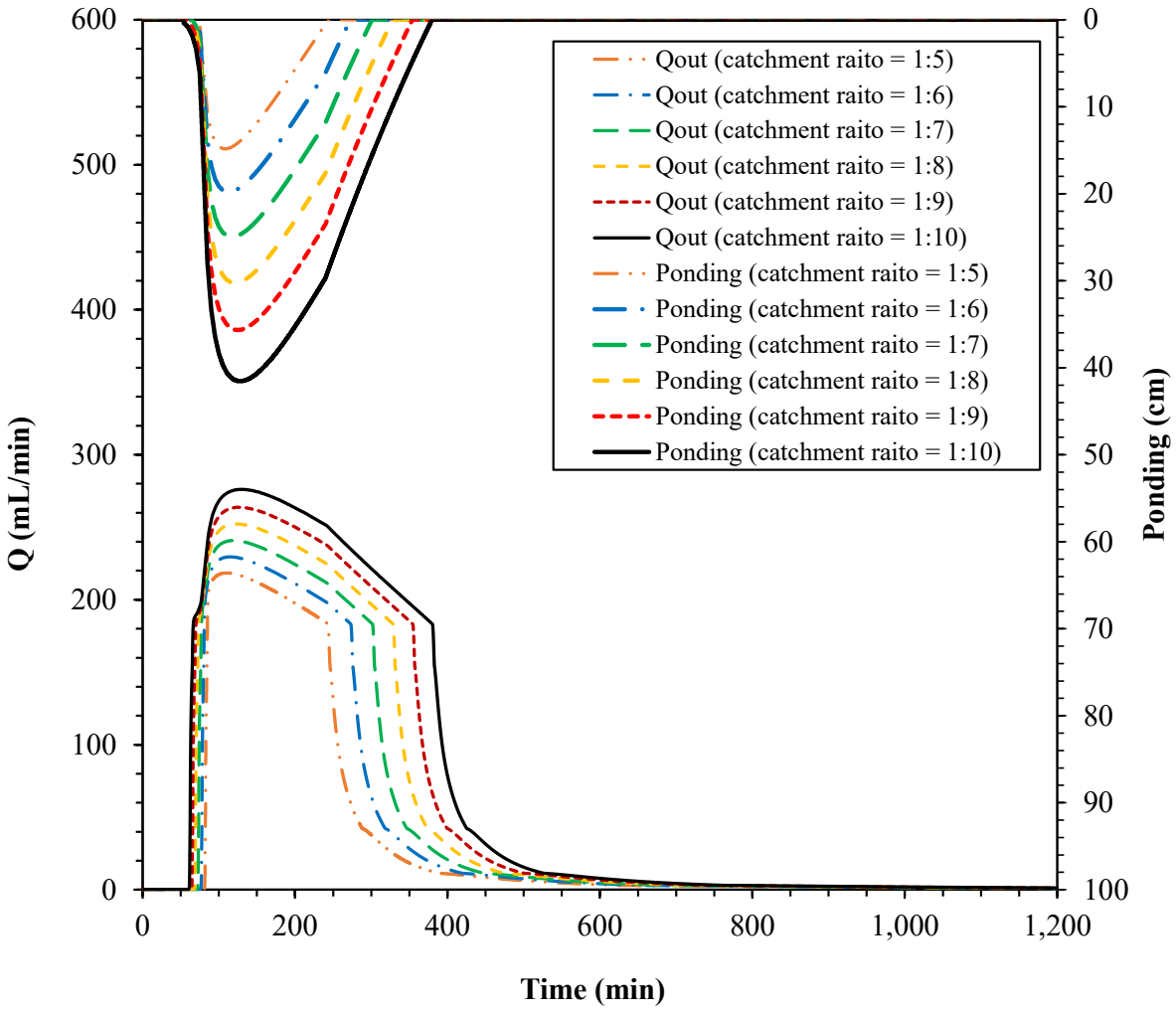

Figure A2.3 Modification bioretention Column 2 by changing the CA/SA ratio. Storm event modeled: 1:100 year.

Chapter 3

Context A3.1 An example of Eq. 3.3-3.5

An example of an optimization problem with 2 minimizing objectives, 4 candidate solutions, and 4 goal vectors are used in Paknejad et al. (2021) to explain this fitness method as shown in Figure A3.4. Candidate solutions CS_2 and CS_4 are parent solutions while CS_1 and CS_3 are offspring solutions, so $N = 2$. In this example, the fitness values of the four candidate solutions are calculated as:

$$Fit_{cs1} = \frac{1}{n_{gv1}} + \frac{1}{n_{gv2}} + \frac{1}{n_{gv3}} + \frac{1}{n_{gv4}} = \frac{1}{2} + \frac{1}{2} + \frac{1}{3} + \frac{1}{4} = \frac{19}{12}$$

$$Fit_{cs2} = \frac{1}{n_{gv1}} + \frac{1}{n_{gv2}} + \frac{1}{n_{gv3}} + \frac{1}{n_{gv4}} = \frac{1}{2} + \frac{1}{2} + \frac{1}{3} + \frac{1}{4} = \frac{19}{12}$$

$$Fit_{cs3} = \frac{1}{n_{gv3}} + \frac{1}{n_{gv4}} = \frac{1}{3} + \frac{1}{4} = \frac{7}{12}$$

$$Fit_{cs4} = \frac{1}{n_{gv4}} = \frac{1}{4}$$

In this case, the fitness values of CS_1 and CS_2 are the same while CS_3 is dominated by CS_4. Using the calculation of fitness value of CS_3 as an example, gv_3 and gv_4 are the two goal vectors that are dominated by CS_3. Therefore, the fitness value of CS_3 is equal to the sum of $\frac{1}{n_{gv3}}$ and $\frac{1}{n_{gv4}}$.

The fitness values of the four goal vectors are calculated as:

$$Fit_{gv1} = \frac{1}{1 + \left(\frac{n_{gv1} - 1}{2N - 1}\right)} = \frac{1}{1 + \left(\frac{2 - 1}{4 - 1}\right)} = \frac{3}{4}$$

$$Fit_{gv2} = \frac{1}{1 + \left(\frac{n_{gv2} - 1}{2N - 1}\right)} = \frac{1}{1 + \left(\frac{2 - 1}{4 - 1}\right)} = \frac{3}{4}$$

$$Fit_{gv3} = \frac{1}{1 + \left(\frac{n_{gv3} - 1}{2N - 1}\right)} = \frac{1}{1 + \left(\frac{3 - 1}{4 - 1}\right)} = \frac{3}{5}$$

$$Fit_{gv4} = \frac{1}{1 + \left(\frac{n_{gv4} - 1}{2N - 1}\right)} = \frac{1}{1 + \left(\frac{4 - 1}{4 - 1}\right)} = \frac{1}{2}$$

Context A3.2 An example of Eq. 3.6-3.7

New fitness value of the four candidate solutions are calculated as:

$$rank_{cs1} = 1 + 0 = 1$$

$$rank_{cs2} = 1 + 1 = 2$$

$$rank_{cs3} = 1 + 0 = 1$$

$$rank_{cs4} = 1 + 1 = 2$$

$$Fit_{cs1} = \frac{1}{n_{gv1}} \times Fit_{gv1} + \frac{1}{n_{gv2}} \times Fit_{gv2} + \frac{1}{n_{gv3}} \times Fit_{gv3} + \frac{1}{n_{gv4}} \times Fit_{gv4} + \frac{1}{rank_{cs1}}$$

$$= \frac{1}{2} \times \frac{3}{4} + \frac{1}{2} \times \frac{3}{4} + \frac{1}{3} \times \frac{3}{5} + \frac{1}{4} \times \frac{1}{2} + \frac{1}{1} = \frac{22}{10}$$

$$Fit_{cs2} = \frac{1}{n_{gv1}} \times Fit_{gv1} + \frac{1}{n_{gv2}} \times Fit_{gv2} + \frac{1}{n_{gv3}} \times Fit_{gv3} + \frac{1}{n_{gv4}} \times Fit_{gv4} + \frac{1}{rank_{cs2}}$$

$$= \frac{1}{2} \times \frac{3}{4} + \frac{1}{2} \times \frac{3}{4} + \frac{1}{3} \times \frac{3}{5} + \frac{1}{4} \times \frac{1}{2} + \frac{1}{2} = \frac{17}{10}$$

$$Fit_{cs3} = \frac{1}{n_{gv3}} \times Fit_{gv3} + \frac{1}{n_{gv4}} \times Fit_{gv4} + \frac{1}{rank_{cs3}} = \frac{1}{3} \times \frac{3}{5} + \frac{1}{4} \times \frac{1}{2} + \frac{1}{1} = \frac{53}{40}$$

$$Fit_{cs4} = \frac{1}{n_{gv4}} \times Fit_{gv4} + \frac{1}{rank_{cs4}} = \frac{1}{4} \times \frac{1}{2} + \frac{1}{2} = \frac{5}{8}$$

Tables:

Table A3.1 Basic parameters and setup of the SWMM model, with the modified Green-Ampt as the infiltration model

Parameters	Description	Setup
N-Imperv	Manning's N for impervious area	0.015
N-Perv	Manning's N for pervious area	0.397
Dstore-Imperv	Depth of depression storage on impervious area (mm)	1.067
Dstore-Perv	Depth of depression storage on previous area (mm)	5.336
%Zero-Imperv	Percent of impervious area with no depression storage	43.563
Suction Head	Soil capillary suction head (mm)	343
Conductivity	Soil saturated hydraulic conductivity (mm/hr)	2
Initial Deficit	Difference between soil porosity and initial moisture content	0.447

Table A3.2 Basic parameters and setup of the dynamic wave in the SWMM model

Parameters	**Setup**
Inertial Terms	Dampen
Normal Flow Criterion	Slop & Froude
Force Main Equation	Hazen-Williams
Minimum Variable Time Step (sec)	0.5
Minimum Nodal Surface Area (sq. meters)	1.14
Head Convergence Tolerance (meters)	0.0015

Table A3.3 Examples of subcatchment land use in the study area

Subcatchment ID	Greenspace (%)	Concrete (%)	Roof (%)
1002	77.17	22.83	0
1036	89.37	10.63	0
1047	85.32	14.11	0.57
1083	77.67	22.33	0
1117	69.08	30.92	0
1250	23.15	67.86	9
1253	55.33	16.71	27.97
1260	60.17	29.47	10.37

Table A3.4 The design storms used in the City of Calgary (COC, 2011)

Time (min)	Intensity (mm/hr) for Return Period					
	2yr	5yr	10yr	25yr	50yr	100yr
0	0.000	0.000	0.000	0.000	0.000	0.000
5	5.589	7.622	8.972	10.716	12.024	13.283
10	7.955	10.866	12.807	15.283	17.168	18.961
15	16.695	23.029	27.274	32.555	36.673	40.516
20	58.763	87.477	106.693	132.056	150.050	168.138
25	22.201	30.772	36.520	43.630	49.196	54.372
30	13.232	18.142	21.432	25.552	28.750	31.748
35	9.731	13.306	15.694	18.719	21.040	23.236
40	7.831	10.695	12.604	15.041	16.895	18.660
45	6.624	9.040	10.647	12.711	14.271	15.763
50	5.782	7.887	9.284	11.088	12.444	13.746
55	5.158	7.032	8.275	9.885	11.090	12.251
60	4.675	6.371	7.493	8.953	10.041	11.093

Figures:

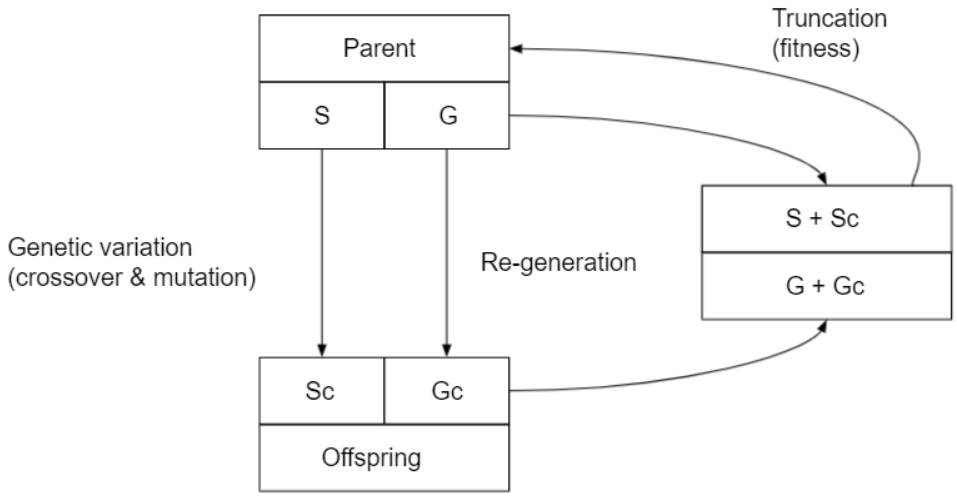

Figure A3.1 An elitist framework of PICEA-g (Wang, 2013)

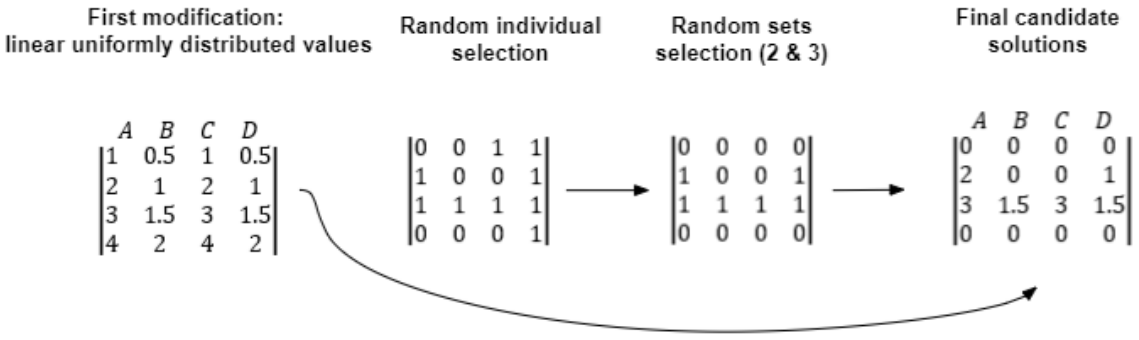

Figure A3.2 An example of initializing first candidate solutions with 4 decision variables and 4 sets of solutions

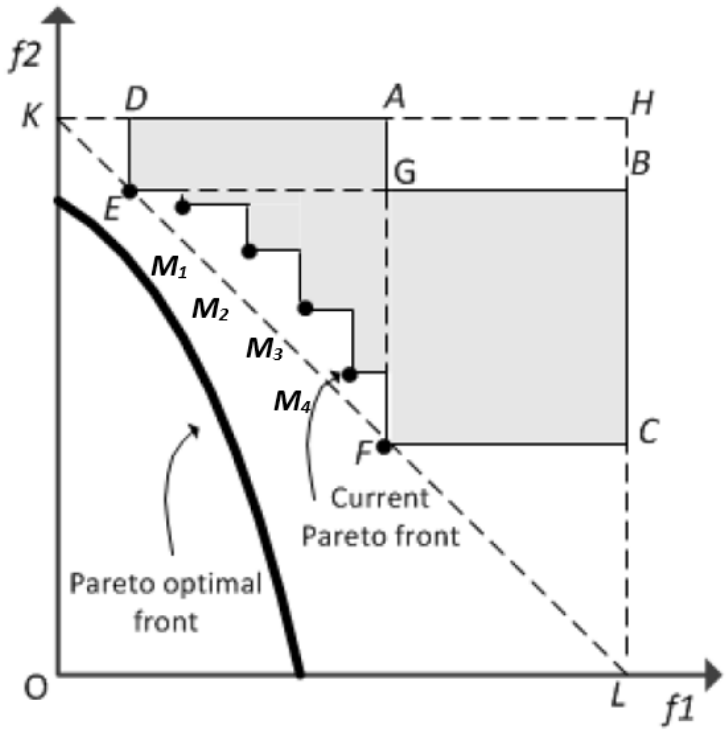

Figure A3.3 An example of two objective problem using the cutting plane (Wang, 2013).

Goal vectors are randomly generated inside the bound space. In the original PICEA-g algorithm, the bound space of goal vectors is *OKHL*. The *cutting plane* cuts the bound space from *OKHL* to $DAGBCFM_{4\text{-}1}E$ (grey area), where *E* and *F* are the extreme points and $M_{1\text{-}4}$ are the non-dominated solutions. In the original bound space, any goal vectors that fall inside the area $OKDEM_{1\text{-}4}FL$ cannot be dominated by any solutions, while any goal vectors that fall inside the area *AHNG* could be dominated by all solutions, which means any goal vectors that fall outside the area $DAGBCFM_{4\text{-}1}E$ (gray area) are wasted and useless. In the meantime, objective *f2* is far from the Pareto optimal front rather than object *f1* (pick any point along with *EF*). Because *GBCF*'s area is larger than *DAGE*'s, more goal vectors fall inside the area *GBCF* rather than *DAGE* with the *cutting plane* approach, distributing more efforts on steering solutions towards objective *f2* in the next generation.

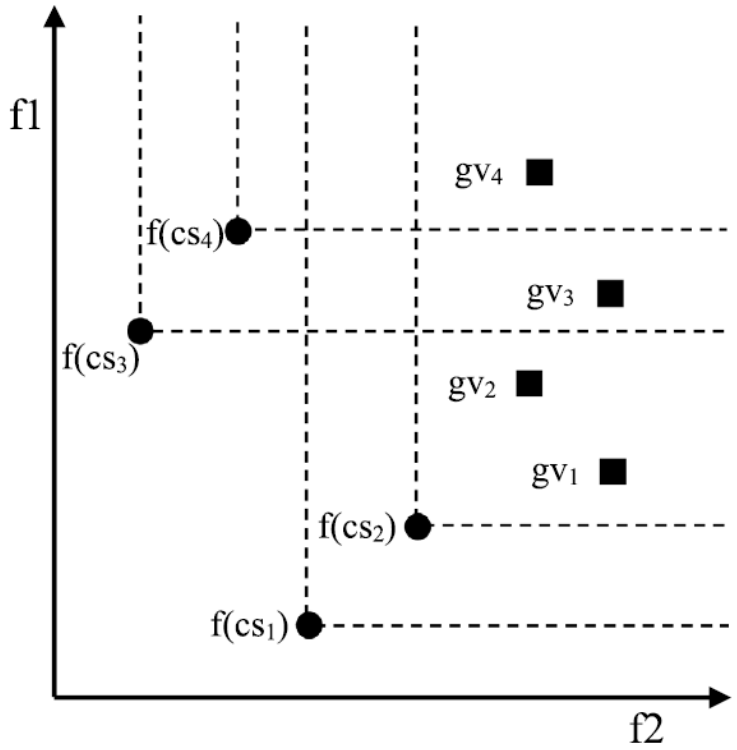

Figure A3.4 An example of how to calculate fitness value in a two-objective problem (Paknejad et al., 2021)

Algorithms:

Algorithm 3.1 Pseudo code of PICEA-g (Modified from Wang (2013))

```
Input: N, Ng, MaxGen
%% N = size of solution, Ng = size of goal vectors, MaxGen = maximum number of generations
Output: BS, BF
%% BS = best solutions, BF = best objective values
CS = initialize solution (N)     % CS = candidate solutions
GV = random goal vectors generator (Ng,Gbounds)
% GV = goal vectors,  Gbounds = Defined space or range for goal vectors
F = achieve object values (CS)    % F = objective values
for gen = 1 to MaxGen
    CSc = genetic variation operator (CS)
    Fc = achieve object values (CSc)
    GVc = random goal vectors generator  (Ng,Gbounds)
    JointCS = CS + CSc
    JointGV = GV + GVc
    Calculate fitness of each individual of JointCS and JointGV
    Sorting JointCS and JointGC by their fitness
    CS = truncation (JointCS)    % select best N solutions from JointCS
    GV = truncation (JointGV)    % select best Ng goal vectors from JointGV
end
BS = CS
BF = achieve object values (BS)
return BS BF
```

Algorithm 3.2 Pseudo code of crossover

```
Input: parents, bounds
%% parents = parent population, bounds = decision variables boundaries
Output: offspring
%% offspring = offspring population
1  generate two chaotic sequences x1 and x2 using the logistic map
2  randomly select two types of LID, t1 and t2 (index of type1 LID)
3 for  j = 1 to N     % N = size of parent population
4          if x1(j) <= 0.5
5               offspring(j,t1) = parents(j,t1) + (uBound(t1) - parents(j,1t)) * x2(t1)*0.5;
6               offspring(j,t2) = parents(j,t2) - (parents(j,t2) - lBound(t2)) * x2(t2)*0.5;
7          else
5               offspring(j,t1) = parents(j,t1) - ( parents(j,t1) - lBound(t1)) * x2(t1)*0.5;
6               offspring(j,t2) = parents(j,t2) + (uBound(t2) - parents(j,t2)) * x2(t2)*0.5;
%%  lBound and uBound are the lower boundaries and upper boundaries of decision variables
7          end
8       end
9  end
10 return offspring
```

Algorithm 3.3 Pseudo code of mutation

```
Input: parents, bounds, fitnessCS
%% parents = parent population, bounds = decision variables boundaries
%%  fitnessCS = fitness value of each solution set (rows of parent population)
Output: offspring
%% offspring = offspring population
set xovProb = 0.7    % xvob = probability of crossover between a pair
for  j = 1 to N     % size of parent population (rows)
    if rand  <=  xovProb      % rand is a random number in [0,1], crossover operates when rand <= xovProb
        parent1 = parents(j,:)
        parent2 = roulette wheel (parents, fitnessCS)
        generate a chaotic sequence x using the logistic map
        for var = 1 to noVar      % noVar is the total number of decision variables
            if x(var) <= 0.5
                offspring(j,var) = parent1(var)
            else
                offspring(j,var) = parent2(var)
            end
            check if offspring population inside the bounds, if not, replace with bounds
        end
    end
end
return offspring
```